# COMPUTATIONAL STUDIES OF *MYCOBACTERIUM TUBERCULOSIS* L, D-TRANSPEPTIDASE2

**THANDOKUHLE NTOMBELA**

**216073335**


**2018**

# COMPUTATIONAL STUDIES OF *MYCOBACTERIUM TUBERCULOSIS* L, D-TRANSPEPTIDASE2

**THANDOKUHLE NTOMBELA**

**216073335**

**2018**

A thesis submitted to the School of Pharmacy and Pharmacology, Faculty of Health Science, University of KwaZulu-Natal, Westville, for the degree of Master of Medical Science.

This is the thesis in which the chapters are written as a set of discrete research publications, with an overall introduction and final summary. Typically, these chapters will have been published in internationally recognized, peer-reviewed journals.

This is to certify that the content of this thesis is the original research work of Mr. Thandokuhle Ntombela
As the candidate's supervisor, I have approved this thesis for submission.

Supervisor: Signed: ---------- Name: **Dr. B. Honarparvar** Date: ----------

Co-Supervisor: Signed: ---------- Name: **Prof. H. G. Kruger** Date: ----------

Co-Supervisor: Signed: ---------- Name: **Dr. G. E. M. Maguire** Date: ----------

# ABSTRACT

Tuberculosis (TB) is still one of the most highly elusive lethal transmittable diseases to eradicate and persist to be a major threat to public health due to emergence of drug resistance. Drug-resistant is steadily increasing worldwide, therefore, there is an urgent need for development of improved efficacious antibiotics and novel drug targets to successfully contain the disease. Peptidoglycan layer (PG) is the major attribute in bacterial cell envelope and is essential for protection and growth in all bacterial species including *Mycobacterium tuberculosis*(*Mtb*).

The biosynthesis pathway for PG is extremely intricate and involves numerous interconnected metabolites such as *N*-acetylmuramic(NAM) acid and *N*-acetylglucosamine(NAG), that are required during transpeptidation. These two sugar molecules are linked together by a $\beta$ (1-4) glycosidic bond and the NAM attaches 3-5 amino acid peptide stems. Consequently, the peptidoglycan strands are cross linked by transpeptidases, namely D, D- and L, D-transpeptidases, forming crucial 4→3 and 3→3 cross-linkages respectively. Both D, D- and L, D-transpeptidases need to be inhibited concomitantly to eradicate the bacterium. L, D-transpeptidase 2 ($Ldt_{Mt2}$) is one of the paralogs that is essential for *Mtb* growth, cell morphology and virulence during the chronic stage of the disease. This paralog has major influence in drug resistance and persistence of tuberculosis.

The traditional $\beta$-lactam family of antibiotics have been reported to be effective against *Mtb* following the inactivation of $\beta$-lactamases (BlaC) known to rapidly hydrolyze the core $\beta$-lactam ring. The classic penicillins inhibit D, D-transpeptidases, while L, D transpeptidases are blocked by carbapenems. Despite several studies in this field, to the best of our knowledge, limited attention has been paid to the inhibition mechanism of $Ldt_{Mt2}$ using carbapenem derivatives. In this regard, we need to explore reliable alternative strategies that are most cost-effective in terms of investigating the interactions of FDA approved carbapenems against *Mtb* L, D-Transpeptidases and study the role of explicit water molecule confined in the active site. As a result, computational chemistry has provided the possibility to sightsee and investigate this problem with relatively cost effective computational techniques.

In this thesis, we applied a hybrid quantum mechanics and molecular mechanics techniques (QM:MM), Our own *N*-layered Integrated molecular Orbital and Molecular Mechanics (ONIOM) approach, to investigate the binding interaction energies of carbapenems (biapenem, imipenem, meropenem and tebipenem) against L, D-transpeptidase 2. Furthermore, the role of

explicit water molecule confined in the active site was also explored using the same hybrid method to ascertain the nature of binding interaction energies of carbapenems against $Ldt_{Mt2}$. In all the investigated carbapenem─$Ldt_{Mt2}$ complexes, the carbapenems and the catalytic active site residues of $Ldt_{Mt2}$ (Cys205, His187, Ser188, His203 and Asn207) were treated at QM (B3LYP/6-31+G(d)) level of theory whereas the remaining part of the complexes were treated at MM level (AMBER force field). The explicit water molecules near the carbapenems were considered and treated at QM as well.

The obtained findings of Gibbs free energy (ΔG), enthalpy (ΔH) and entropy (ΔS) for all studied complexes showed that the carbapenems exhibit reasonable binding interactions towards $Ldt_{Mt2}$. This can be attributed by the structural dissimilarities of the carbapenems side chain which significantly induce conformational changes in the $Ldt_{Mt2}$. In comparison, the binding free energy calculations of the model system with explicit water molecule yielded significant binding interaction energies. The QTAIM and NBO results confirmed the nature of binding free energies that the topological properties of atoms in molecules and the delocalization of electrons are from a bonding to antibonding orbitals in hydrogen bond interactions and this has enhanced the stability of carbapenem—$Ldt_{Mt2}$ complexes. We believe that molecular insight of the carbapenems binding to $Ldt_{Mt2}$ and the role of explicit solvent will enable us to understand the inhibition mechanisms.

**Keywords:** Tuberculosis (TB); Mycobacterium tuberculosis *(Mtb)*; L, D-transpeptidase2 Carbapenems; Our own N-layered Integrated Molecular Orbital and Molecular Mechanics (ONIOM); Quantum theory of atoms in molecules (QTAIM); Natural bond orbital (NBO).

# DECLARATION

I, Mr. Thandokuhle Ntombela, declare that;

1. The research reported in this thesis, except where otherwise indicated, is my original research.

2. This thesis has not been submitted for any degree or examination at any other university.

3. This thesis does not contain other persons' data, pictures, graphs or other information, unless specifically acknowledged as being sourced from other persons.

4. This thesis does not contain other persons' writing, unless specifically acknowledged as being sourced from other researchers. Where other written sources have been quoted, then:

a. Their words have been re-written, but the general information attributed to them has been referenced

b. Where their exact words have been used, then their writing has been placed in italics, inside quotation marks and referenced.

5. This thesis does not contain text, graphics or tables copied and pasted from the Internet, unless specifically acknowledged, and the source being detailed in the thesis and in the References sections.

A detail contribution to publications that form part and/or include research presented in this thesis is stated (include publications submitted, accepted, in *press* and published).

**Signed:**

# LIST OF PUBLICATIONS

**Publication 1**: ONIOM study of the binding interaction energies for the carbapenems complexed with L, D-Transpeptidase 2 from *Mycobacterium tuberculosis* – Thandokuhle Ntombela, Zeynab Fakhar, Collins U. Ibeji, Thavendran Govender, Glenn E. M. Maguire, Gyanu Lamichhane, Hendrik G. Kruger and Bahareh Honarparvar.

Thandokuhle Ntombela contributed to the design of the project, carried out all the calculations and wrote the paper.
The paper was submitted to the Journal of Computer-aided molecular design, 31st of January 2018.

**Publication 2**: ONIOM study of carbapenems binding interaction energies against L, D-Transpeptidase 2 from *Mycobacterium tuberculosis* with explicit water molecules confined in the active site – Thandokuhle Ntombela, Zeynab Fakhar, Gideon F. Tolufashe, Collins U. Ibeji, Thavendran Govender, Glenn E. M. Maguire, Gyanu Lamichhane, Hendrik G. Kruger and Bahareh Honarparvar.

Thandokuhle Ntombela contributed to the design of the project, carried out all the calculations and wrote the paper.
The submission of this potential publication will be withhold until the shortcomings identified in the thesis are sufficiently addressed.

# ACKNOWLEDGEMENTS

**"By faith and charitable deeds, there are rewards, for faith without deeds is useless or dead"**

James 2: 14

I would first like to express my deepest hearty thanks to the Almighty God for protecting and giving me strength to overcome all odds up until this day. I would like to extend my sincere gratitude to my supervisors, Prof. H.G. Kruger, Dr B Honarparvar, Dr Glenn E.M. Maguire, and Dr Zeynab Fakhar for their remarkable scientific support, patience, and guidance throughout the course of this project.

A Special thank you goes to my father Mr J. Ntombela for supreme love and well wishes for success. I would also like to acknowledge my *late* mother & brother, Mrs M.G. Ntombela & Mr N.J. Ntombela for indoctrinating morals and love for success. *Ngiyabonga ngemfundiso nangeziyalo ezinhle enazitshala kimi.* And least but not last, to Ntombela family, and those who have continued to love, support and encourage me during my years of study thank you so much.

I would also like to thank:

- My fellow colleagues of the Catalysis and Peptide Research Unit, both former and present for their invaluable support.
- My friends: Scebi Mthethwa, Lindokuhle Mbatha, Siphiwe Ndlovu, Mthokozisi Nsele, Dr Rebamang Mosa, and Nomadlozi Hlophe for their continuous moral support and sparking values towards this attainment. My heartfelt gratitude and appreciation is indeed extended to Dr. Zeynab Fakhar for being a sister, colleague, mentor and a good friend always, your invaluable support has thus brought me this far (THANK YOU FOR EVERYTHING).
- The National Research Foundation (NRF) and UKZN for their generous funding during this project.
- The CHPC and UKZN clusters for their computational resources

**"For we walk by FAITH not by sight"**

2 Corinthians 5:7

# Table of Contents

# LIST OF FIGURES

## CHAPTER ONE;



## CHAPTER TWO



## CHAPTER THREE

## APPENDIX A



## APPENDIX B

# LIST OF TABLES

## CHAPTER TWO



## CHAPTER THREE



## APPENDIX A



## APPENDIX B

# LIST OF ABBREVIATIONS

| | |
|---|---|
| AG | Arabinogalactan |
| AMBER | Assisted Model Building with Energy Refinement |
| Asn | Asparagine |
| B3LYP | Becke3 Lee-Yang-Parr |
| BCP | Bond Critical Points |
| CP | Critical Points |
| Cys | Cysteine |
| DFT | Density Functional Theory |
| FDA | Food and Drug Administration |
| HB | Hydrogen Bond |
| His | Histidine |
| HIV | Human Immune Virus |
| LDT | L, D-Transpeptidase |
| $Ldt_{Mt2}$ | L, D-Transpeptidase 2 |
| MA | Mycolic acids |
| MDR-TB | Multi-drug resistant tuberculosis |
| MM | Molecular Mechanics |
| MM-GBSA | Molecular Mechanics/Generalized Born and Surface Area |
| *Mtb* | *Mycobacterium tuberculosis* |
| NBO | Natural Bond Orbital |
| ONIOM | Our own N-layered Integrated molecular Orbital and Molecular Mechanics |
| PDB | Protein Data Bank |
| PG | Peptidoglycan |
| QM | Quantum Mechanics |
| QTAIM | Quantum Theory of Atoms in Molecules |
| Ser | Serine |
| TDM | Trehalose dimycolate |
| WHO | World Health Organization |
| XDR-TB | Extensively drug resistant tuberculosis |

# CHAPTER ONE

# INTRODUCTION

## 1.1 Preface

Tuberculosis (TB) is an infectious disease commonly caused by acid-fast Gram-positive strains of *Mycobacterium tuberculosis* bacilli. TB is regarded as one of the foremost global health issues [1, 2] and the most important infectious disease after HIV/AIDS. Recently, the World Health Organization announced a new statistical report with an estimated 10.4 million TB cases, which indicated a rapid increase of both morbidity and mortality rate [2]. Approximately 95% of TB deaths worldwide are most prevalent in developing countries [2]. The disease is an easily transmittable airborne infection that spreads when people who have active TB sneeze, cough, speak or spit [3]. TB control is much obfuscated by the co-operation of HIV which triggers the reactivation of latent *mycobacterium tuberculosis* (*Mtb*) persisters and has led to the emergence of drug-resistant strains of *M. tuberculosis* [4-6].

The sub-Saharan Africa region suffers the highest incidents of TB while the highest TB-burden occurs in populous countries such as India, Asia, Bangladesh, China, Indonesia, Pakistan, Nigeria and South Africa [7]. In 2014, the WHO estimated the incidence of TB in South Africa to be 860 (776–980) per 100,000 population, which contributed to it becoming amongst the highest burden countries in the world [8].

The remarkable resurgence of TB disseminated *via* the emergence of drug-resistance has resulted in high morbidity and mortality rates [9]. Successful treatment for TB, discovered 40-50 years ago [10], requires the use of multiple antibiotics referred to as front-line drugs (isoniazid, rifampicin, pyrazinamide, and ethambutol) and patients are subjected to a treatment period of 6-9 months. These frontline drug-regimens for drug-susceptible TB are noted to have some side effects if they are improperly used [11, 12]. There are two types of drug-resistance tuberculosis, multi-drug resistance (MDR-TB)[13] and extensively drug resistance (XDR-TB) [13] tuberculosis, respectively. MDR-TB is defined as the resistance of *mycobacterium tuberculosis* strain against isoniazid and rifampicin. XDR-TB is referred to mycobacterium tuberculosis strains that are multi-drug resistance to almost all anti-tubercular drugs, including second-line drugs. Several years ago, an epidemic of drug-resistant TB, multidrug-resistant TB, and extensively drug-resistant TB, which are highly fatal, tremendously expensive and intricate to treat, emerged globally [14]. The major challenge in South Africa is the inadequacy

of TB control tools for detecting isoniazid resistance, the first resistance mutation to be acquired, since the current molecular diagnosis tools only assess rifampicin resistance [15]. Instances of drug resistance strains in South Africa were traced back to the late 1950s (XDR) and 1980s (MDR) [15]. The study conducted by Gandhi *et al.* [16] in the KwaZulu-Natal province indicated that the F15/ LAM4/KZN strain type prevailed among MDR TB and XDR TB cases and has led to nosocomial transmission and high mortality rates [17, 18].

South Africa is ranked sixth in the world in new TB incidents among the 22 countries that express an extreme TB-burden estimated to contribute about 80% of TB cases across the globe [7]. As a result, MDR-TB and XDR-TB persist in being a serious public health concern [19]. Therefore, there is an urgent need for the development of new potent drug therapies aimed at counteracting resistant *Mtb* strains and which can also be co-administered with HIV antiretroviral drugs.

### 1.1.1 Tuberculosis as a global health issue and co-epidemic with HIV

During the early 1980s, the HIV epidemic led to a major rise in TB cases and TB mortality in many countries, especially in southern and eastern parts of Africa [20]. Immunocompromised HIV-positive patients have a high probability to develop active TB infection and significantly enhance the risk of *mycobacterium tuberculosis* reactivation which in turn constitutes many deaths worldwide [21, 22]. Also, HIV co-infection convolution aggravates TB thus increasing the incidents of drug resistant cases by disseminating the infection, while HIV replication is also enhanced in other organs such as the lungs and pleura [23, 24]. Approximately 80% of people infected with HIV in the KwaZulu-Natal, are co-infected with active tuberculosis [25]. Of the people co-infected with HIV and TB in South Africa, an estimated 20% have a MDR strain. In fact, the disease burden in KwaZulu-Natal has been accentuated by the outbreak of XDR-TB among HIV-positive individuals reported in 2005 [25].

In 2015, an estimate of 0.4 million HIV-co-infected TB patients passed on and most deaths were due to TB infection. The actual number of estimated TB deaths in 2015 according to WHO was 1.4 million [26]. In an estimated 1.2 million new TB cases amongst HIV-infected people, the majority of about 71% come from people living in Africa. Although antiretroviral therapy is available for HIV infected individuals, their potency in controlling HIV-associated morbidity and fatality is thus diminished if tuberculosis programmes are not enhanced [27, 28]. Regimens that can provide safe co-operation with antiretroviral therapy are critically needed.

### 1.1.2 *Mycobacterium tuberculosis* and its life cycle

*Mycobacterium tuberculosis* is a rod-shaped, non-motile, aerobic Gram-positive bacillus that was first discovered by the German scientist, Dr Robert Koch, in1882 [29]. *M tuberculosis* is an obligate intracellular bacterium that requires a high oxygen content environment for its survival, therefore the lungs are primarily targeted. *Mtb* can infect a variety of animal species and humans. *Mtb* is a non-spore forming bacteria which can remain alive for years in a latent/dormant state [30] and its replication process differs to other bacteria as it divides every 15-20 hours, which is extremely slow. It is a persistent pathogen and it shares common characteristic features with other infectious agents responsible for sustained infections [31].

*Mtb* infection instigates upon pulmonary exposure, resulting from inhalation of active bacilli from the atmosphere [32]. The chances of being infected by active bacilli are influenced and escalated by various "infrastructural" factors, that often involves overcrowded conditions with respect to work, transport, schools and the living environment [33]. Prior to *bacilli* internalization, innate immune response or pro-inflammatory response from the host is stimulated to release phagocytic cells to contain mycobacterium tuberculosis [30, 34] which are then transported towards the alveolar epithelium layer in the lungs. The infected macrophages call upon other mononuclear cells and T lymphocytes from the surrounding blood vessels to form organized dynamical structures known as granulomata [34].

As the primary lesion matures into granuloma, the infected macrophages are surrounded by a number of foamy macrophages and a fibrous cuff forms while the central region of the granuloma accumulates caseous debris (**Figure 1**) [30, 35, 36]. The active form of tubercle in the caseous region dissipates through blood plasma to various parts of the body, ultimately resulting in active bacilli being expelled into the environment *via* the lungs and sputum. *Mycobacterium tuberculosis* can remain within the host organism for quite lengthy periods in dormant state and can still resuscitate [30]. Immunocompetent HIV infected individuals are most prone for *Mtb* reactivation.

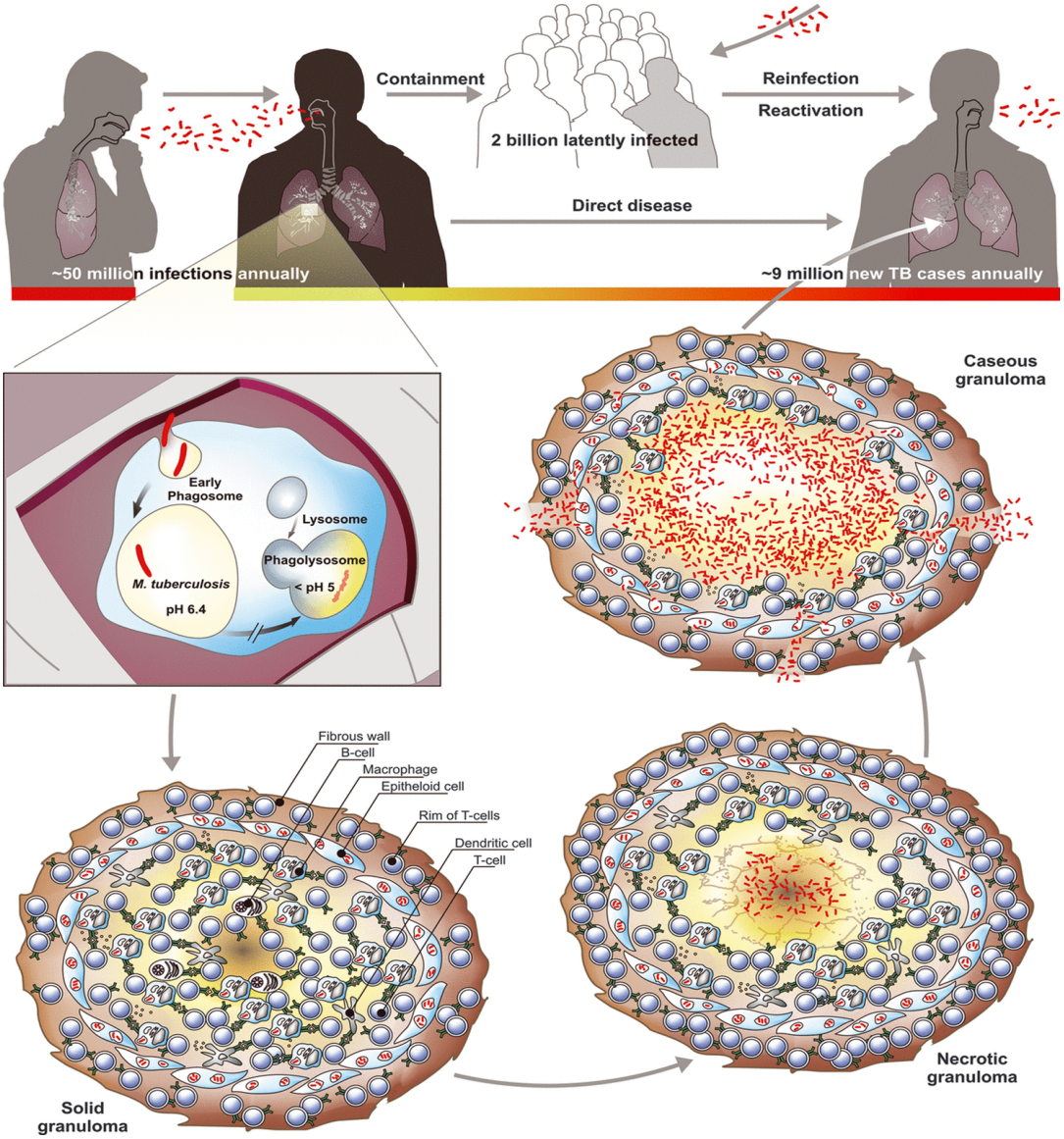


**Figure 1.** Schematic diagram representation of mycobacterium tuberculosis life cycle during infection [30]. Reprinted with permission from reference 50. *Copyright* 2012. *Federation of European Microbiological Societies (FEMS).*

### 1.1.3 Mycobacterium tuberculosis composition

#### 1.1.3.1 Cell wall structure

The cell envelope of *M. tuberculosis* is a highly intricate hydrophobic arrangement of distinct glycolipids and mycolic acids. Mycolic acids are elongated chains of branched fatty acids either covalently bound to the cell wall or to the toxic form of glycolipid, trehalose dimycolate (TDM)[37]. The cell wall is made up of two layers, the inner- and the outer-layer, bound by a plasma membrane [38]. The outer membrane bound layer is composed of lipids and proteins freely linked to the cell wall with fatty acid chains matching the inner membrane-bound layer fatty acids. The inner membrane bound layer comprises of mycolic acids (MA), arabinogalactan (AG), and peptidoglycan (PG) covalently tethered together to form a MA-AG-

PG complex that outspreads from the plasma membrane beginning with PG and ending with MAs [38]. The PG complex structure enhances the protection in *mycobacterium tuberculosis* against various drugs that are unable to penetrate through the cell wall and reach the cytoplasm to successfully destroy the cells.

The complex structure of the cell wall also consists of muropeptide sugar molecules, *N*-acetylglucosamine (NAG) and *N*-acetylmuramic acid (NAM) [39]. These sugar molecules are linked to each other through a β (1-4)-glycosidic bond in affiliation with three to five amino acid-long peptide stems [39-41]. The peptidoglycan layer is crucial to maintain rigidity and turgor pressure thus, serves as a structural permeability barrier in the cell envelope [42]. A mesh-wax-like coat of mycolic acid and glycolipids are joined to arabinogalactan that is successively linked to *N*-acetylmuramic acid subunits in the peptidoglycan layer [43]. *Mtb* share a common peptide-stem sequence with *Escherichia coli* and *M. subtilis* but with minor distinctions [40].

The amidation on the D-glutamate (D-Glu), diaminopimelate (Dap) moieties and a high proportion (80%) of Dap-Dap (3→3) transpeptide linkages are catalysed by the enzyme L, D-transpeptidase and 20% of cross-linkages, the classical 4→3 are catalysed by D, D-transpeptidase also known as penicillin binding proteins [39, 44, 45]. *Mtb* L, D-transpeptidases are susceptible to β-lactam antibiotics as a result of effective inactivation of chromosomally encoded *β*-lactamase known to hydrolyse the *β*-lactam ring of carbapenems [46].

#### 1.1.3.2 Peptidoglycan layer

Peptidoglycan (PGN) is a key component of the bacterial cell envelope in both Gram-negative and Gram-positive bacteria. The peptidoglycan layer forms part of the structural basis for most bacteria as it is made of macromolecules that encompasses the cytoplasmic membrane to protect the bacterium from exploding due to the osmotic pressure of the cytoplasm [47]. Peptidoglycan provides protection as it serves as a framework for attaching various surface polymers to maintain the integrity and overall shape of the persisters. The action of enzymes, glycosyltransferases in polymerization and transpeptidases in cross-linkages formation of the peptide stems, help congregate the peptidoglycan from sugar pentapeptide subunits [48, 49]. The peptidoglycan layer is formed from two alternating amino sugars *N*-acetylmuramic acid and *N*-acetylglucosamine, held together by a β-1, 4 glycosidic bond, coupled by a short oligopeptide stem attached to mycolic acids and glycolipids, that forms a wax-like coat in the outer layer, covalently linked to arabinogalactan [43].

The biosynthetic route of peptidoglycan is a complex process that initiates in the cytoplasm with the synthesis of a muramyl pentapeptide precursor comprising a terminal D-Ala-D-Ala. Bacterial *N*-acetylglucosamine synthesis from fructose-6-phosphate involves four enzymes to successfully complete the synthesis of the peptidoglycan layer that includes [39]: glucosamine-6-phosphate synthase (GlmS), phosphoglucosamine mutase (GlmM), glucosamine-1-phosphate acetyltransferase and *N*-acetylglucosamine-1-phosphate uridyltransferase (GlmU) [39]. GlmS is an aminotransferase enzyme that is essential for the conversion of fructose-6-P to glucosamine-6-P through the activity of fructose-6-phosphate aminotransferase (GlmS) using L-glutamine [39, 50]. GlmM is involved in the biosynthesis process of UDP-GlcNAc by isomerizing glucosamine-6-P to glucosamine-1-P, respectively [39, 51]. The two final steps of cell wall biosynthesis are catalysed by *N*-acetylglucosamine-1-phosphate uridyltransferase (GlmU). GlmU is a bifunctional enzyme that catalyse the acetyltransfer from acetyl-coA to glucosamine-1-phosphate (GlcN-1-P) to yield *N*-acetylglucosamine-1-phosphate (GlcNAc-1-P) which is then converted to UDP-GlcNAc by uridyltransfer from uridine 5-triphosphate (UTP) in the presence $Mg^{2+}$ [52].

The UDP-GlcNAc, the precursor for NAG, is transformed to UDP-MurNAc upon addition of the lactyl group to glucosamine. The UDP-MurNAc is then converted to UDP-MurNAc pentapeptide by addition of five amino acids including the dipeptide D-alanyl-D-alanine. The metabolic pathway of L-alanine is basically formed through reductive amination process of pyruvate (**Figure 2**). As a consequent, the bacterial cell wall requires the D-alanine precursor for peptidoglycan biosynthesis and for survival. Therefore, the L-alanine precursor is predominantly available as a source of nitrogen in most bacteria [53].

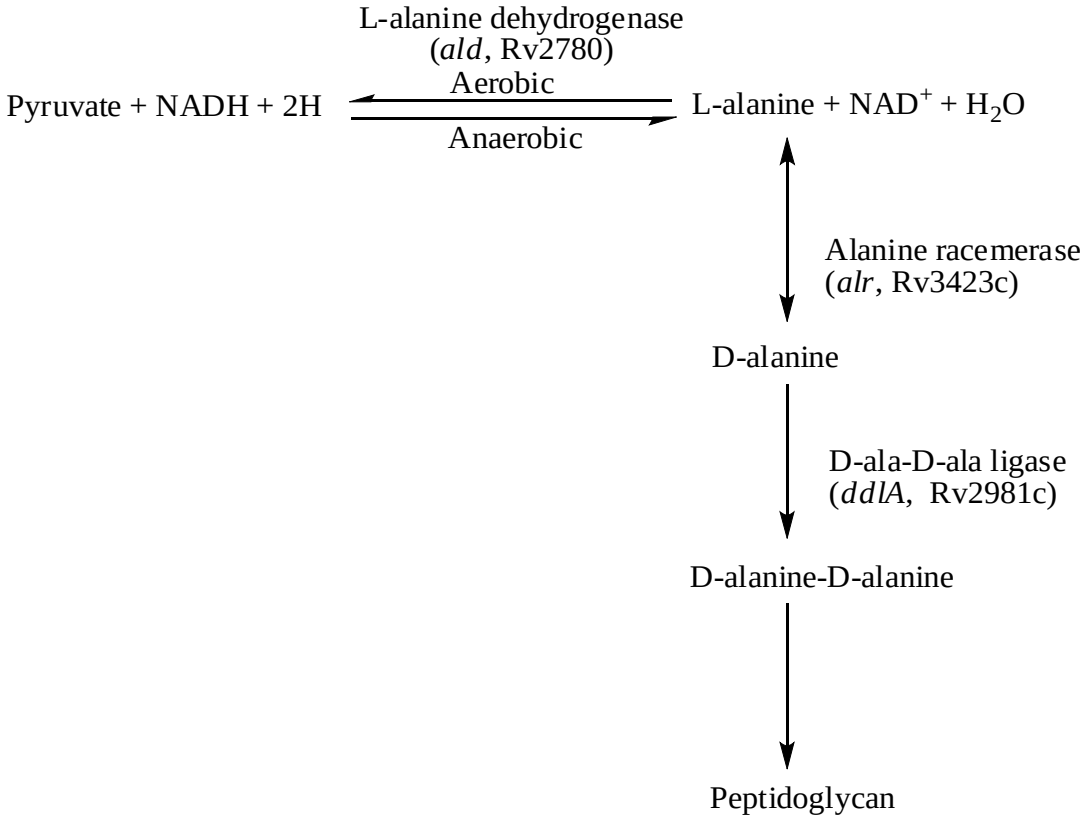


**Figure 2.** Illustrative representation of interconversion of L-alanine to D-alanine during peptidoglycan biosynthesis [54].

The alanine racemase is dependent on pyridoxal phosphate for catalysing the interconversion of L-alanine amino acid into D-alanine, the essential precursor for peptidoglycan, which then joined to D-alanyl-D-alanine moiety through the action of D-Ala-D-Ala ligase (**Figure 2**) [55, 56]. PG is covalently linked to arabinogalactan that is also connected to mycolic acid lipid layer that consists of three classes of lipids (alpha-, keto- and methoxymycolates) (**Figure 3**) [57]. The oxygenated mycolic lipid layer plays a significant role in inducing the growth of mycobacterium tuberculosis's intra-macrophages [58]. Mycolic acids vary in their configuration as alpha-mycolic acids have two cis-configuration cyclopropane rings while keto- and methoxymycolates have either cis- or trans- configuration of the cyclopropane ring.

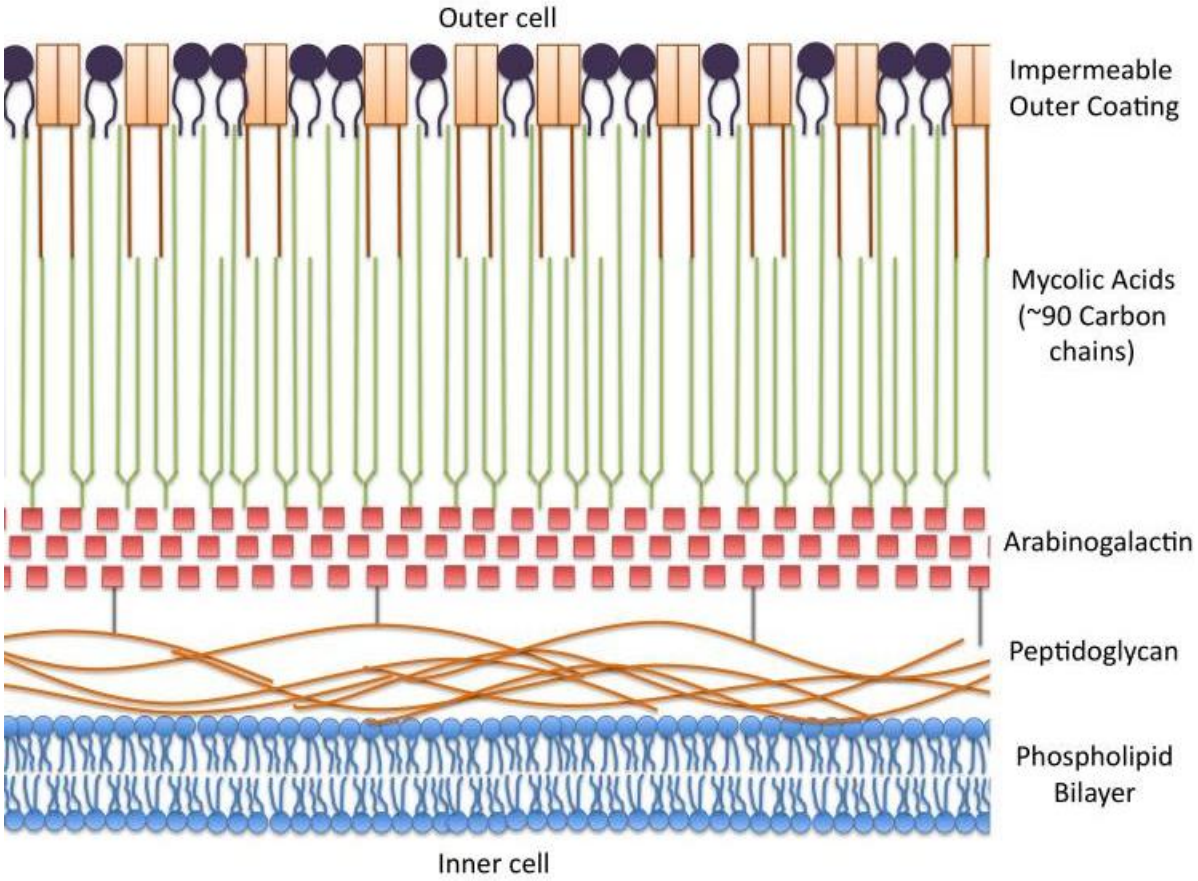


**Figure 3.** Schematic diagram of mycobacterium tuberculosis cell wall composition [59]. Reprinted with permission from reference 69. *Copyright* 2011. *Yale Journal of Biology and Medicine* (YJBM).

### 1.1.4 L, D-Transpeptidase function and structure

L, D-transpeptidases (Ldt) are regarded as a novel family of peptidases comprising of a cysteine residue in the active-site and is different from D, D transpeptidases by having serine as a catalytic residue. Ldt function by catalysing the formation of crucial 3→3 cross-linkages and also serves numerous other cellular functions [60]. The primary step of Ldt involves the nucleophilic attack of the meso-diaminopimelic acid (meso-Dap$^3$) carbonyl of the tetrapeptide stem, which then lead to the formation of the thioester bond between carbonyl and catalytic cysteine of L, D-transpeptidase. The secondary step involves the nucleophilic attack of the subsequent acyl enzyme by the amine group of the meso-Dap$^3$ side chain from the second stem-peptide substrate thus resulting in the formation of 3→ 3 cross-linkages. Consequently, the D, D-transpeptidases is also playing a critical role in the biosynthesis process of the peptidoglycan layer by catalysing the formation of 4→3 cross-linkages (D-Ala$^4$─meso-Dap$^3$) [61]. In most bacterial species, L, D-transpeptidases have an insignificant role of forming 3→3 cross-linkages during the biosynthesis process of peptidoglycan as observed in *Escherichia coli* where the 3→3 cross-linkages were formed during the exponential and stationary phases of

growth [62]. *Mycobacterium tuberculosis* exhibit elevated content of about 80% 3→3 cross-linkages compared to other bacterial species [63]. Previously, L, D-transpeptidase 2, $Ldt_{Mt2}$ (MT2594, the product of gene Rv2518c), was characterized in *Mtb*, which thus proved that the loss of virulence and deteriorated growth in *Mtb* strain was reliant to the lack of $Ldt_{Mt2}$ during the chronic phase of the disease [64]. Apart from $Ldt_{Mt2}$, *Mtb* has four other paralogs of which one, $Ldt_{Mt1,}$ displays $Ldt_{Mt2}$ properties ($Ldt_{Mt1}$-$Ldt_{Mt5}$) [45, 63]. Previous studies show that L, D-transpeptidase ($Ldt_{fm}$) in mutated *Enterococcus faecium* plays a significant role in favour of the pathogen's survival as it triggers the adaptive response to *β*-lactam antibiotics which are hydrolysed by lactamase enzyme thus promoting elevated level of drug resistance.

#### 1.1.4.1 Structure of L, D-transpeptidase 2

The L, D-transpeptidase enzyme (PDB code: 3TUR) [65] comprises of two chains, A and B with 527 amino acids [65]. Each chain contains two domains; the N-terminal domain extending with 150-250 residues, held in an antiparallel fold and a C-terminal catalytic domain extending by 254-407 residues [65]. These two domains are joined together by a short stretch of residues (251-253) making a complete functional protein [60]. The active site lid includes His300-Asp323 residues in a spiral loop of two normal β-sheets. The active site of L, D-transpeptidase comprises of a catalytic triad of Cys354, His336 and Ser337 residues with His336 and Ser337 being buried in the cavity while Cys354 is exposed to bulk solvent and is reachable through two paths (A, B) [66].

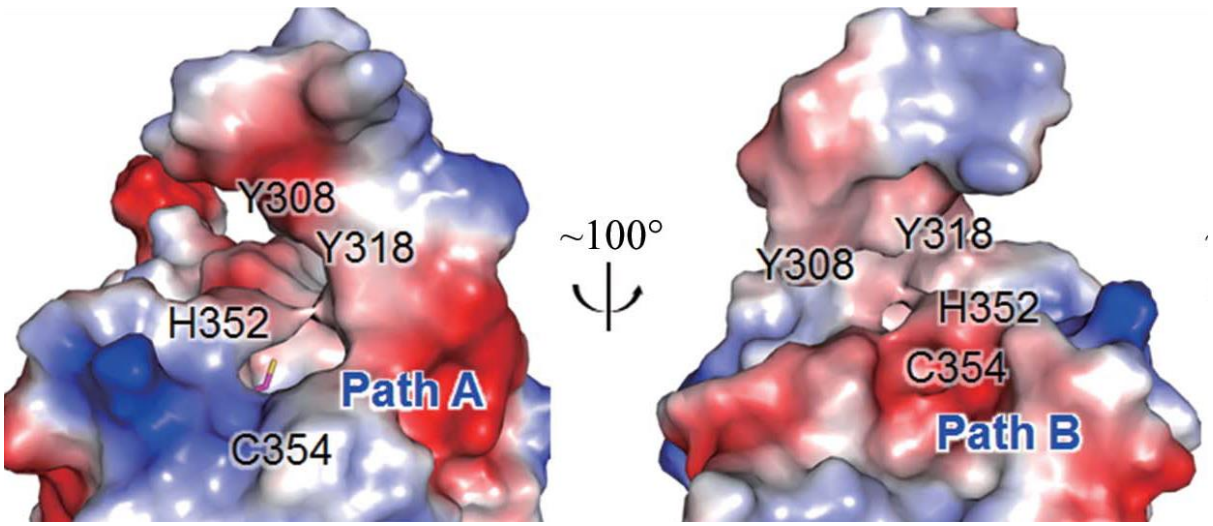


**Figure 4.** 3-D structure of $Ldt_{Mt2}$ showing active site lid in an open conformation [65, 66].

### 1.1.5 Application of carbapenems antibiotics

Carbapenems are a subfamily of β-lactam antibiotics that were discovered by Merck & Co from the soil bacteria *Streptomyces cattleya* [67]. These compounds exhibit a broad spectrum of activity with bactericidal effects against Gram-negative and Gram-positive bacteria including both aerobic and non-aerobic species [68]. The β-lactam antibiotics resemble the peptide precursor of the peptidoglycan layer, NAM/NAG chain, by having a D-Alanyl-D-Alanine configuration at the terminal amino acid residues. These features allow antibiotics to easily bind to the penicillin binding protein (PBP) site and irreversibly bind to the active site serine residue, thus preventing the formation of cross-linkages thereby causing disruption of the cell wall [69]. The carbapenems vary mainly in their side chain configuration at C2 and C6 which also reflects their variant stability, resistance, stimulation, and inhibition of the β-lactamase enzyme [70]. Carbapenems structurally differ from other β-lactams in that position 1 is substituted with a sulphur atom and a double bond is present between C2-C3 of the 5-membered ring as depicted in **Figure 5**.

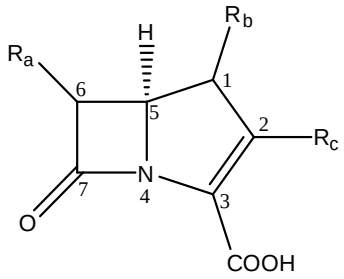


**Figure 5.** Structural core of β-lactam antibiotic

The combination of a β-lactamase inhibitor (clavulanate) and amoxicillin shows an efficient bactericidal effect against TB infected patients and even those that were reported to have developed resistance by inhibition of the mycobacterium β-lactamase (BlaC) enzyme [46, 71, 72]. Previous studies reveal that the $Ldt_{Mt2}$ enzyme is very susceptible to amoxicillin-clavulanic acid [45].

Dehydropeptidase (DHP-1) is an enzyme located in the renal tubule of the kidney and has an ability to degrade imipenem. Imipenem remains unchanged in solution and possesses a wide spectrum of activity against aerobic and anaerobic bacteria [73, 74]. Imipenem was recommended clinically to be co-administered with cilastatin following rapid degradation by the DHP-1 [67, 70]. However, meropenem was later approved for clinical use as it was stable against DHP-1 degradation and is also resistant to *Mtb* BlaC β-lactamase and can therefore be administered

alone [70]. Disruption of the permeability barrier of the cell wall components will increase the ability of antibiotics penetration towards the inside of the cell. Therefore, full inhibition of L, D transpeptidase is essentially a significant way to curb the proliferation of *mycobacterium tuberculosis* and thus more insight on mechanism of carbapenems can provide useful information for rational drug design. The loss of $Ldt_{Mt2}$ in *M. tuberculosis* leads to a transformed cell size, growth, and virulence which thus exposes the bacterium to increased susceptibility to amoxicillin [75, 76]. However, it was pointed out before, that inhibition of both $Ldt_{Mt1}$ (first generation β-lactams) and $Ldt_{Mt2}$ (carbapenems) would offer a better chance of avoiding the development of drug resistance [77].

Previous experimental literature stated that imipenem irreversibly inhibited $Ldt_{Mt1}$ which is known to contribute in the formation of 3→3 transpeptide cross-linkages [78]. Lavollay *et al.* [63] conducted a study of this enzyme believed to have generated major cross-linkages during the stationary phase of *Mycobacterium tuberculosis*. In their findings, $Ldt_{Mt1}$ was also associated with the structural adaptation of the pathogen during the non-replicative state [63].

Studies exploring carbapenem mechanism of inhibition against $Ldt_{Mt2}$ have authenticated their potency against extensively drug-resistant TB strains and are therefore well suited as possible drug candidates for TB treatment [65, 66, 79]. *In-vitro* studies demonstrated that penems (faropenem) and the carbapenems (doripenem, biapenem and tebipenem) have bactericidal activity against *Mycobacterium tuberculosis* in the absence of β-lactamase inhibitors [80].

Lately, several computational methods have been used to study carbapenems against $Ldt_{Mt2}$ which provided very useful molecular views of possible mechanisms of inhibitors and the receptor [65, 75, 77, 81-83].

### 1.1.6 Computational work and importance of the study

The peptidoglycan biosynthesis pathway is a key functional process necessary for mycobacterium tuberculosis morphology and growth and has been intensively explored by Lamichhane *et al.* [75]. The functions performed by various *Mycobacterium tuberculosis* enzymes yield fundamental metabolites required in the peptidoglycan biosynthesis. This includes vital targets for rational drug design (GlmS, GlmM, GlmU, MurA, MurB, MurC, MurD, MurE and MurF) which the bacterium utilizes to synthesize the rigid architectural peptidoglycan layer. In that study, the essential metabolites of an organism were identified using genetic and biochemical techniques and then afterwards followed by application of computational approaches, Discovery Studio 2.5.5, to retrieve the mimics of the essential metabolites by pharmacophore identification [75].

Recently, studies exploring the catalytic mechanism of L, D transpeptidase 2 from mycobacterium tuberculosis emerged [81] giving more insight into the binding interactions between the substrate and $Ldt_{Mt2}$. In that study, the experimentally proposed mechanism for $Ldt_{Mt2}$ was extensively investigated by quantum mechanics/molecular mechanic (QM/MM) molecular dynamic (MD) simulations. The free energy results obtained by PMF analysis agreed with the proposed experimental mechanism and have shown that the acylation step is the rate-limiting step in the catalytic mechanism. A comprehensive analysis of the substrate-protein interactions revealed the significance of involved residues, such as Met303, Tyr318, Trp340, His352, and Asn356, in binding of the substrate and stabilization of the transition state [81]. Silva *et al.* [77] also investigated the mechanism of the inhibition reaction of mycobacterium tuberculosis L, D-transpeptidase 2 by carbapenems using hybrid QM/MM MD simulations and a QM/MM umbrella sampling technique to obtain the free energy profile for $Ldt_{Mt2}$ catalytic mechanism. According to the proposed mechanism, the acylation step was confirmed to be preceded by a thiol–imidazole pair formation (Cys354 and His336 catalytic residues) in its zwitterionic form. The significance of this mechanism reveals that during acyl-enzyme formation the His336 plays a crucial role in proton abstraction from Cys354 thiol group which fulfil the acylation step. In this regard, the theoretical findings with the new proposed mechanism agreed in principle with the experimental data.

Considering the significance of Cys354, His336 and water molecule during acylation of $\beta$-lactams, the proceeding theoretical MD simulation study conducted by Silva *et al.* [84] explored the binding affinities of imipenem and meropenem against $Ldt_{Mt2}$. The binding free energies

for inhibitor/ex-$Ldt_{Mt2}$ complexes were calculated from a 25 ns MD simulation using MM/GBSA and SIE approaches and the obtained findings from the study revealed that imipenem complex adopted a closed conformation while for meropenem complex remained in an open conformation after the whole MD simulation. This further required validation by longer MD simulation runs to bring more insight on conformational opening and closing of the complexes [84]. Consequently, the β-hairpin flap dynamics seem to have a major contribution in accommodating the inhibitor within the pocket binding site. Recently the MD simulation study exploring differential flap dynamics in $Ldt_{Mt2}$ revealed that during the binding process of the inhibitor, the enzyme undergoes some conformational changes in the flap region [85]. The distance analysis amongst all the anticipated tip–tip distances of flap residues revealed the crucial role in mitigating the flap conformations. The study provided a very insightful overview of the ligand binding process accommodated by rapid β-hairpin flap dynamics reliant on open and closed conformations.

An integrated computational method, a two-layered ONIOM approach, developed by Morokuma and colleagues [86-89] has been used to study large molecular complex systems. The ONIOM (our *N*-layered integrated molecular orbital plus molecular mechanics) approach is a hybrid method known to combine different QM method as well as MM method for large systems to provide accurate calculations. The $Ldt_{Mt2}$ is a very large enzyme which requires hybrid methods to be studied when complexed with inhibitors. We proceeded with a two-layered ONIOM method to investigate the binding interaction energies for FDA approved carbapenems against $Ldt_{Mt2}$ enzyme. Furthermore, the inclusion and the role of explicit water molecules confined in the active site of $Ldt_{Mt2}$ was also investigated to ascertain the nature of binding interaction energies for carbapenems.

## 1.2 Computational background

Computational chemistry is a fast-growing branch of chemistry intended to investigate chemical and biochemical challenges at an atomic and molecular aspect using theoretical methods encompassed in computer programs. Computational chemistry has been significantly useful in studying chemical biological systems with an aim of acquiring adequate insight about macromolecular targets to help design novel drugs based on fundamental information of targets. There are various theoretical methods in computational chemistry, namely, QM, MM and MD that are routinely used to study the chemical behaviour of molecular systems [90].

### 1.2.1 Quantum Mechanics

In the early 1920s Max Born and colleagues minted the term "quantum mechanics" which later appeared for the first time in Born's paper titled *"Zur Quantenmechanik"* in 1924 [91]. Quantum mechanics is a branch of physics that deals with physical states of matter and the chemical behaviour of molecular systems on the scale of atoms and subatomic particles and has gained momentum in diverse fields of science.

#### 1.2.1.1 Ab-initio methods

*Ab-initio* methods form part of quantum chemistry and is the most commonly used electronic structure method in both theoretical and computational chemistry. Despite the method being the most accurate, its calculations are very expensive in terms of time and computational resources [92, 93]. These methods are guided by the principles of quantum mechanics derived from theoretical chemical theory and can produce very high accuracy given the suitable large basis set are used. The distinct levels of theory for instance of Moller-Plesset (MP*n*) includes the effect of electron correlation, Hartree-Fock (HF) and Configuration Interaction (CI) [92].

#### 1.2.1.2 Density functional theory

Kohn Hohenberg and Kohn Sham initiated a different quantum mechanical modelling method, density functional theory (DFT), that uses density functional models intended to improve the electronic structures by using electron density instead of wave function [94] to evaluate structural energies at ground state [94-96]. DFT operates by two fundamental useful theorems proposed by its inventors which uses electron density functional to explore the electronic structures of the systems [94]. The first theorem demonstrates that the ground state properties of complex-electronic systems are unique functional of electron density that relies on 3-dimensional coordinates. The second theorem states that the functional of the system that transmit the

ground state energy delivers the lowest energy dependent on the real input of the ground state density [95]. The Becke3LYP [97] correlation functional using designated basis set is known for its accuracy and relatively little computational cost [98]. A basis set is defined as a set of functions used to denote the electronic wave function in Hatree-Fock method or density functional theory for effective approximation of atoms in molecules. The hybrid model Becke3LYP is frequently used for organic compounds and yield good geometries for molecular, organic and organometallic compounds [99].

#### 1.2.1.3 Semi-empirical methods

Semi-empirical methods are represented by their use of empirically derived parameters for simplifying the approximation of the Schrodinger equation [100]. This method is based on the Hatree-Fock method that acknowledges the correlation effect of the method and is mostly applied on large molecular systems [93]. Semi-empirical methods only employ QM calculations specifically for the valence electrons in the system. The most commonly used functionals for semi-empirical methods are AM1, PM3, PM6, ZINDO and INDO [100]. These diverse functionals use experimental data and lower the computational cost by reducing the integrals for approximation of results.

### 1.2.2 Molecular mechanics

Molecular mechanics applies principles of classical mechanics to model molecular systems and it is mostly used to study varying molecular systems in terms of size and complexity to predict their relative potential energies using force fields and their quality of parameterization [101]. The empirical force field method utilizes classical mechanics with the perception that the total steric energy of the structure relies on the sum of complex interactions.

MM methods typically have lower accuracy and are relatively less expensive than quantum mechanical methods in terms of computational resources [101, 102]. The major detriment of molecular mechanic methods is that the quality of the calculations is enormously reliant on empirical parameters. The experimental studies or high-level of *ab initio* calculations normally determines the parameters based on the small number of model systems [102]. The most well-known force fields include; Merk Molecular Force Field (MMFF) [103], AMBER [104, 105]and Universal Force Field (UFF) [106]. In our case, the AMBER force field [104] was applied and it utilizes a simple harmonic model that features torsions, bond stretch and angle bends, and standard functions for Van der Waal and electrostatic interactions [107]. These force-fields were

significantly designed for certain families of compounds and the researchers should ensure the suitability of the force-field for the proposed model system under investigation.

### 1.2.3 ONIOM hybrid method (QM/MM)

ONIOM (our own n-layered Integrated molecular Orbital and molecular Mechanics) is an onion-scale-like method that combines QM and MM methods in multiple layers [88, 108]. The ONIOM hybrid method was first developed by Morokuma *et al.* [87, 109] to investigate small and large molecular systems. In this method, the results are combined to predict the high-level calculation for the real system which is quite expensive. ONIOM is applicable for geometry optimizations, calculation of energies and vibrational frequencies for complex molecular systems [87]. The ONIOM approach sufficiently provides accurate calculations for molecular systems, treated at three distinct levels (or layers) of theory, namely: low, medium and high layer. The low layer encompasses the entire system and, in most cases, is evaluated with an inexpensive method such as a MM method. Geometry optimization calculations of the partitioned system treated with diverse levels of theory in separate regions, the model system being in QM and the real system (larger region) treated by MM become easier [110]. The middle layer, also known as the intermediate model region, normally is considered in the case of a three-layered ONIOM model and often constitute of a portion larger than that of model system (high layer). The high layer comprises of a smaller region, the model system, usually treated with the precisely accurate QM method, DFT[109]. In our two-layered ONIOM hybrid method the catalytic residues (, His187, Ser188 and Cys205) as well as the carbapenem inhibitors were treated at high layer with DFT and the remaining part of the system at low layer with AMBER force field [104, 105].

For a two-layered ONIOM model system, the calculations were performed with the following schemes:

$$E_{ONIOM} = E_{real\ low} + E_{model\ high} - E_{model,low} \quad (\mathbf{1})$$

### 1.2.3.1 ONIOM binding free energy calculations

For ONIOM calculations the versatile pre-and post-processor graphical user interface (GUI) [111], Gauss View program, implemented in Gaussian 09 [112] package was used to model, view and prepare the input files for all the enzyme-inhibitor complexes. The binding free energies of the four selected FDA approved carbapenems were investigated for $Ldt_{Mt2}$ using Gauss view program and ONIOM model implemented in Gaussian 09 [112] package: ONIOM (B3LYP/6-31G(d): AMBER). The ONIOM binding interaction energy can be calculated as follow:

$$\Delta G_{ONIOM} \approx \Delta G = G_{complex} - (G_{protein} + G_{ligand}) (\mathbf{2})$$

Where, ΔG denotes the total binding energy of the system, $G_{complex}$ is the energy of complex (enzyme + ligand) and $G_{protein}$ and $G_{ligand}$ are the energies obtained individually from the enzyme and ligand respectively. The details of the computational methods are presented in the respective chapters.

## 1.3 Aim and Objectives

This study has two aims:

1. To generate a computational chemistry model using a two-layered ONIOM method and to calculate the binding interaction energies between carbapenems and $Ldt_{Mt2}$ from *Mycobacterium tuberculosis*. To achieve this, the following objectives were outlined:
    - To determine the binding free energies of carbapenems against $Ldt_{Mt2}$ during the complexation process using a DFT-B3LYP functional in a two-layered ONIOM method.
    - To determine the topological properties of the carbapenem-$Ldt_{Mt2}$ complexes using AIM200 software.
    - To determine the intermolecular interactions by second perturbation theory using NBO analysis approach.
2. To examine using an ONIOM computational model with explicit water molecule confined in the active site to ascertain the nature of binding interaction energies of carbapenems. To achieve this, the following objectives were outlined:
    - To evaluate the role of water molecule in the binding interface of carbapenems and $Ldt_{Mt2}$ using a DFT-B3LYP functional with 6-31+G(d) basis set.

- To determine the binding free energies of carbapenem—water—$Ldt_{Mt2}$ complexes.
- To determine the binding features of carbapenems in a water mediated $Ldt_{Mt2}$ complexes using Ligand scout.
- To determine the topological properties of the carbapenem—water—$Ldt_{Mt2}$ complexes using AIM200 software.
- To determine the intermolecular interactions of carbapenem—water—$Ldt_{Mt2}$ complexes by second perturbation theory using NBO analysis approach.

### 1.4 Thesis outline

This project evaluated the potential of the computational chemistry method, ONIOM (QM/MM), as an appropriate method for studying large systems. **Chapter 2** outlines the use of an integrated two-layered ONIOM method for determination of binding interaction energies of carbapenems against $Ldt_{Mt2}$. **Chapter 3** outlines the exploitation of the ONIOM computational model with explicit water molecule confined in the active site of L, D transpeptidase 2 to ascertain the nature of binding interaction energies of carbapenems. **Chapter 4** presents the conclusion and significance of the study.

## References


[1] Falzon, D., Raviglione, M., Bel, E. H., Gratziou, C., Bettcher, D., and Migliori, G. B. (2015) The role of eHealth and mHealth in tuberculosis and tobacco control: a WHO/ERS consultation, *European Respiratory Journal 46*, 307-311.

[2] (WHO), W. H. O. (2016) World Health Organization. *Global tuberculosis report* 2016 [cited 25 November 2016]; Available from http://apps.who.int/iris/bitstream/10665/250441/1/9789241565394-eng.pdf?ua=1.

[3] Guptal, K., and Atreja, A. (2006) Transmission of tuberculous infection and its control in health care facilities, *NTI Bulletin 42*, 63-67.

[4] Bucher, H. C., Griffith, L. E., Guyatt, G. H., Sudre, P., Naef, M., Sendi, P., and Battegay, M. (1999) Isoniazid prophylaxis for tuberculosis in HIV infection: a meta-analysis of randomized controlled trials, *Aids 13*, 501-507.

[5] Daley, C. L., Small, P. M., Schecter, G. F., Schoolnik, G. K., McAdam, R. A., Jacobs Jr, W. R., and Hopewell, P. C. (1992) An Outbreak of Tuberculosis with Accelerated Progression among Persons Infected with the Human Immunodeficiency Virus: An Analysis Using Restriction-Fragment—Length Polymorphisms, *N Engl J Med 326*, 231-235.

[6] Shafer, R., Singh, S., Larkin, C., and Small, P. (1995) Exogenous reinfection with multidrug-resistant Mycobacterium tuberculosis in an immunocompetent patient, *Tubercle and Lung Disease 76*, 575-577.

[7] World Health Organisation (WHO), http://www.who.int/tb/publications/global_report/gtbr14_main_text.pdf: Accessed 20 November 2016. ( 2014) Global Tuberculosis Report.

[8] Organization, W. H. (2014) *Global status report on alcohol and health 2014*, World Health Organization.

[9] Mukadi, Y. D., Maher, D., and Harries, A. (2001) Tuberculosis case fatality rates in high HIV prevalence populations in sub-Saharan Africa, *Aids 15*, 143-152.

[10] Seung, K., and Rich, M. L. (2016) Diagnosis and Treatment of Drug-Resistant Tuberculosis, *Tuberculosis: The Essentials 237*, 170.

[11] Swindells, S. (2012) New drugs to treat tuberculosis, *F1000 Med Rep 4*.

[12] Matteelli, A., Migliori, G. B., Cirillo, D., Centis, R., Girard, E., and Raviglion, M. (2007) Multidrug-resistant and extensively drug-resistant Mycobacterium tuberculosis: epidemiology and control, *Expert Rev Anti Infect Ther 5*, 857-871.

[13] Jaramillo, E. (2008) *Guidelines for the programmatic management of drug-resistant tuberculosis*, World Health Organization.

[14] Young, D. B., Perkins, M. D., Duncan, K., and Barry, C. E., 3rd. (2008) Confronting the scientific obstacles to global control of tuberculosis, *J Clin Invest 118*, 1255-1265.

[15] Cohen, K. A., Abeel, T., Manson McGuire, A., Desjardins, C. A., Munsamy, V., Shea, T. P., Walker, B. J., Bantubani, N., Almeida, D. V., Alvarado, L., Chapman, S. B., Mvelase, N. R., Duffy, E. Y., Fitzgerald, M. G., Govender, P., Gujja, S., Hamilton, S., Howarth, C., Larimer, J. D., Maharaj, K., Pearson, M. D., Priest, M. E., Zeng, Q., Padayatchi, N., Grosset, J., Young, S. K., Wortman, J., Mlisana, K. P., O'Donnell, M. R., Birren, B. W., Bishai, W. R., Pym, A. S., and Earl, A. M. (2015) Evolution of Extensively Drug-Resistant Tuberculosis over Four Decades: Whole Genome Sequencing and Dating Analysis of Mycobacterium tuberculosis Isolates from KwaZulu-Natal, *PLOS Medicine 12*, e1001880.

[16] Gandhi, N. R., Brust, J. C., Moodley, P., Weissman, D., Heo, M., Ning, Y., Moll, A. P., Friedland, G. H., Sturm, A. W., and Shah, N. S. (2014) Minimal diversity of drug-resistant Mycobacterium tuberculosis strains, South Africa, *Emerg. Infect. Dis. 20*, 426.

[17] Gandhi, N. R., Shah, N. S., Andrews, J. R., Vella, V., Moll, A. P., Scott, M., Weissman, D., Marra, C., Lalloo, U. G., and Friedland, G. H. (2010) HIV coinfection in multidrug-and extensively drug-

resistant tuberculosis results in high early mortality, *American journal of respiratory and critical care medicine 181*, 80-86.
[18] Ioerger, T. R., Koo, S., No, E.-G., Chen, X., Larsen, M. H., Jacobs Jr, W. R., Pillay, M., Sturm, A. W., and Sacchettini, J. C. (2009) Genome analysis of multi-and extensively-drug-resistant tuberculosis from KwaZulu-Natal, South Africa, *PloS one 4*, e7778.
[19] http://www.who.int/mediacentre/factsheets/fs104/en/.
[20] Organization, W. H. (2015) *Global tuberculosis report 2015*, World Health Organization.
[21] Aaron, L., Saadoun, D., Calatroni, I., Launay, O., Memain, N., Vincent, V., Marchal, G., Dupont, B., Bouchaud, O., and Valeyre, D. (2004) Tuberculosis in HIV-infected patients: a comprehensive review, *Clin Microbiol Infect 10*, 388-398.
[22] Selwyn, P. A., Sckell, B. M., Alcabes, P., Friedland, G. H., Klein, R. S., and Schoenbaum, E. E. (1992) High risk of active tuberculosis in HIV-infected drug users with cutaneous anergy, *Jama 268*, 504-509.
[23] Badri, M., Ehrlich, R., Wood, R., Pulerwitz, T., and Maartens, G. (2001) Association between tuberculosis and HIV disease progression in a high tuberculosis prevalence area, *Int J Tuberc Lung Dis 5*, 225-232.
[24] Collins, K. R., Quinones-Mateu, M. E., Toossi, Z., and Arts, E. J. (2002) Impact of tuberculosis on HIV-1 replication, diversity, and disease progression, *AIDS Rev 4*, 165-176.
[25] Gandhi, N. R., Moll, A., Sturm, A. W., Pawinski, R., Govender, T., Lalloo, U., Zeller, K., Andrews, J., and Friedland, G. (2006) Extensively drug-resistant tuberculosis as a cause of death in patients co-infected with tuberculosis and HIV in a rural area of South Africa, *The Lancet 368*, 1575-1580.
[26] Samanta, P. N., and Das, K. K. (2016) Prediction of binding modes and affinities of 4-substituted-2, 3, 5, 6-tetrafluorobenzenesulfonamide inhibitors to the carbonic anhydrase receptor by docking and ONIOM calculations, *J. Mol. Graphics Modell. 63*, 38-48.
[27] De Cock, K., and Chaisson, R. (1999) Will DOTS do it? A reappraisal of tuberculosis control in countries with high rates of HIV infection [Counterpoint], *Int J Tuberc Lung Dis 3*, 457-465.
[28] Corbett, E. L., Marston, B., Churchyard, G. J., and De Cock, K. M. (2006) Tuberculosis in sub-Saharan Africa: opportunities, challenges, and change in the era of antiretroviral treatment, *The Lancet 367*, 926-937.
[29] Lawn, S. D., and Zumla, A. I. (2011) Tuberculosis, *Lancet 378*, 57-72.
[30] Gengenbacher, M., and Kaufmann, S. H. (2012) Mycobacterium tuberculosis: success through dormancy, *FEMS microbiology reviews 36*, 514-532.
[31] Zumla, A., Raviglione, M., Hafner, R., and von Reyn, C. F. (2013) Tuberculosis, *N Engl J Med 368*, 745-755.
[32] http://www.cdc.gov/tb/education/corecurr/pdf/chapter2.pdf.
[33] Schmidt, C. W. (2008) Linking TB and the Environment: An Overlooked Mitigation Strategy, *Environ Health Perspect 116*, A478-485.
[34] Scordo, J. M., Knoell, D. L., and Torrelles, J. B. (2016) Alveolar epithelial cells in Mycobacterium tuberculosis infection: active players or innocent bystanders?, *J Innate Immun 8*, 3-14.
[35] Neyrolles, O. (2014) Mycobacteria and the greasy macrophage: getting fat and frustrated, *Infect Immun 82*, 472-475.
[36] Russell, D. G., Cardona, P. J., Kim, M. J., Allain, S., and Altare, F. (2009) Foamy macrophages and the progression of the human tuberculosis granuloma, *Nat Immunol 10*, 943-948.
[37] Glickman, M. S., Cox, J. S., and Jacobs Jr, W. R. (2000) A Novel Mycolic Acid Cyclopropane Synthetase Is Required for Cording, Persistence, and Virulence of Mycobacterium tuberculosis, *Molecular Cell 5*, 717-727.
[38] Brennan, P. J. (2003) Structure, function, and biogenesis of the cell wall of Mycobacterium tuberculosis, *Tuberculosis (Edinb) 83*, 91-97.
[39] Barreteau, H., Kovac, A., Boniface, A., Sova, M., Gobec, S., and Blanot, D. (2008) Cytoplasmic steps of peptidoglycan biosynthesis, *FEMS Microbiol Rev 32*, 168-207.

[40] Vollmer, W. (2008) Structural variation in the glycan strands of bacterial peptidoglycan, *FEMS Microbiol Rev 32*, 287-306.
[41] Meroueh, S. O., Bencze, K. Z., Hesek, D., Lee, M., Fisher, J. F., Stemmler, T. L., and Mobashery, S. (2006) Three-dimensional structure of the bacterial cell wall peptidoglycan, *Proc Natl Acad Sci U S A 103*, 4404-4409.
[42] Hett, E. C., and Rubin, E. J. (2008) Bacterial growth and cell division: a mycobacterial perspective, *Microbiol Mol Biol Rev 72*, 126-156, table of contents.
[43] Brennan, P. J., and Crick, D. C. (2007) The cell-wall core of Mycobacterium tuberculosis in the context of drug discovery, *Curr Top Med Chem 7*, 475-488.
[44] Cordillot, M., Dubée, V., Triboulet, S., Dubost, L., Marie, A., Hugonnet, J.-E., Arthur, M., and Mainardi, J.-L. (2013) In Vitro Cross-Linking of Mycobacterium tuberculosis Peptidoglycan by l,d-Transpeptidases and Inactivation of These Enzymes by Carbapenems, *Antimicrob Agents Chemother 57*, 5940-5945.
[45] Gupta, R., Lavollay, M., Mainardi, J. L., Arthur, M., Bishai, W. R., and Lamichhane, G. (2010) The Mycobacterium tuberculosis protein LdtMt2 is a nonclassical transpeptidase required for virulence and resistance to amoxicillin, *Nat Med 16*, 466-469.
[46] Hugonnet, J.-E., Tremblay, L. W., Boshoff, H. I., Barry, C. E., and Blanchard, J. S. (2009) Meropenem-Clavulanate Is Effective Against Extensively Drug-Resistant Mycobacterium tuberculosis, *Science 323*, 1215-1218.
[47] Typas, A., Banzhaf, M., Gross, C. A., and Vollmer, W. (2012) From the regulation of peptidoglycan synthesis to bacterial growth and morphology, *Nat Rev Microbiol 10*, 123-136.
[48] Ostash, B., and Walker, S. (2005) Bacterial transglycosylase inhibitors, *Curr Opin Chem Biol 9*, 459-466.
[49] Sauvage, E., Kerff, F., Terrak, M., Ayala, J. A., and Charlier, P. (2008) The penicillin-binding proteins: structure and role in peptidoglycan biosynthesis, *FEMS Microbiol Rev 32*, 234-258.
[50] Badet, B., Vermoote, P., and Le Goffic, F. (1988) Glucosamine synthetase from Escherichia coli: kinetic mechanism and inhibition by N3-fumaroyl-L-2, 3-diaminopropionic derivatives, *Biochemistry 27*, 2282-2287.
[51] Mengin-Lecreulx, D., and van Heijenoort, J. (1993) Identification of the glmU gene encoding N-acetylglucosamine-1-phosphate uridyltransferase in Escherichia coli, *J. Bacteriol. 175*, 6150-6157.
[52] Mengin-Lecreulx, D., and Van Heijenoort, J. (1994) Copurification of glucosamine-1-phosphate acetyltransferase and N-acetylglucosamine-1-phosphate uridyltransferase activities of Escherichia coli: characterization of the glmU gene product as a bifunctional enzyme catalyzing two subsequent steps in the pathway for UDP-N-acetylglucosamine synthesis, *J. Bacteriol. 176*, 5788-5795.
[53] Prosser, G. A., and de Carvalho, L. P. (2013) Metabolomics reveal d-alanine: d-alanine ligase as the target of d-cycloserine in Mycobacterium tuberculosis, *ACS Med. Chem. Letts. 4*, 1233-1237.
[54] Desjardins, C. A., Cohen, K. A., Munsamy, V., Abeel, T., Maharaj, K., Walker, B. J., Shea, T. P., Almeida, D. V., Manson, A. L., and Salazar, A. (2016) Genomic and functional analyses of Mycobacterium tuberculosis strains implicate ald in D-cycloserine resistance, *Nat. Genet. 48*, 544-551.
[55] Halouska, S., Fenton, R. J., Zinniel, D. K., Marshall, D. D., Barletta, R. l. G., and Powers, R. (2014) Metabolomics analysis identifies d-Alanine-d-Alanine ligase as the primary lethal target of d-Cycloserine in mycobacteria, *Journal of proteome research 13*, 1065.
[56] LeMagueres, P., Im, H., Ebalunode, J., Strych, U., Benedik, M. J., Briggs, J. M., Kohn, H., and Krause, K. L. (2005) The 1.9 Å Crystal Structure of Alanine Racemase from Mycobacterium tuberculosis Contains a Conserved Entryway into the Active Site†, *Biochemistry 44*, 1471-1481.
[57] Brennan, P. J., and Nikaido, H. (1995) The envelope of mycobacteria, *Annu Rev Biochem 64*, 29-63.

[58] Riley, L. W. (2006) Of mice, men, and elephants: Mycobacterium tuberculosis cell envelope lipids and pathogenesis, *J Clin Invest 116*, 1475-1478.
[59] Smith, J. P. (2011) Nanoparticle delivery of anti-tuberculosis chemotherapy as a potential mediator against drug-resistant tuberculosis, *Yale J. Biol. Med 84*, 361.
[60] Biarrotte-Sorin, S., Hugonnet, J.-E., Delfosse, V., Mainardi, J.-L., Gutmann, L., Arthur, M., and Mayer, C. (2006) Crystal Structure of a Novel β-Lactam-insensitive Peptidoglycan Transpeptidase, *J. Mol. Biol. 359*, 533-538.
[61] Cordillot, M., Dubée, V., Triboulet, S., Dubost, L., Marie, A., Hugonnet, J.-E., Arthur, M., and Mainardi, J.-L. (2013) In vitro cross-linking of Mycobacterium tuberculosis peptidoglycan by l, d-transpeptidases and inactivation of these enzymes by carbapenems, *Antimicrob. Agents Chemother. 57*, 5940-5945.
[62] Mainardi, J.-L., Villet, R., Bugg, T. D., Mayer, C., and Arthur, M. (2008) Evolution of peptidoglycan biosynthesis under the selective pressure of antibiotics in Gram-positive bacteria, *Fems Microbiology Reviews 32*, 386-408.
[63] Lavollay, M., Arthur, M., Fourgeaud, M., Dubost, L., Marie, A., Veziris, N., Blanot, D., Gutmann, L., and Mainardi, J.-L. (2008) The peptidoglycan of stationary-phase Mycobacterium tuberculosis predominantly contains cross-links generated by L, D-transpeptidation, *J. Bacteriol. 190*, 4360-4366.
[64] Gupta, R., Lavollay, M., Mainardi, J.-L., Arthur, M., Bishai, W. R., and Lamichhane, G. (2010) The Mycobacterium tuberculosis protein LdtMt2 is a nonclassical transpeptidase required for virulence and resistance to amoxicillin, *Nat Med 16*, 466-469.
[65] Erdemli, S. B., Gupta, R., Bishai, W. R., Lamichhane, G., Amzel, L. M., and Bianchet, M. A. (2012) Targeting the cell wall of Mycobacterium tuberculosis: structure and mechanism of L,D-transpeptidase 2, *Struct. 20*, 2103-2115.
[66] Kim, H. S., Kim, J., Im, H. N., Yoon, J. Y., An, D. R., Yoon, H. J., Kim, J. Y., Min, H. K., Kim, S.-J., and Lee, J. Y. (2013) Structural basis for the inhibition of Mycobacterium tuberculosis L, D-transpeptidase by meropenem, a drug effective against extensively drug-resistant strains, *Acta Crystallogr. Sect. D. Biol. Crystallogr. 69*, 420-431.
[67] Zhanel, G. G., Johanson, C., Embil, J. M., Noreddin, A., Gin, A., Vercaigne, L., and Hoban, D. J. (2005) Ertapenem: review of a new carbapenem, *Expert review of anti-infective therapy 3*, 23-39.
[68] Shah, P. M., and Isaacs, R. D. (2003) Ertapenem, the first of a new group of carbapenems, *J. Antimicrob. Chemother. 52*, 538-542.
[69] Fisher, J. F., Meroueh, S. O., and Mobashery, S. (2005) Bacterial resistance to beta-lactam antibiotics: compelling opportunism, compelling opportunity, *Chem Rev 105*, 395-424.
[70] Norrby, S. R. (1995) Carbapenems, *Med. Clin. North Am. 79*, 745-759.
[71] Hugonnet, J. E., and Blanchard, J. S. (2007) Irreversible inhibition of the Mycobacterium tuberculosis beta-lactamase by clavulanate, *Biochemistry 46*, 11998-12004.
[72] Zumla, A., Nahid, P., and Cole, S. T. (2013) Advances in the development of new tuberculosis drugs and treatment regimens, *Nat Rev Drug Discov 12*, 388-404.
[73] Kropp, H., Gerckens, L., Sundelof, J. G., and Kahan, F. M. (1985) Antibacterial activity of imipenem: the first thienamycin antibiotic, *Review of Infectious Diseases 7*, S389-S410.
[74] Birnbaum, J., Kahan, F. M., Kropp, H., and Macdonald, J. S. (1985) Carbapenems, a new class of beta-lactam antibiotics: Discovery and development of imipenem/cilastatin, *Am. J. Med. 78*, 3-21.
[75] Lamichhane, G., Freundlich, J. S., Ekins, S., Wickramaratne, N., Nolan, S. T., and Bishai, W. R. (2011) Essential metabolites of Mycobacterium tuberculosis and their mimics, *MBio 2*, e00301-00310.
[76] Schoonmaker, M. K., Bishai, W. R., and Lamichhane, G. (2014) Nonclassical transpeptidases of Mycobacterium tuberculosis alter cell size, morphology, the cytosolic matrix, protein localization, virulence, and resistance to β-lactams, *J. Bacteriol. 196*, 1394-1402.

[77] Silva, J. R. A., Govender, T., Maguire, G. E., Kruger, H. G., Lameira, J., Roitberg, A. E., and Alves, C. N. (2015) Simulating the inhibition reaction of Mycobacterium tuberculosis L, D-transpeptidase 2 by carbapenems, *Chem. Commun. 51*, 12560-12562.
[78] Correale, S., Ruggiero, A., Capparelli, R., Pedone, E., and Berisio, R. (2013) Structures of free and inhibited forms of the L, D-transpeptidase LdtMt1 from Mycobacterium tuberculosis, *Acta Crystallogr. Sect. D. Biol. Crystallogr. 69*, 1697-1706.
[79] Both, D., Steiner, E. M., Stadler, D., Lindqvist, Y., Schnell, R., and Schneider, G. (2013) Structure of LdtMt2, an L,D-transpeptidase from Mycobacterium tuberculosis, *Acta Crystallogr D Biol Crystallogr 69*, 432-441.
[80] Dhar, N., Dubée, V., Ballell, L., Cuinet, G., Hugonnet, J.-E., Signorino-Gelo, F., Barros, D., Arthur, M., and McKinney, J. D. (2015) Rapid cytolysis of Mycobacterium tuberculosis by faropenem, an orally bioavailable β-lactam antibiotic, *Antimicrob. Agents Chemother. 59*, 1308-1319.
[81] Silva, J. R. r. A., Roitberg, A. E., and Alves, C. u. N. (2014) Catalytic mechanism of L, D-transpeptidase 2 from Mycobacterium tuberculosis described by a computational approach: insights for the design of new antibiotics drugs, *J. Chem. Inf. Mod. 54*, 2402-2410.
[82] Schoonmaker, M. K., Bishai, W. R., and Lamichhane, G. (2014) Nonclassical transpeptidases of Mycobacterium tuberculosis alter cell size, morphology, the cytosolic matrix, protein localization, virulence, and resistance to beta-lactams, *J Bacteriol 196*, 1394-1402.
[83] Fakhar, Z., Govender, T., Maguire, G. E. M., Lamichhane, G., Walker, R. C., Kruger, H. G., and Honarparvar, B. (2017) Differential flap dynamics in l,d-transpeptidase2 from mycobacterium tuberculosis revealed by molecular dynamics, *Molecular BioSystems 13*, 1223-1234.
[84] Silva, J. R. A., Bishai, W. R., Govender, T., Lamichhane, G., Maguire, G. E., Kruger, H. G., Lameira, J., and Alves, C. N. (2016) Targeting the cell wall of Mycobacterium tuberculosis: a molecular modeling investigation of the interaction of imipenem and meropenem with L, D-transpeptidase 2, *J. Biomol. Struct. Dyn. 34*, 304-317.
[85] Fakhar, Z., Govender, T., Maguire, G. E., Lamichhane, G., Walker, R. C., Kruger, H. G., and Honarparvar, B. (2017) Differential flap dynamics in l, d-transpeptidase2 from mycobacterium tuberculosis revealed by molecular dynamics, *Molecular BioSystems*.
[86] Morokuma, K. (2009) Theoretical studies of structure, function and reactivity of molecules— A personal account, *Proc Jpn Acad Ser B Phys Biol Sci 85*, 167-182.
[87] Dapprich, S., Komáromi, I., Byun, K. S., Morokuma, K., and Frisch, M. J. (1999) A new ONIOM implementation in Gaussian98. Part I. The calculation of energies, gradients, vibrational frequencies and electric field derivatives, *Comput. Theor. Chem. 461*, 1-21.
[88] Morokuma, K. (2002) New challenges in quantum chemistry: quests for accurate calculations for large molecular systems, *Philosophical Transactions of the Royal Society of London A: Mathematical, Physical and Engineering Sciences 360*, 1149-1164.
[89] Vreven, T., Byun, K. S., Komaromi, I., Dapprich, S., Montgomery, J. A., Morokuma, K., and Frisch, M. J. (2006) Combining Quantum Mechanics Methods with Molecular Mechanics Methods in ONIOM, *J Chem Theory Comput 2*, 815-826.
[90] Schreiner, P. R. (2007) Relative Energy Computations with Approximate Density Functional Theory—A Caveat!, *Angew. Chem. Int. Ed. 46*, 4217-4219.
[91] Born, M. (1924) Über Quantenmechanik, *Zeitschrift für Physik 26*, 379-395.
[92] Frank, J. (1999) Introduction to computational chemistry, *Editorial Offices October*.
[93] Honarparvar, B., Govender, T., Maguire, G. E., Soliman, M. E., and Kruger, H. G. (2013) Integrated approach to structure-based enzymatic drug design: molecular modeling, spectroscopy, and experimental bioactivity, *Chem. Rev. 114*, 493-537.
[94] Hohenberg, P., and Kohn, W. (1964) Inhomogeneous electron gas, *Phys. Rev. 136*, B864.
[95] Kohn, W., and Sham, L. J. (1965) Self-consistent equations including exchange and correlation effects, *Phys. Rev. 140*, A1133.
[96] Jones, R. O., and Gunnarsson, O. (1989) The density functional formalism, its applications and prospects, *Reviews of Modern Physics 61*, 689.

[97] Becke, A. D. (1993) Density-functional thermochemistry. III. The role of exact exchange, *J. Chem. Phys. 98*, 5648-5652.
[98] Lee, C., Yang, W., and Parr, R. G. (1988) Development of the Colle-Salvetti correlation-energy formula into a functional of the electron density, *Physical review B 37*, 785.
[99] Osuna, S., Morera, J., Cases, M., Morokuma, K., and Sola, M. (2009) Diels− Alder reaction between cyclopentadiene and C60: An analysis of the performance of the ONIOM method for the study of chemical reactivity in fullerenes and nanotubes, *J. Phys. Chem. A 113*, 9721-9726.
[100] Foresman, J., and Frish, E. (1996) Exploring chemistry, *Gaussian Inc., Pittsburg, USA*.
[101] Bultinck, P., De Winter, H., Langenaeker, W., and Tollenare, J. P. (2003) *Computational medicinal chemistry for drug discovery*, CRC Press.
[102] Allinger, N. L. (2010) *Molecular structure: understanding steric and electronic effects from molecular mechanics*, John Wiley & Sons.
[103] Halgren, T. A. (1996) Merck molecular force field. I. Basis, form, scope, parameterization, and performance of MMFF94, *J. Comput. Chem. 17*, 490-519.
[104] Case, D. A., Cheatham, T. E., Darden, T., Gohlke, H., Luo, R., Merz, K. M., Onufriev, A., Simmerling, C., Wang, B., and Woods, R. J. (2005) The Amber biomolecular simulation programs, *J. Comput. Chem. 26*, 1668-1688.
[105] Cornell, W. D., Cieplak, P., Bayly, C. I., Gould, I. R., Merz, K. M., Ferguson, D. M., Spellmeyer, D. C., Fox, T., Caldwell, J. W., and Kollman, P. A. (1995) A second generation force field for the simulation of proteins, nucleic acids, and organic molecules, *J. Am. Chem. Soc. 117*, 5179-5197.
[106] Rappé, A. K., Casewit, C. J., Colwell, K., Goddard Iii, W., and Skiff, W. (1992) UFF, a full periodic table force field for molecular mechanics and molecular dynamics simulations, *J. Am. Chem. Soc. 114*, 10024-10035.
[107] Rogers, D. W. (2003) *Computational chemistry using the PC*, John Wiley & Sons.
[108] Vreven, T., and Morokuma, K. (2000) On the application of the IMOMO (integrated molecular orbital+ molecular orbital) method, *J. Comput. Chem. 21*, 1419-1432.
[109] Vreven, T., Byun, K. S., Komáromi, I., Dapprich, S., Montgomery, J. A., Morokuma, K., and Frisch, M. J. (2006) Combining quantum mechanics methods with molecular mechanics methods in ONIOM, *J. Chem. Theo. Comp. 2*, 815-826.
[110] Vreven, T., Morokuma, K., Farkas, Ö., Schlegel, H. B., and Frisch, M. J. (2003) Geometry optimization with QM/MM, ONIOM, and other combined methods. I. Microiterations and constraints, *J. Comput. Chem. 24*, 760-769.
[111] Dennington, R., Keith, T., and Millam, J. (2009) Semichem Inc, *Shawnee Mission KS, GaussView, Version 5*.
[112] Frisch, M., Trucks, G., Schlegel, H., Scuseria, G., Robb, M., Cheeseman, J., Scalmani, G., Barone, V., Mennucci, B., and Petersson, G. (2009) Gaussian 2009, *See Supporting Information f or full citation*.

# CHAPTER TWO

## ONIOM study of the binding interaction energies for the carbapenems complexed with L, D-Transpeptidase 2 from *Mycobacterium tuberculosis*

**Thandokuhle Ntombela, [a] Zeynab Fakhar, [b] Collins U. Ibeji, [a] Thavendran Govender, [a] Glenn E. M. Maguire, [a, c] Gyanu Lamichhane, [d] Hendrik G. Kruger[a*] and Bahareh Honarparvar[a*]**

[a]Catalysis and Peptide Research Unit, School of Health Sciences, University of KwaZulu-Natal, Durban 4001, South Africa.

[b]Department of Chemistry, Faculty of Natural and Agricultural Sciences, University of Pretoria, Lynnwood Road, Hatfield 0002, Pretoria, South Africa.

[c]School of Chemistry and Physics, University of KwaZulu-Natal, 4001 Durban, South Africa.

[d]Center for Tuberculosis Research, Division of Infectious Diseases, School of Medicine, Johns Hopkins University, Baltimore, MD 21205, USA.

***Corresponding authors:** Honarparvar@ukzn.ac.za (Dr Bahareh Honarparvar), (Prof. Hendrik G. Kruger) kruger@ukzn.ac.za, Telephone: + 27 31 2601845, Fax: +27 31 2603091, Catalysis and Peptide Research Unit, School of Health Sciences, University of KwaZulu-Natal, Durban 4041, South Africa.

## Abstract

Tuberculosis remains a dreadful disease that has claimed many human lives worldwide. Elimination of the causative agent *mycobacterium tuberculosis* remains elusive. Multidrug-resistant TB is rapidly increasing worldwide; therefore, there is an urgent need for improving the current antibiotics and novel drug targets to successfully curb the TB burden. L, D-transpeptidase 2 is an essential protein in *Mtb* that is responsible for virulence and growth during the chronic stage of the disease. Both D, D- and L, D-transpeptidases need to be inhibited concurrently to eradicate the bacterium. It was recently discovered that classic penicillins only inhibit D, D-transpeptidases, while L, D transpeptidases are blocked by carbapenems. This has contributed to drug resistance and persistence of tuberculosis. Herein, a hybrid two-layered ONIOM (B3LYP/6-31G+(d):AMBER) model was used to extensively investigate the binding interactions of $Ldt_{Mt2}$ complexed with four carbapenems (biapenem, imipenem, meropenem, and tebipenem) to ascertain molecular insight of the drug-enzyme complexation event. In the studied complexes, the carbapenems together with catalytic triad active site residues of $Ldt_{Mt2}$ (His187, Ser188 and Cys205) were treated at with QM [B3LYP/6-31+G(d)], while the remaining part of the complexes were treated at MM level (AMBER force field). The resulting Gibbs free energy (ΔG), enthalpy (ΔH) and entropy (ΔS) for all complexes showed that the carbapenems exhibit reasonable binding interactions towards $Ldt_{Mt2.}$

Increasing the number of amino acid residues that form hydrogen bond interactions in the QM layer showed significant impact in binding interaction energy differences and the binding stabilities of the carbapenems inside the active pocket of $Ldt_{Mt2}$. The theoretical binding free energies obtained in this study reflect the same trend of the experimental results. The electrostatic, hydrogen bond and Van der Waals interactions between the carbapenems and $Ldt_{Mt2}$ were also assessed. To further examine the nature of intermolecular interactions for carbapenem-$Ldt_{Mt2}$ complexes, AIM and NBO analysis were performed for the QM region (carbapenems and the active residues of $Ldt_{Mt2}$) of the complexes. These analyses revealed that the hydrogen bond interactions and charge transfer from the bonding to anti-bonding orbitals enhances the binding and stability of carbapenem-$Ldt_{Mt2}$ complexes.

**Keywords:** Tuberculosis (TB); Mycobacterium tuberculosis *(Mtb)*; L, D-transpeptidase 2 ($Ldt_{Mt2}$); Carbapenems; Our Own N-layered Integrated Molecular Orbital and Molecular Mechanics (ONIOM); Quantum theory of atoms in molecules (QTAIM); Natural bond orbital (NBO).

## 1.0 Introduction

Tuberculosis is an infectious disease caused by *mycobacterium tuberculosis* bacilli that threatens many lives worldwide. Despite the advanced efforts made to improve TB treatment, the eradication of the disease is still an enormous challenge. Recent statistics from the World Health Organisation (WHO) reveal that about 10.4 million new TB cases were reported in 2016[1]. The growing incidences of multi-drug resistant (MDR-TB) and extensively drug-resistant (XDR-TB) strains of *mycobacterium tuberculosis* complicates the treatment regimens currently available thus threatening a return to a pre-antibiotic era[2, 3].

The upsurge of resistance to currently available anti-TB therapeutics leads to rapid dissemination of the infection. In South Africa, the incident cases of MDR and XDR continue to be a leading burden to public health care, as the disease remains the foremost cause of death[4]. For HIV patients, South Africa has the highest TB burden amongst 22 Sub-Saharan countries and has the highest figures of HIV-infected people suffering from TB, which contributes to high incidence cases of multi-drug resistant tuberculosis[5]. In the light of this fact, development of novel anti-tubercular therapeutic agents is urgently required[6].

The peptidoglycan moiety of *Mtb* involves 4→3 and 3→3 peptide cross-links facilitated by D, D-transpeptidase and L, D-transpeptidase (LDT) enzymes, respectively. Disruption of

peptidoglycan biosynthesis and cross-linking requires complete inhibition of both transpeptidases which subsequently kills the bacteria[6, 7]. Most bacterial species possess approximately less than 10% of 3→3 cross-linkages catalysed by LDTs during the exponential and stationary phase of growth. *Mtb* is the only known *mycobacterium* that demonstrates a high content of 3→3 crosslinks (80%) making this enzyme family an attractive target[8-10].

Carbapenems are a well-known class of *β*-lactam antimicrobial agents with reported inhibitory properties against different transpeptidases[8, 11, 12]. In particular, carbapenem derivatives are known as effective compounds against L, D-transpeptidase 2 from *mycobacterium tuberculosis*[8, 9]. This enzyme has thus been identified by various researchers as a possible target for TB inhibition[9, 10, 13-17]. Erdemli *et al*.,[9] established that L, D-transpeptidase 2 ($Ldt_{Mt2}$), is the product of gene MT2594 in *Mtb*. A *Mtb* strain lacking $Ldt_{Mt2}$ leads to alteration of colony morphology, loss of virulence and enhanced susceptibility to amoxicillin–clavulanate during the chronic phase of infection. Therefore, $Ldt_{Mt2}$ is vital for the physiology of the peptidoglycan and is essential for the virulence of *Mtb*[6, 9, 18]. Catalysis occurs at the active site (residues Cys354, His336, and Ser337) of $Ldt_{Mt2}$ and involves two reaction steps namely, acylation and deacylation[9]. In this proposed mechanism, a proton (R-SH) transfer occurs from Cys354 to the His336 followed by a nucleophilic attack ($R\text{-}S^-$) on the carbonyl group of the substrate by the sulfur of Cys354. However, the presence of His352 and Asn356 residues provides the possibility of hydrogen bond formation and hydrophobic interactions which can stabilize the enzyme-inhibitor complex. The carbapenems' thio-side chain can also be potentially tailored to accommodate the protein surface and to optimize inhibition of $Ldt_{Mt2}$. In addition, earlier experimental observations reconfirmed that the thio-side chain of the carbapenem derivatives fulfils an important role to optimize the inhibitor efficiency by forming critical hydrogen bonds inside the active site pocket[18].

Besides several publications in the field of computer-aided drug discovery for the potential anti-HIV agents made by our research group[19-21], the theoretical binding free energies of the commercially available inhibitors against $Ldt_{Mt2}$ were also reported using MM-GBSA and solvation interaction energy (SIE) methods[22]. The role of $Ldt_{Mt2}$ flap opening and closing upon complexation of the substrate and three carbapenems, namely: ertapenem, imipenem and meropenem, was also reported using 140 ns molecular dynamics simulation with explicit water solvent[23]. The determined binding affinities showed more favorable free binding energies for ertapenem and meropenem than imipenem in the closed conformation of the *β*-hairpin flap[23].

Despite several studies in this field, to the best of our knowledge, limited attention has been paid to the inhibition mechanism of $Ldt_{Mt2}$ using carbapenem derivatives.

The n-layered integrated molecular orbital and molecular mechanics (ONIOM)[24-28] method is a hybrid QM/MM technique used to compute interaction energies using the combination of quantum mechanical method (QM) with a molecular mechanics (MM) force field[29, 30]. This multi-layered method is utilized mostly in large biosystems where the model and real system are consistently treated with accurate level of theories[24-28]. In this approach, the active residues and ligand are treated with a high level of theory (Density Functional Theory or *ab initio*) while the remaining part of the system is treated at a lower level (AMBER force field)[31-34].

In this study, the molecular orbital calculations were performed for four selected FDA-approved carbapenems (biapenem, imipenem, meropenem, and tebipenem) complexed to $Ldt_{Mt2}$ using a two-layer ONIOM (QM:MM) approach. Structures of the carbapenems for the present work are presented in **Figure 1**.

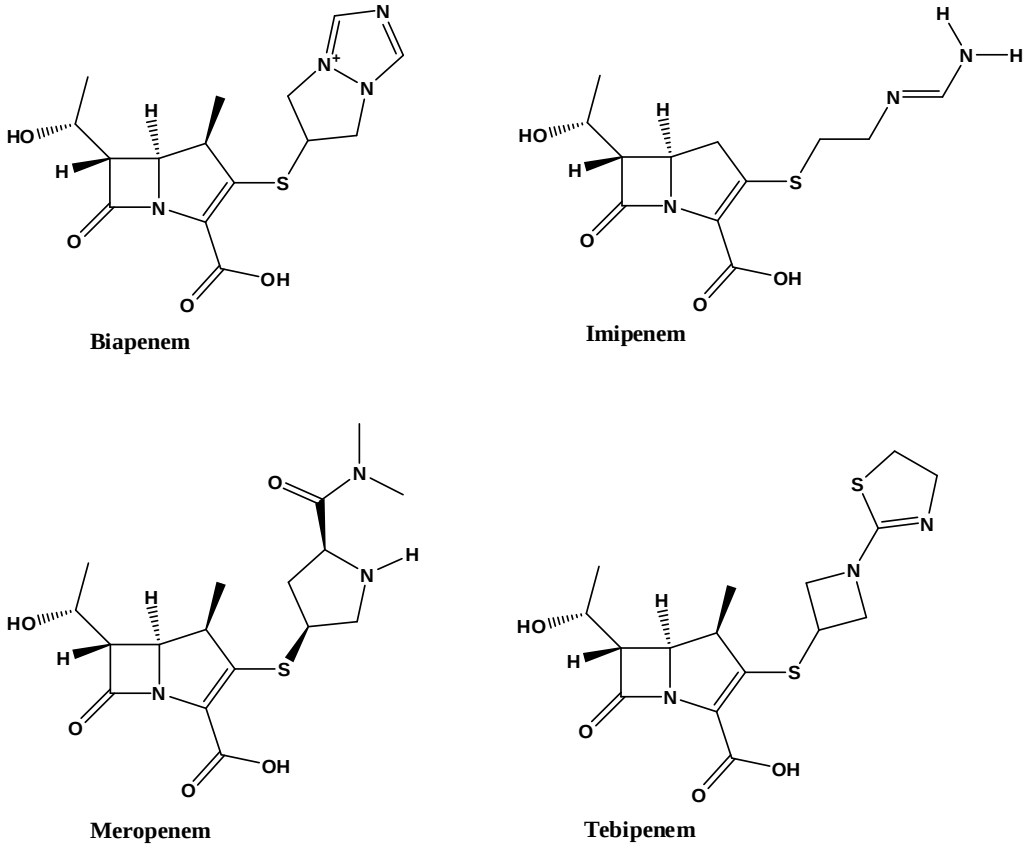


**Figure 1.** The structures of the selected FDA approved carbapenems that are active against L, D transpeptidase 2.

For further analysis of the calculated ONIOM binding free energies, we investigated the electrostatic and hydrogen bonding interactions for these inhibitor-enzyme complexes. For further analysis of the intermolecular interactions between $Ldt_{Mt2}$ and the selected carbapenems, QTAIM[35] and NBO[36] analysis were performed on the QM region of the biosystems (carbapenems and the active residues of $Ldt_{Mt2}$). The AIM topological indices assessed the nature of hydrogen bond interactions through molecular orbital interactions and NBO analysis determined the electron charge transfer between carbapenems and the active residues of $Ldt_{Mt2.}$ Our hypothesis is that this computational study will provide a greater level of insight into the crucial interactions of the inhibitor during complexation. This in turn, will be useful for the design of novel and more potent anti-TB drugs from carbapenem inhibitors.

## 2.0 Material and Methods

### 2.1 System preparation

The enzyme-inhibitor complex structures of *M.tb* $Ldt_{Mt2}$ were prepared by superimposing Chain A of 3TUR[9] complexed with the natural substrate and 3VYP[37] meropenem-bound complex. The covalently bound meropenem from 3VYP was restored by deletion of the covalent bond between the sulfur atom of cysteine residue and the carbonyl carbon of $\beta$-lactam ring. The $\beta$-lactam ring was restored, and the hydrogen atoms were added and optimized. This complexed structure was then used as a reference to model other complexes by superimposing other inhibitors into the same geometry using PyMOL[38].

A molecular dynamics (MD) calculation was performed on the starting complex to affix the missing protons using X-leap[39] software. The MD simulations were carried out using Amber 14 with the ff99SB[40] force field (for proteins) and GAFF[41] for the inhibitors. The complexes were solvated with TIP3P[42] explicit water in a cubic box with 10 Å distance and counterions were added to neutralize the complexes. Partial Mesh Ewald (PME)[43] method was applied for long range electrostatic forces with cut-off of 12 Å. All bonds to hydrogen atoms was constrained using the SHAKE algorithm.[44] Two-stage geometric minimization was performed by 2500 steps of steepest decent minimization followed by 2500 of conjugated gradient to remove clashes and bad contacts. To accurately assign the protonation states of the residues in the enzyme at pH=7.8, the empirical PropKa web server[45] was used.

The prepared complexes were then subjected for ONIOM[24-28] calculations. The ONIOM input files together with the optimized output files of all complexes are provided in PDB format with the supplementary materials.

### 2.2 ONIOM hybrid (QM:MM) method

All the calculations were performed using the Gaussian09[46] program. It was established in numerous studies[47-49] that the Becke3LYP[51, 52] functional yields energies in good agreement with high-level *ab initio* methods. The two-layered ONIOM[24, 25, 50] hybrid approach (B3LYP/6-31+G (d): AMBER) invented by Morokuma *et al.*,[29] was employed to assess the binding affinities within the selected carbapenem-$Ldt_{Mt2}$ complexes. In this ONIOM[24-28] model, the catalytic active residues of the $Ldt_{Mt2}$ enzyme (His187, Ser188 and Cys205) and the selected FDA-approved inhibitors were modeled using density functional theory (DFT)[51, 52], B3LYP[53, 54] functional and the 6-31+G(d)[55, 56] basis set. The remaining part of the enzyme was kept at the low level of theory (MM)[26, 57] with an AMBER force field.

A full geometry optimization was performed for the selected carbapenem-$Ldt_{Mt2}$ complexes. Normal mode frequency analyses were performed at the same level of theory to examine the nature of stationary points to be in real minimum potential energy surface with no negative frequency. The total interaction energies are defined as:

$$\Delta E_{ONIOM} = \Delta E_{model,high} + \Delta E_{real,low} - \Delta E_{model,low} \qquad (\mathbf{1})$$

Where, $\Delta E_{\text{model}}$ denote the energies of the model system defined at high and low level of theory and $\Delta E_{\text{real}}$ denote the whole (real) system. Thus, the equivalent binding interaction ONIOM energies of the complex systems are determined as follows:

$$\Delta G_{ONIOM} \approx \Delta G = G_{carbapenem-\text{LdtMt2}} - (G_{\text{carbapenem}} + G_{\text{LdtMt2}}) \qquad (\mathbf{2})$$

The thermodynamic quantities (enthalpies and entropies and it different entropic contributions) were also attained from frequency calculations. The different entropic contributions (rotation, translation, and vibration) for carbapenem-$Ldt_{Mt2}$ complexes were calculated as follows:

$$\Delta S_{total} = \Delta S_{carbapenem-\text{LdtMt2}} - (\Delta S_{carbapenems} + \Delta S_{\text{LdtMt2}}) \qquad (\mathbf{3})$$

### 2.3 Mode of interactions and hydrogen-bond analysis

The LigPlot[58] program generated the 2-D representation of protein-ligand complexes from the output file of the PDB input file. This program gives an informative representation of

intermolecular interactions (hydrogen bond and hydrophobic interactions) that exist between the protein and the ligand. The hydrogen bonds[59-61] and hydrophobic interactions for eight selected carbapenem-$Ldt_{Mt2}$ complexes were analysed using LigPlot[58]. The hydrogen bond distances between the carbapenems and $Ldt_{Mt2}$ in the complexes were determined using Discovery Studio[62] to attain the proximity of cysteine towards the $\beta$-lactam's carbonyl group. This is essential for determining the binding mode of carbapenems interacting with $Ldt_{Mt2}$ and to provide the best inhibitor pose relative to the catalytic residues.

### 2.4 QTAIM calculations

The quantum theory of atoms in molecules (QTAIM) invented by Bader[63] is a theoretical tool that enables hydrogen bond analysis. The hydrogen bonds (HB) between a hydrogen donor and acceptor groups are connected by a Bond Critical Point (BCP). The basis of the theory is fundamentally reliant on the critical points (CPs) of the molecular electronic charge density $\rho$(r). The critical points are described by three eigenvalues of Hessian matrix ($\lambda_1$, $\lambda_2$, and $\lambda_3$) based on the molecular electronic charge densities. Popelier and Bader[64] used the AIM analysis to characterize the significance of chemical interactions that strictly involves the hydrogen bonding between clustered systems[64]. The two measures are proposed, electron density $\rho$(r) and the Laplacian of the electron density $\nabla^2 \rho$(r), assessed at the BCP of two hydrogen bonded atoms. The location of BCP strongly relies on the electronegativities of the interacting atoms in molecules. Another important parameter is the bond ellipticity ($\varepsilon$), defined as follows:

$$\varepsilon = \left[\left(\frac{\lambda_1}{\lambda_2}\right) - 1\right] \qquad (\mathbf{4})$$

Where $\lambda_1$ and $\lambda_2$ are perpendicular curvatures of the density at the BCP described by the large values of electron density. The ellipticity provides a significant measure of $\pi$-bond nature and delocalization of the electronic charge and determines the bond stability.

### 2.5 Natural bond orbital (NBO)

The natural bond orbital (NBO) analysis[36] is an appropriate method used to study the effect of electron charge transfer between QM region of $Ldt_{Mt2}$ and carbapenems using the second perturbation theory of NBO analysis using NBO3.1 program implemented in Gaussian 09 software[46]. The NBO analysis was achieved based on the molecular wave functions distorted into one-centre (lone pair) and two centres (bond) representations. The Fock matrix diagonal elements in the NBO depiction represent the energies for localized bonds, lone pairs, and anti-

bonds of the studied systems. The stabilization energy $E^{(2)}$ associated with $i \rightarrow j$ delocalization is explicitly estimated by the following equation:

$$E^{(2)} = \Delta Eij = qi\frac{F(i,j)^2}{\varepsilon_j - \varepsilon_i} \quad \textbf{(5)}$$

Where $q_i$ denotes the $i$th donor orbital occupancy, $\varepsilon_i$, and $\varepsilon_j$ are the diagonal elements (orbital energies) and $F(i, j)$ is the off-diagonal element, respectively, associated with the NBO Fock matrix. The higher the value of $E^{(2)}$, the more charge transfer between electron donors and electron acceptors[36].

## 3.0 Results and Discussion

During geometry optimization it was observed that the two carbapenems experienced slight movement inside the binding site of $Ldt_{Mt2}$ (**Figure 2**) as expected[22]. The short-range distances between the sulfur atom of the catalytic cysteine residue and the carbonyl carbon of the $\beta$-lactam ring of the carbapenem were in the range of 3.550 Å to 3.942 Å.

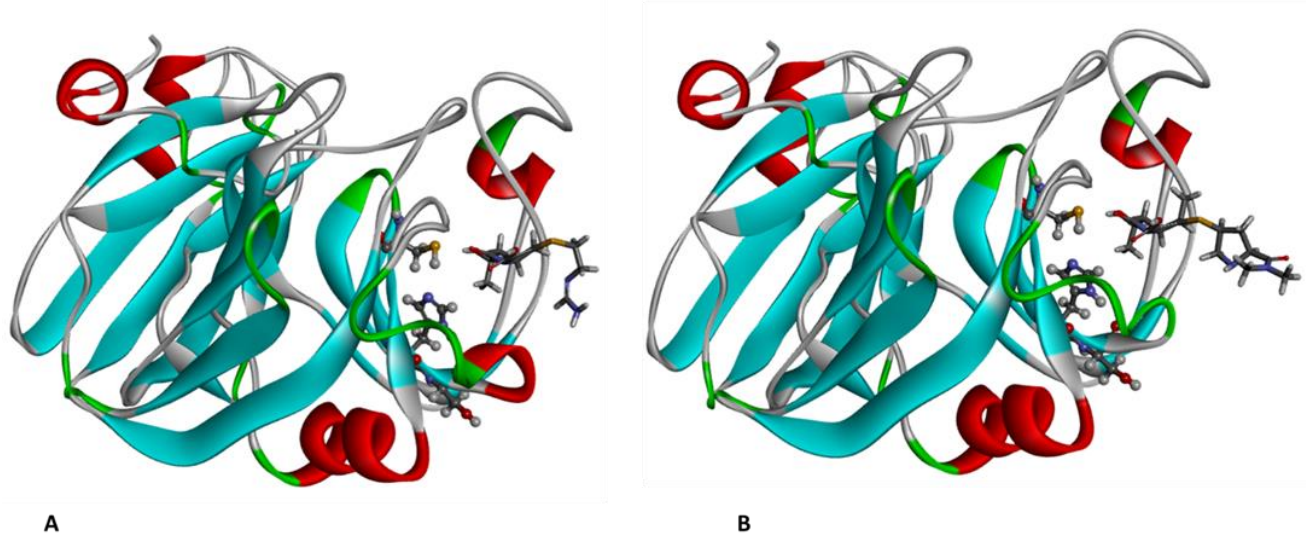


**Figure 2.** 3D-structure of **A**. Imi—$Ldt_{Mt2}$ and **B**. Mero—$Ldt_{Mt2}$ complexes, the inhibitor is presented as wireframe and the considered active pocket residues as ball and stick (**Figure 3S**). The ONIOM (Gaussian) input files as well as the optimized output files of all inhibitor—enzyme complexes are also provided with the supplementary material.

The superimposed 3D structures of 3TUR ($Ldt_{Mt2}$ in complex with peptidoglycan fragment as natural substrate) and 3VYP (meropenem—$Ldt_{Mt2}$ adduct), as well as other superimposed complexes are presented in **Figures 1S** and **2S** (Supplementary material).

**ONIOM interaction energies**

A descriptive illustration of our ONIOM model is shown in **Figure 3**, where the carbapenems and the catalytic residues of $Ldt_{Mt2}$ were treated at QM (B3LYP/6-31+G(d)) level and the remaining part of the complexes was treated at MM level (AMBER force field).

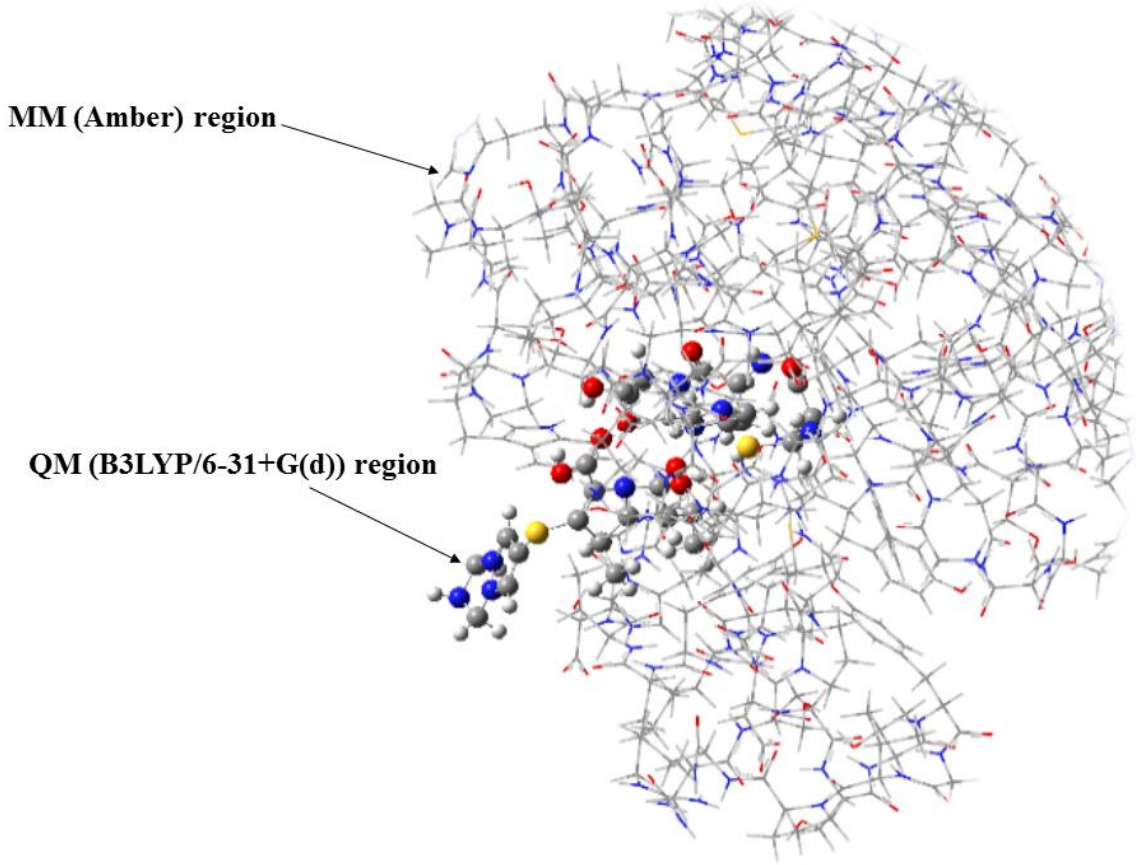


**Figure 3.** A two-layered QM:MM ONIOM (B3LYP/6-31G+(d): AMBER) model of Bia-$Ldt_{Mt2}$ complex. Active site residues His187, Ser188 and Cys205 were also treated at the same QM level. The ONIOM (Gaussian) input files as well as the optimized output files of all inhibitor-enzyme complexes are also provided with the supplementary material (**Figure 4S**).

To assess the binding affinities of the selected carbapenems against $Ldt_{Mt2}$ using the ONIOM method, we included the three catalytic triad residues (Cys205, His187, Ser188) of $Ldt_{Mt2}$ and carbapenems at QM level of theory (**Table 1**). After that, two more residues (His203 and Asn207), found to be in close contact with the carbapenems, were also included at the QM level (**Table 1S**) to ascertain the fundamental role they have in thermodynamic properties.

As for the comparison of our two applied ONIOM models, the first model with three active site residues (His187, Ser188 and Cys205) treated at the QM level of theory exhibited less negative theoretical binding free energies (**Table 1**) in comparison to the second model with five active site residues (His187, Ser188, His203, Cys205 and Asn207) **(Table 1S)**.

The fist model followed the experimental trend, while the second model, with five catalytic residues at the QM level, the binding energy trend for tebipenem and imipenem was reversed **(Table 1S)**.

The selected carbapenems possess a common thiol-group with varying side chains that distinguish them from each other. The side chains are said to play an integral role in stabilizing the complex by forming electrostatic and van der Waals interactions during the binding process.

**Table 1**. The binding free energies (kcal mol$^{-1}$) for FDA-approved carbapenem-Ldt$_{Mt2}$ complexes evaluated using ONIOM (B3LYP/6-31+G (d): AMBER). [reported experimental data[9, 65] and calculated theoretical results]

| **Complexes** | **$\Delta G_{bind}$(Exp)** | **$\Delta G_{bind}$(Calc)** | **$\Delta H$** | **$\Delta S_{Total}$** | **$\Delta S_{trans}$** | **$\Delta S_{rot}$** | **$\Delta S_{vib}$** |
|---|---|---|---|---|---|---|---|
| | **kcal mol$^{-1}$** | **kcal mol$^{-1}$** | **kcal mol$^{-1}$** | **cal mol$^{-1}$ K$^{-1}$** | **cal mol$^{-1}$ K$^{-1}$** | **cal mol$^{-1}$ K$^{-1}$** | **cal mol$^{-1}$ K$^{-1}$** |
| **Imi-Ldt$_{Mt2}$** | -9.82 | -23.88 | -43.58 | -66.08 | -42.95 | -34.78 | 11.65 |
| **Tebi-Ldt$_{Mt2}$** | -9.35 | -23.80 | -42.49 | -62.67 | -43.68 | -36.25 | 17.26 |
| **Bia-Ldt$_{Mt2}$** | -8.96 | -23.18 | -44.06 | -70.03 | -43.43 | -35.48 | 8.88 |
| **Mero-Ldt$_{Mt2}$** | -8.16 | -14.89 | -41.86 | -91.64 | -43.68 | -35.99 | -11.97 |

Gibb's free energy (**$\Delta G$**), Enthalpies (**$\Delta H$**), Entropies **($\Delta S$**) and entropic contribution, translational (**$\Delta S_{trans}$**), rotational (**$\Delta S_{rot}$**), vibrational **($\Delta S_{vib}$**) are derived from equations 2 and 3. The ONIOM (Gaussian) input files as well as the optimized output files of all inhibitor—enzyme complexes are also provided with the supplementary material.

Our group previously reported a longer MD (140 ns) simulation study that aimed to investigate the role of flap dynamics during the binding process of the natural substrate as well as three carbapenems[23]. Their results for the carbapenem-Ldt$_{Mt2}$ complexes, namely; Mero-Ldt$_{Mt2}$ , Erta-Ldt$_{Mt2}$, and Imi-Ldt$_{Mt2}$ gave binding free energies ($\Delta G_{bind}$) of; -40.42 kcal mol$^{-1}$, -37.91 kcal mol$^{-1}$ and -34.47 kcal mol$^{-1}$, respectively[23]. In contrast to that, the experimental binding energy trend for Mero-Ldt$_{Mt2}$ and Imi-Ldt$_{Mt2}$ is reversed (there is no reported value for ertapenem). Therefore, to further improve the model for these inhibitor-enzyme complexes, a hybrid two layered ONIOM approach was chosen to explore the non-covalent binding interaction energies as another method to investigate the pre-complex stability prior to carbapenems binding.

It was noted that for Imi-Ldt$_{Mt2}$ and Mero-Ldt$_{Mt2}$ complexes, the theoretical order of Gibb's binding free energies varied to that of our previous study[23]. The theoretical Gibb's free energies ($\Delta G$) for carbapems-Ldt$_{Mt2}$ complexes range from -23.88 to -14.89 kcal mol$^{-1}$. However, Imi-

$Ldt_{Mt2,}$ Tebi-$Ldt_{Mt2}$ and Bia-$Ldt_{Mt2}$ have comparable Gibb's free energies $\Delta G$ (-23.88 kcal $mol^{-1}$, -23.80 kcal $mol^{-1}$ and -23.18 kcal $mol^{-1}$, respectively) with a discrepancy of 0.08─0.7 kcal $mol^{-1}$ and the relative energy differences are in good agreement with experimental data (**Table 1**). Even though Mero-$Ldt_{Mt2}$ complex shows the lowest binding energy for both experimental and theoretical results, the calculated theoretical results display larger relative differences compared to the experimental results.

The enthalpy contribution ($\Delta H$) for carbapenem-$Ldt_{Mt2}$ complexes ranges from -44.06 to -41.86 kcal $mol^{-1}$. This indicates that the non-covalent complexation process is exothermic. The enthalpy contribution ($\Delta H$) of Bia-$Ldt_{Mt2}$ and Imi-$Ldt_{Mt2}$ complexes is -44.06 kcal $mol^{-1}$ and -43.58 kcal $mol^{-1}$ respectively and are comparable. Moreover, the enthalpy contribution ($\Delta H$) for all complexes are slightly similar (**Table 1)**. Finally, the Mero-$Ldt_{Mt2}$ complex has the weakest enthalpy contribution of $\Delta H$= -41.86 kcal $mol^{-1}$, which contributes to the weak calculated binding free energy ($\Delta G$ = -14.89 kcal $mol^{-1}$).

In the case of entropy contribution ($\Delta$S), it was noted that Mero-$Ldt_{Mt2}$ shows the most negative entropy $\Delta S$ = -91.64 cal $mol^{-1}$ $K^{-1}$. The higher entropy signifies reduced degrees of freedom of the inhibitors in the protein active pocket. This contributes to the less favourable binding free energy for meropenem. Bia-$Ldt_{Mt2}$ exhibits a negative entropy of $\Delta S$ = -70.03 cal $mol^{-1}$ $K^{-1}$, while that of Imi-$Ldt_{Mt2}$ is -66.08 cal $mol^{-1}$ $K^{-1}$ and Tebi-$Ldt_{Mt2}$, with the most favourable entropy response at -62.67 cal $mol^{-1}$ $K^{-1}$. This overcomes its smaller enthalpy value rendering it the second highest in Gibb's binding energy. Additionally, among the entropy components, the translational ($\Delta S_{trans}$) and rotational ($\Delta S_{rot}$) values for all considered complexes are in close range, while the vibrational entropies ($\Delta S_{vib}$) differs significantly in all complexes and this could be attributed to the thio-side chain of each considered carbapenem. Mero-$Ldt_{Mt2}$ is the only complex that displays a negative vibrational entropy with contributes significantly to the overall entropy value.

**Hydrogen bonding interactions**

The fundamental role of hydrogen bonds in target-drug affinities has been significantly explored[59, 66, 67]. Moreover, protein conformation is driven by hydrogen bond formation, which thus optimizes hydrophobic interactions and leads to increased binding affinities of complex molecules[59]. The van der Waals and electrostatic interactions in complexes are crucial for maintaining stability between protein-ligand arrays. Hydrogen bond interactions serve a

significant role in stabilizing the inhibitor inside the binding pocket although these are considered as weak interactions[68]. Structural analyses of the carbapenems show significant interactions with $Ldt_{Mt2}$ amino acids (His203, Asn207, Ser202, Cys205, Thr201, His187, Thr171, Trp191, Ser192, and Tyr169) in the catalytic cavity. In most cases, the hydroxyethyl substituent, carbonyl oxygen, and nitrogen of the carbapenem $\beta$-lactam ring are responsible for hydrogen bond formation. In order to obtain more details and understanding of these interactions, the distances of hydrogen bonds between ligands and receptors were analysed with Discovery studio[62] before and after optimization (**Figure 4**). The measured intermolecular bond distances, for all the selected carbapenem-$Ldt_{Mt2}$ complexes, between the sulfur atom of the catalytic cysteine and carbonyl carbon of the $\beta$-lactam ring were adequately in proximity for nucleophilic attack as expected. It was observed that in all complexes, the average bond distance between the sulfur atom of cysteine and carbonyl carbon of the $\beta$-lactam ring had increased (after optimization) with a concomitant decrease in the distance from the hydroxyl hydrogen to the sulfur. As a result, the carbonyl oxygen also participated in forming hydrogen bonds with the His203 and Asn207. (See details shown in supplementary material **Figure 5S**.)

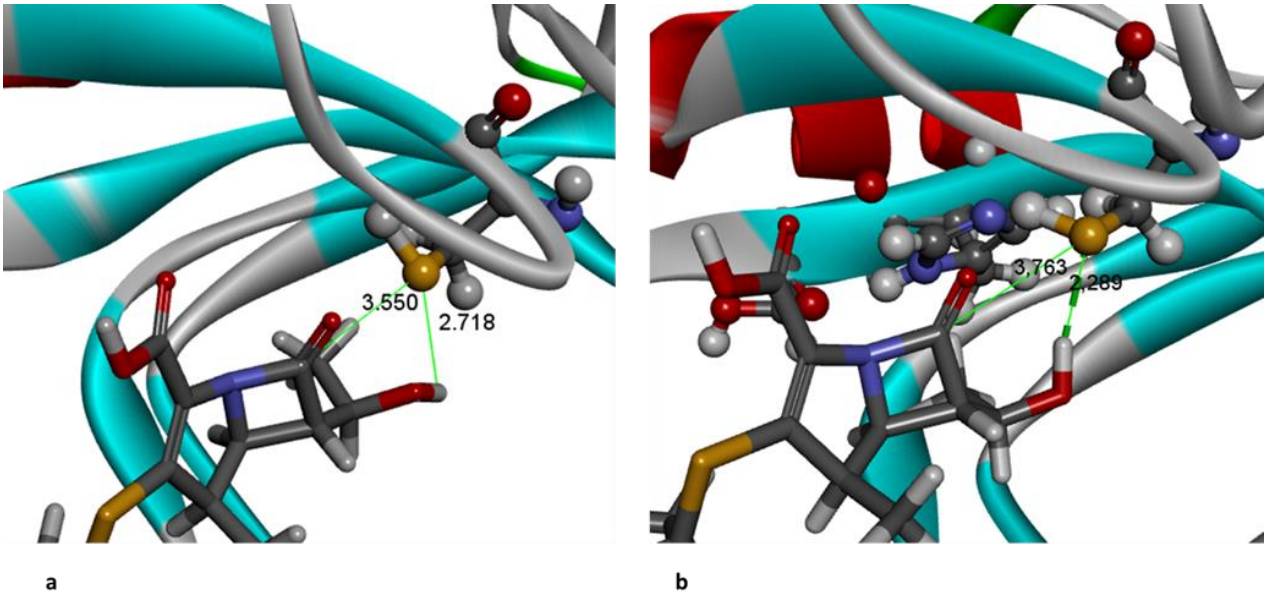


**Figure 4.** Schematic representation of hydrogen bond interactions and their respective distances (**A**) Before optimization (**B**) After optimization. The ONIOM (Gaussian) input files as well as the optimized output files of all inhibitor-enzyme complexes are also provided with the supplementary material.

**Hydrogen bond modes of interaction in carbapenem-Ldt$_{Mt2}$ complexes**

To further examine the nature of the calculated binding free energies for the FDA approved inhibitors complexed with Ldt$_{Mt2}$, the LigPlot[58] program was used to reveal the possible intermolecular hydrogen bond and electrostatic interactions between the carbapenem-Ldt$_{Mt2}$ complexes. The critical amino acid residues such as His203, Asn207, Ser202, Cys205, Thr201, His187, Thr171, Trp191, Ser192, and Tyr169, (These correspond to His352, Asn356, Ser351, Cys354, Thr350, His336, Thr320, Trp340, Ser341, and Tyr318 of the original crystal structure), directly interact with the inhibitor by forming hydrogen bonds and hydrophobic interactions (**Figure 5**). The details of other complexes are depicted in the supplementary materials (**Figure 6S**).

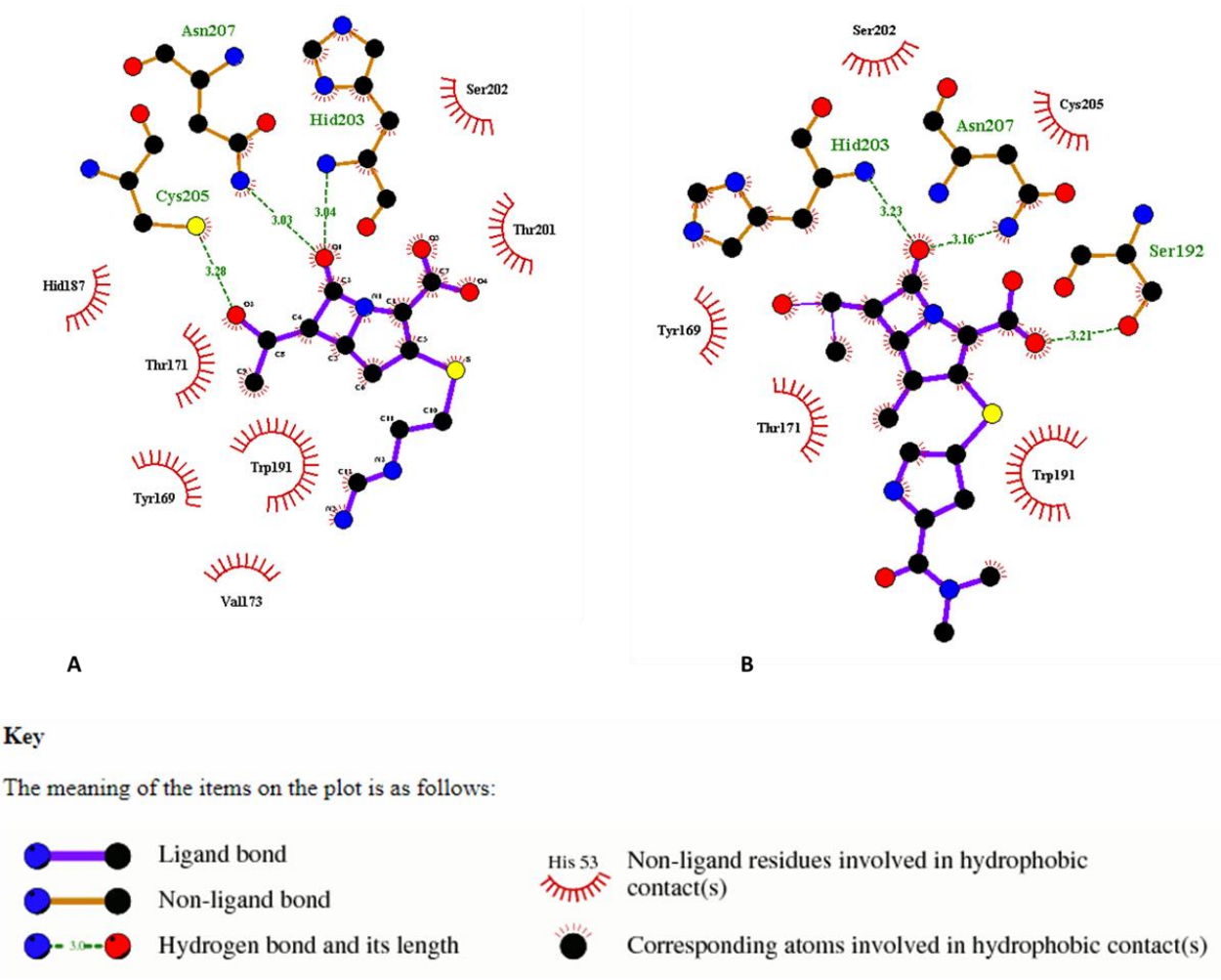


**Figure 5.** A 2-D schematic representation of hydrogen bond and hydrophobic interactions between catalytic amino acid residues and the carbapenems (**A.** Imipenem and **B.** Meropenem). Red dotted lines represent hydrogen bond interactions.

The plots show hydrogen bonding and electrostatic interactions occurring between the inhibitors and the catalytic active site residues of $Ldt_{Mt2}$. As it is observed, the arrangement of the catalytic amino acids residues displays a consistent pattern in proximity to the *β*-lactam ring of all the carbapenems.

**QTAIM analysis**

The quantum theory of atoms in molecules (QTAIM) has been used to characterize and quantify the H-bonding interactions for carbapenem-$Ldt_{Mt2}$ complexes as described by Bader[63, 69]. After geometry optimization of the carbapenem-$Ldt_{Mt2}$ complexes using a two-layered ONIOM (B3LYP/6-31G+(d): AMBER) model, the QM region of carbapenem-$Ldt_{Mt2}$ complexes (catalytic triad residues: His187, Ser188, and Cys205 and the selected carbapenems), were truncated and the wave functions of the QM region were calculated using B3LYP/6-31G+(d). Followed by the *ab initio* wave function calculations, the electron topography of carbapenem-$Ldt_{Mt2}$ complexes were generated using AIM2000 software package[70]. The topological analysis of the electron charge density provides the location of the critical points wherein the gradient of electron density is insignificant[35]. The BCP, which determine the existence or non-existence of hydrogen bond interactions and the molecular graph to connect the bond paths of critical points of the studied truncated systems, were obtained. The Imi-$Ldt_{Mt2}$ and Mero-$Ldt_{Mt2}$ complexes are shown in **Figure 6**. In general, if a hydrogen bond does exist between two atoms, the range of $\rho(r)$ and $\nabla^2 \rho(r)$ are between 0.002–0.035 a.u. and 0.024–0.139 a.u., respectively[71]. The topological parameters for the truncated carbapenem-$Ldt_{Mt2}$ complexes are tabulated in **Table 2**.

According to **Table 2**, the $\rho(r)$ and $\nabla^2 \rho(r)$ values for carbapenem-$Ldt_{Mt2}$ complexes vary in terms of their respective interacting atoms at specific critical points (CP). However, the minimum and maximum for both the $\rho(r)$ and $\nabla^2 \rho(r)$ in all the studied carbapenem-$Ldt_{Mt2}$ complexes interactions are 0.0053─0.0245 and 0.0184─0.0594 a.u, respectively. In this regard, Imi-$Ldt_{Mt2}$, Tebi-$Ldt_{Mt2}$ and Bia-$Ldt_{Mt2}$ have comparable $\rho(r)$ and $\nabla^2 \rho(r)$ values that determine the strength of the hydrogen bond interactions and authenticate the existence of hydrogen bond formation at each BCP, represented by red dots in the molecular graph plot (**Figure 6**.). It is noteworthy that the average values for $\rho(r)$ and $\nabla^2 \rho(r)$ of **HB's** for each complex also corresponds to the theoretical and experimental Gibb's binding free energies.

The Laplacian of charge density at the bond critical point, $\nabla^2 \rho(r)$, is defined as the sum of three preliminary curvatures of the function at each point of the space. The sign of $\nabla^2 \rho(r)$ serves an

integral role in the determination of whether the charge density is locally depleted $\nabla^2 \rho(r)>0$, or locally concentrated $\nabla^2 \rho(r)<0$. Consequently, the standard measures of hydrogen bonds are characterized by $H(r)<0$ and $\nabla^2 \rho(r)<0$ for strong hydrogen bonds, whereas the medium hydrogen bonds with $H(r)<0$ and $\nabla^2 \rho(r)>0$, and $H(r)>0$, and $\nabla^2 \rho(r)>0$ are determined to be the weak ones[72]. The observed phenomena in the case of $\nabla^2 \rho(r)$ values in **Table 2** appear positive while some of the values of $H(r)$ appear negative. This indicates that the bond nature is considered as being partially covalent-partially electrostatic (Pc-Pe)[73]. The two parameters, $\nabla^2 \rho(r)$ and $H(r)$ at BCP are normally used to categorize and characterize hydrogen bonds. Distance analysis is another crucial factor in determining the bond strength between interacting atoms induced by electronegativity because of electron charge density.

**Table 2**. AIM topological parameters including electron density (**ρ**) and their Laplacian of electron density (**$\nabla^2\rho$**) in a.u. and energetic parameters ***G(r)***, ***H(r)***, and ***V(r)*** in (kcal/mol) in carbapenem-$Ldt_{Mt2}$ complexes calculated at the B3LYP/6-31+G(d).

| **Hydrogen bonds** | **Complexes interactions** | ***ρ (r)*** | **$\nabla^2\rho$ (r)** | ***G(r)*** | ***H(r)*** | ***V(r)*** | **Ellipticity (ε)** |
|---|---|---|---|---|---|---|---|
| | **Imi-$Ldt_{Mt2}$** | | | | | | |
| **HB1** | $O_{56}H\cdots S_{36}$ | 0.0232 | 0.0574 | 0.0154 | 0.0010 | 0.0164 | 0.0359 |
| **HB2** | $C_{55}H\cdots C_{11}$ | 0.0053 | 0.0184 | 0.0034 | -0.0012 | 0.0022 | 0.6362 |
| | **Tebi-$Ldt_{Mt2}$** | | | | | | |
| **HB1** | $O_{81}H\cdots S_{36}$ | 0.0230 | 0.0565 | 0.0151 | 0.0010 | 0.0161 | 0.0370 |
| **HB2** | $C_{80}H\cdots C_{11}$ | 0.0069 | 0.0233 | 0.0045 | -0.0013 | 0.0031 | 0.1980 |
| | **Bia-$Ldt_{Mt2}$** | | | | | | |
| **HB1** | $O_{76}H\cdots S_{70}$ | 0.0233 | 0.0569 | 0.0153 | 0.0011 | 0.0163 | 0.0388 |
| **HB2** | $C_{75}H\cdots C_{45}$ | 0.0072 | 0.0245 | 0.0047 | -0.0014 | 0.0033 | 0.1500 |
| | **Mero-$Ldt_{Mt2}$** | | | | | | |
| **HB1** | $O_{86}H\cdots S_{81}$ | 0.0245 | 0.0594 | 0.0161 | 0.0013 | 0.0175 | 0.0393 |
| **HB2** | $C_{85}H\cdots C_{56}N$ | 0.0080 | 0.0275 | 0.0054 | -0.0015 | 0.0039 | 0.1495 |

KEG, Lagrangian kinetic energy density *G(r)*, KEK, Hamiltonian kinetic energy density *H(r)*, VIR, Virial filed function *V(r)*.

The ellipticity ($\varepsilon$) values of each bond critical point for all carbapenem-$Ldt_{Mt2}$ complexes are reported in **Table 2**. Ellipticity is the important measure of the bond's stability *i.e.* high ellipticity value signifies unstable bonds.[74] The ellipticity of the carbapenem-$Ldt_{Mt2}$ complexes ranges from 0.0359─0.6362 a.u. It is noted that **HB1** is dominant for all complexes. The $\varepsilon$ values for **HB1** also follow the same trend of the binding free energies (experimental and theoretical). It is worth pointing out that the hydrogen bonds in the QM region of all carbapenem-complexes demonstrate stable electrostatic interactions, considering the average amount of ellipticity as Imi—$Ldt_{Mt2}$ > Tebi—$Ldt_{Mt2}$ > Bia—$Ldt_{Mt2}$ ≈ Mero—$Ldt_{Mt2}$ and this trend is consistent with the obtained binding free energies.

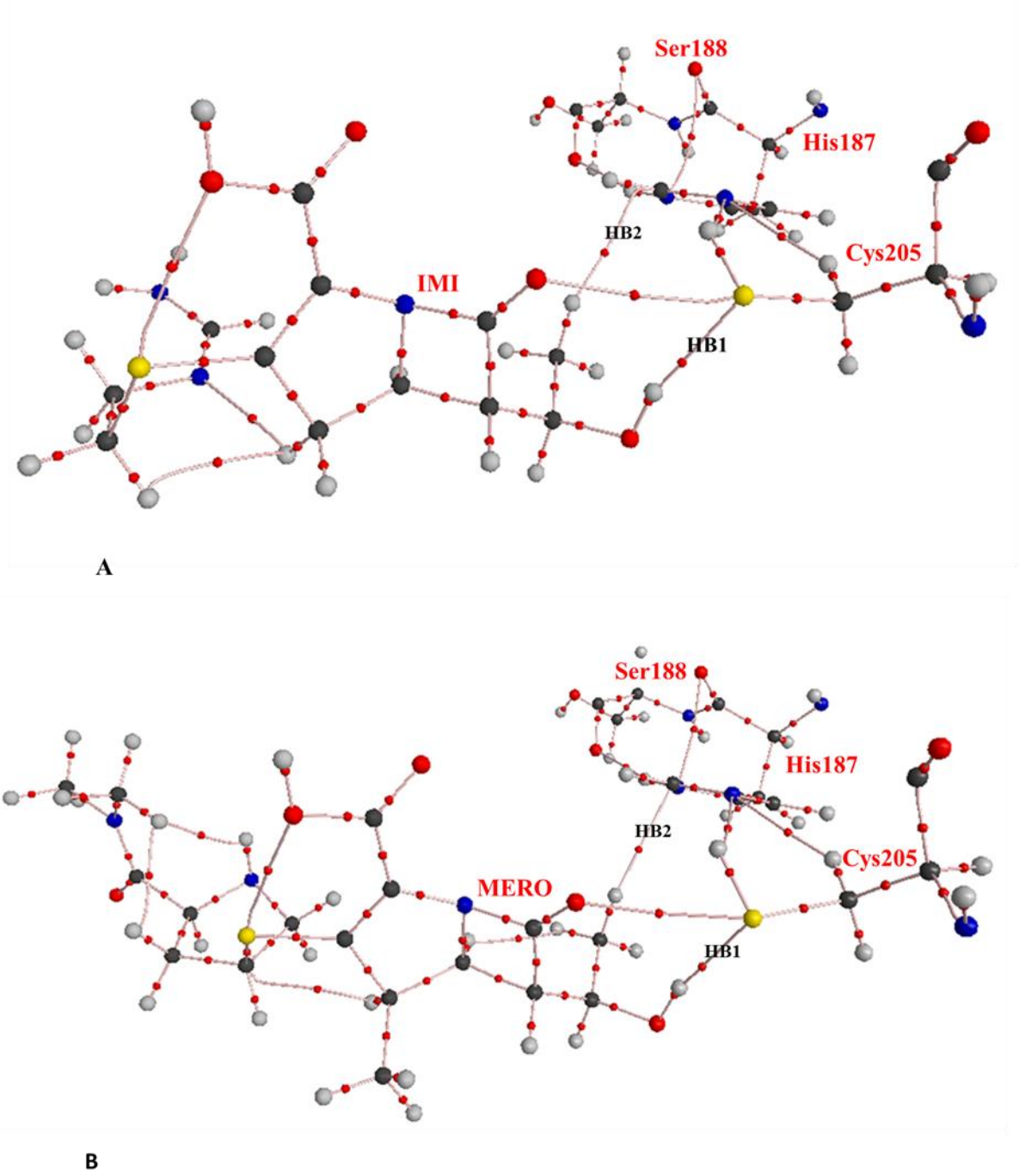


**Figure 6.** Molecular graph of **A**. Imi-$Ldt_{Mt2}$ and **B**. Mero-$Ldt_{Mt2}$ complexes generated using AIM2000 software. Small red spheres and lines correspond to the bond critical points (BCP) and the bond paths, respectively. See details of the molecular graph for other complexes in **Figure 7S**.

**Natural Bond Orbital analysis**

In the NBO analysis[36], electronic wave functions are elucidated in terms of a set of occupied Lewis and a set of unoccupied non-Lewis localized orbitals. The delocalization effect can be recognized by the existence of off-diagonal elements of the Fock matrix. The intensities of delocalization interactions are predicted by the second-order perturbation theory $E^{(2)}$[36]. Based on the optimized ground state geometries of the QM region of the carbapenem-$Ldt_{Mt2}$ complexes using the B3LYP/6-311+G(d), the NBO analysis of donor-acceptor (bond-anti-bonding) interactions have been assessed. The **HB1** is also dominant in all complexes. The stabilization energies associated with delocalization of electrons is the strongest in S36⋯O56─H73 (**HB1**) of the Imi-$Ldt_{Mt2}$ complex by 15.80 kcal $mol^{-1}$. In the Mero-$Ldt_{Mt2}$ complex, the S81⋯⋯O86─H87 (**HB1**) have the strongest stabilization energy of 17.45 kcal $mol^{-1}$ as shown in **Table 3**.

The other carbapenem-$Ldt_{Mt2}$ complexes (Tebi-$Ldt_{Mt2}$ and Bia-$Ldt_{Mt2}$) also exhibited the strongest stabilization energies in **HB1** interactions. This observation reveals that even for the complexes with moderate and weak binding affinities, electron charge transfer will still occur from donor to acceptor units (**Table 3**). The charge transfer between the lone pair (LP) and the anti-bonding (BD*) orbitals, as shown in **Figure 7**, exhibit larger stabilization $E^2$ values. As a result, this indicates the possibility of electron charge transfer from donors to acceptors. The formation of hydrogen bonds provides sufficient evidence for the considerable electron charge transfer from the lone pair orbital to anti-bonding orbital. Hence, the NBO analysis agrees with the QTAIM results in justifying the stability of the carbapenem-$Ldt_{Mt2}$ complexes denoted by ONIOM Gibbs free binding interaction energies.

**Table 3**. Second-order perturbation energies E $^{(2)}$ (kcal mol$^{-1}$) corresponding to the most important charge transfer interaction (donor→ acceptor) in the carbapenem-Ldt$_{Mt2}$ complexes at the B3LYP/6-31G level.

| **Complex/ Interactions** | **Donor NBO(*i*) *n*(O)** | **Acceptor NBO(*j*) σ*(O─H)** | ***E*** $^{(2)}$ **(kcalmol$^{-1}$) (O)→σ*(O─H)** |
|---|---|---|---|
| **Imi-Ldt$_{Mt2}$** | | | |
| **HB1** | BD (1) S36─H37 | BD*(1) O56─H73 | 0.22 |
| | LP (2) S36 | BD*(1) O56─H73 | 15.80 |
| **HB2** | BD (1) C55─H60 | BD*(1) C11─H12 | 0.12 |
| | BD (1) C11─H12 | BD*(1) C55─H60 | 0.28 |
| **Tebi-Ldt$_{Mt2}$** | | | |
| **HB1** | BD (1) S36─H37 | BD*(1) O81─H82 | 0.17 |
| | LP (1) S36 | BD*(1) O81─H82 | 1.64 |
| | LP (2) S36 | BD*(1) O81─H82 | 15.80 |
| **HB2** | BD (1) C11─H12 | BD*(1) C80─H84 | 0.27 |
| **Bia-Ldt$_{Mt2}$** | | | |
| **HB1** | BD (1) S70─H71 | BD*(1) O76─H79 | 0.12 |
| | LP (1) S70 | BD*(1) O76─H79 | 2.77 |
| | LP (2) S70 | BD*(1) O76─H79 | 16.47 |
| **HB2** | BD (1) C75─H78 | BD*(1) C45─H46 | 0.22 |
| | BD (1) C45─H46 | BD*(1) C75─H78 | 0.17 |
| **Mero-Ldt$_{Mt2}$** | | | |
| **HB1** | BD (1) S81─H82 | BD*(1) O86─H87 | 0.16 |
| | LP (1) S81 | BD*(1) O86─H87 | 1.42 |
| | LP (2) S81 | BD*(1) O86─H87 | 17.45 |
| **HB2** | BD (1) C85─H89 | BD*(1) C56─N58 | 0.24 |
| | BD (2) C56─N58 | BD*(1) C85─H89 | 0.73 |
| | BD (2) C56─N58 | BD*(1) C85─H89 | 0.40 |

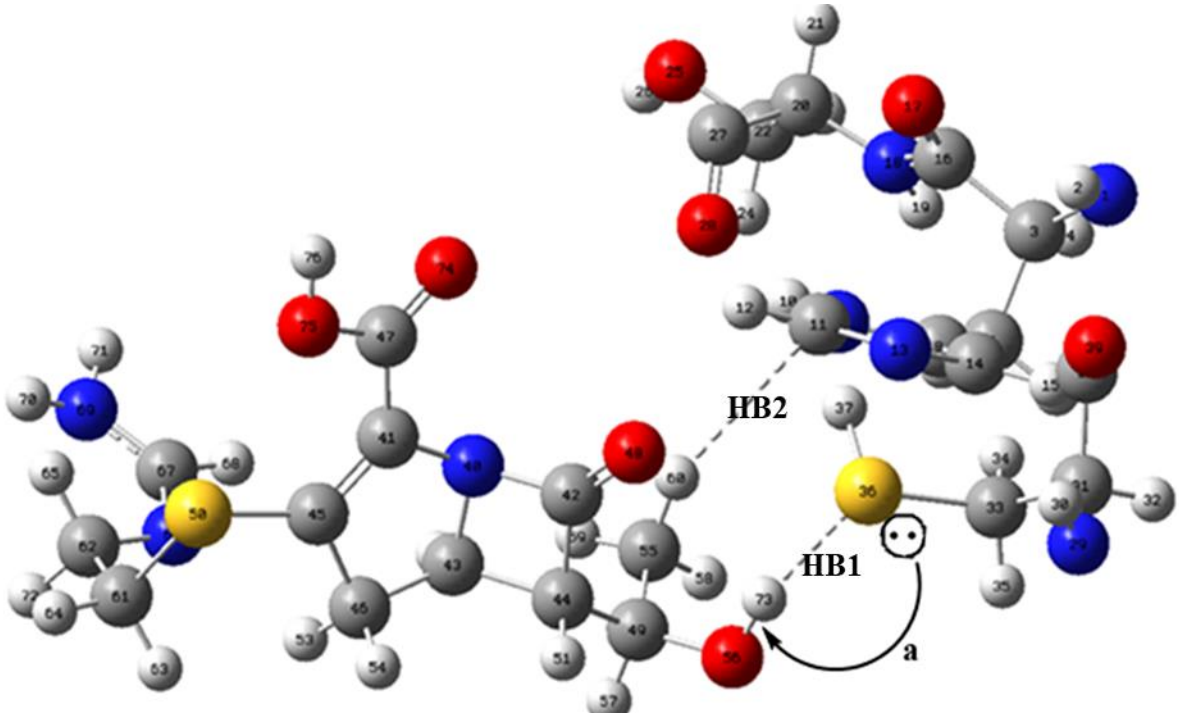


**Figure 7.** Depiction of electron transfers for Imi-Ldt$_{Mt2}$ complex derived by second-order perturbation theory of NBO analysis. The curved arrows (**a**) depict the direction of charge transfer: (**a**) LP (S) → σ* (O─H) listed in **Table 3**. See other depictions in **Figure 8S**

## 4.0 Conclusion

In this study, a two-layered ONIOM (B3LYP/6-31+G(d): Amber) model was used to evaluate the efficacy of FDA approved carbapenems antibiotics towards Ldt$_{Mt2}$ by calculating their binding interaction energies, hydrogen bond measurements, AIM and performing NBO analyses. The four carbapenem-Ldt$_{Mt2}$ complexes, namely Imi-Ldt$_{Mt2}$, Tebi-Ldt$_{Mt2}$, Bia-Ldt$_{Mt2}$, and Mero-Ldt$_{Mt2}$, were undertaken for this study. The Gibb's free energies (ΔG) obtained in this study corresponded with the experimental trend. As for enthalpies (ΔH) and entropies (ΔS), the favorable contributions of ligand–receptor electrostatic, hydrogen bond and van der Waals interactions to binding free energies for calculated complexes (carbapenems-Ldt$_{Mt2}$) suggests a suitable theoretical model that can be useful in advancing the *β*-lactam antibiotics as potential anti-TB drug agents. Moreover, the QTAIM topological indices provide an accurate indication of the critical hydrogen bond formation that contribute to the stability of the carbapenem-Ldt$_{Mt2}$ complexes. The AIM analysis agrees with the extent of charge transfer between carbapenems and Ldt$_{Mt2}$ shown by the NBO second order perturbation theory. NBO analysis was used to elucidate the data concerning charge transfer of electrons between carbapenems and Ldt$_{Mt2}$. Both analyses reveal that the prominent non-covalent interactions within the complexes correlates to the ONIOM calculated binding free energies.

The ONIOM method provides better relative binding free energies of these complexes than the previous molecular dynamics studies. The outcome of this study highlights the nature of the non-covalent interactions of $Ldt_{Mt2}$ with carbapenems which could be helpful for rational drug design of novel anti-TB drugs with relatively improved efficacies.

## Competing interests

The authors declare that they have no competing interests.


## Acknowledgements

We thank the College of Health Sciences (CHS), Aspen Pharmacare, MRC and NRF for financial support. We are also grateful to the CHPC (www.chpc.ac.za) and UKZN cluster for computational resources.

# References


[1] (WHO), W. H. O. (2017) World Health Organization. *Global tuberculosis report* 2016 [cited 16 January 2018]; Available from: www.who.int/tb/publications/global_report/en/.

[2] Cegielski, J. P. (2010) Extensively drug-resistant tuberculosis:"there must be some kind of way out of here", *Clin. Infect. Dis. 50*, S195-S200.

[3] Cole, S. T., and Riccardi, G. (2011) New tuberculosis drugs on the horizon, *Curr. Opin. Microbiol. 14*, 570-576.

[4] Gandhi, N. R., Moll, A., Sturm, A. W., Pawinski, R., Govender, T., Lalloo, U., Zeller, K., Andrews, J., and Friedland, G. (2006) Extensively drug-resistant tuberculosis as a cause of death in patients co-infected with tuberculosis and HIV in a rural area of South Africa, *The Lancet 368*, 1575-1580.

[5] Organization, W. H. (2014) World Health Organization global tuberculosis report, *Geneva: World Health Organization(accessed on 14 February 2017)*.

[6] Gupta, R., Lavollay, M., Mainardi, J. L., Arthur, M., Bishai, W. R., and Lamichhane, G. (2010) The Mycobacterium tuberculosis protein $Ldt_{Mt2}$ is a nonclassical transpeptidase required for virulence and resistance to amoxicillin, *Nat. Med. 16*, 466-469.

[7] Mainardi, J.-L., Villet, R., Bugg, T. D., Mayer, C., and Arthur, M. (2008) Evolution of peptidoglycan biosynthesis under the selective pressure of antibiotics in Gram-positive bacteria, *FEMS Microbiol. Rev. 32*, 386-408.

[8] Lavollay, M., Arthur, M., Fourgeaud, M., Dubost, L., Marie, A., Veziris, N., Blanot, D., Gutmann, L., and Mainardi, J.-L. (2008) The peptidoglycan of stationary-phase Mycobacterium tuberculosis predominantly contains cross-links generated by L, D-transpeptidation, *J. Bacteriol. 190*, 4360-4366.

[9] Erdemli, S. B., Gupta, R., Bishai, W. R., Lamichhane, G., Amzel, L. M., and Bianchet, M. A. (2012) Targeting the cell wall of Mycobacterium tuberculosis: structure and mechanism of L,D-transpeptidase 2, *Structure 20*, 2103-2115.

[10] Li, W. J., Li, D. F., Hu, Y. L., Zhang, X. E., Bi, L. J., and Wang, D. C. (2013) Crystal structure of L,D-transpeptidase $Ldt_{Mt2}$ in complex with meropenem reveals the mechanism of carbapenem against Mycobacterium tuberculosis, *Cell Res. 23*, 728-731.

[11] Papp-Wallace, K. M., Endimiani, A., Taracila, M. A., and Bonomo, R. A. (2011) Carbapenems: past, present, and future, *Antimicrob. Agents Chemother. 55*, 4943-4960.

[12] Wietzerbin, J., Das, B. C., Petit, J. F., Lederer, E., Leyh-Bouille, M., and Ghuysen, J. M. (1974) Occurrence of D-alanyl-(D)-meso-diaminopimelic acid and meso-diaminopimelyl-meso-diaminopimelic acid interpeptide linkages in the peptidoglycan of Mycobacteria, *Biochemistry 13*, 3471-3476.

[13] Böth, D., Steiner, E. M., Stadler, D., Lindqvist, Y., Schnell, R., and Schneider, G. (2013) Structure of $Ldt_{Mt2}$, an L, D-transpeptidase from Mycobacterium tuberculosis, *Acta Crystallogr. D. 69*, 432-441.

[14] Cordillot, M., Dubée, V., Triboulet, S., Dubost, L., Marie, A., Hugonnet, J.-E., Arthur, M., and Mainardi, J.-L. (2013) In vitro cross-linking of Mycobacterium tuberculosis peptidoglycan by l, d-transpeptidases and inactivation of these enzymes by carbapenems, *Antimicrob. Agents Chemother. 57*, 5940-5945.

[15] Correale, S., Ruggiero, A., Capparelli, R., Pedone, E., and Berisio, R. (2013) Structures of free and inhibited forms of the L, D-transpeptidase LdtMt1 from Mycobacterium tuberculosis, *Acta Crystallogr. D. 69*, 1697-1706.

[16] Dubée, V., Triboulet, S., Mainardi, J.-L., Ethève-Quelquejeu, M., Gutmann, L., Marie, A., Dubost, L., Hugonnet, J.-E., and Arthur, M. (2012) Inactivation of Mycobacterium tuberculosis L, D-transpeptidase LdtMt1 by carbapenems and cephalosporins, *Antimicrob. Agents Chemother. 56*, 4189-4195.

[17] Schoonmaker, M. K., Bishai, W. R., and Lamichhane, G. (2014) Nonclassical transpeptidases of Mycobacterium tuberculosis alter cell size, morphology, the cytosolic matrix, protein localization, virulence, and resistance to β-lactams, *J. Bacteriol. 196*, 1394-1402.

[18] Kim H. S, K. J., Im H. N, Yoon J. Y, An D. R, Yoon H. J, Kim J. Y, Min H. K, Kim S. J, Lee J. Y, Han B. W, Suh S. W. (2013) Structural basis for the inhibition of Mycobacterium tuberculosis L,D-transpeptidase by meropenem, a drug effective against extensively drug-resistant strains, Acta Crystallogr D Biol Crystallogr D69, 420-431.

[19] Nizami, B., Sydow, D., Wolber, G., and Honarparvar, B. (2016) Molecular insight on the binding of NNRTI to K103N mutated HIV-1 RT: molecular dynamics simulations and dynamic pharmacophore analysis, *Mol. BioSyst. 12*, 3385-3395.

[20] Honarparvar, B., Pawar, S. A., Alves, C. N., Lameira, J., Maguire, G. E., Silva, J. R. A., Govender, T., and Kruger, H. G. (2015) Pentacycloundecane lactam vs lactone norstatine type protease HIV inhibitors: binding energy calculations and DFT study, *J. Biomed. Sci. 22*, 15.

[21] Honarparvar, B., Govender, T., Maguire, G. E., Soliman, M. E., and Kruger, H. G. (2013) Integrated approach to structure-based enzymatic drug design: molecular modeling, spectroscopy, and experimental bioactivity, *Chem. Rev 114*, 493-537.

[22] Silva, J. R. A., Bishai, W. R., Govender, T., Lamichhane, G., Maguire, G. E., Kruger, H. G., Lameira, J., and Alves, C. N. (2016) Targeting the cell wall of Mycobacterium tuberculosis: a molecular modeling investigation of the interaction of imipenem and meropenem with L, D-transpeptidase 2, *J. Biomol. Struct. Dyn. 34*, 304-317.

[23] Fakhar, Z., Govender, T., Maguire, G. E. M., Lamichhane, G., Walker, R. C., Kruger, H. G., and Honarparvar, B. (2017) Differential flap dynamics in l,d-transpeptidase2 from mycobacterium tuberculosis revealed by molecular dynamics, *Mol. BioSyst. 13*, 1223-1234.

[24] Svensson, M., Humbel, S., Froese, R. D., Matsubara, T., Sieber, S., and Morokuma, K. (1996) ONIOM: A multilayered integrated MO+ MM method for geometry optimizations and single point energy predictions. A test for Diels-Alder reactions and Pt (P (t-Bu) 3) 2+ H2 oxidative addition, *J. Phys. Chem. A 100*, 19357-19363.

[25] Dapprich, S., Komáromi, I., Byun, K. S., Morokuma, K., and Frisch, M. J. (1999) A new ONIOM implementation in Gaussian98. Part I. The calculation of energies, gradients, vibrational frequencies and electric field derivatives, *Comput. Theor. Chem 461*, 1-21.

[26] Vreven, T., and Morokuma, K. (2000) On the application of the IMOMO (integrated molecular orbital+ molecular orbital) method, *J. Comput. Chem 21*, 1419-1432.

[27] Karadakov, P. B., and Morokuma, K. (2000) ONIOM as an efficient tool for calculating NMR chemical shielding constants in large molecules, *Chem. Phys. Lett 317*, 589-596.

[28] Banáš, P., Jurečka, P., Walter, N. G., Šponer, J., and Otyepka, M. (2009) Theoretical studies of RNA catalysis: hybrid QM/MM methods and their comparison with MD and QM, *Methods 49*, 202-216.

[29] Morokuma, K. (2009) Theoretical studies of structure, function and reactivity of molecules— A personal account, *Proc. Jpn. Acad. Ser. B Phys. Biol. Sci. 85*, 167-182.

[30] Maseras F., M. K. (1995) IMOMM: A new integrated ab initio + molecular mechanics geometry optimization scheme of equilibrium structures and transition states. , *J. Comp. Chem. 16*, 1170-1179.

[31] Zheng, F., and Zhan, C.-G. (2008) Rational design of an enzyme mutant for anti-cocaine therapeutics, *J. Comput-Aided. Mol. Des. 22*, 661-671.

[32] Ruangpornvisuti, V. (2004) Recognition of carboxylate and dicarboxylates by azophenol–thiourea derivatives: a theoretical host–guest investigation, *Comput. Theor. Chem 686*, 47-55.

[33] Samanta, P. N., and Das, K. K. (2016) Prediction of binding modes and affinities of 4-substituted-2, 3, 5, 6-tetrafluorobenzenesulfonamide inhibitors to the carbonic anhydrase receptor by docking and ONIOM calculations, ***J*** *Mol Graph Model 63*, 38-48.

[34] Promsri, S., Chuichay, P., Sanghiran, V., Parasuk, V., and Hannongbua, S. (2005) Molecular and electronic properties of HIV-1 protease inhibitor C 60 derivatives as studied by the ONIOM method, *Comput. Theor. Chem 715*, 47-53.
[35] Bader, R., and Molecules, A. I. (1990) A Quantum Theory, Clarendon, Oxford, England.
[36] Reed, A. E., Curtiss, L. A., and Weinhold, F. (1988) Intermolecular interactions from a natural bond orbital, donor-acceptor viewpoint, *Chemical Reviews 88*, 899-926.
[37] Li, W.-J., Li, D.-F., Hu, Y.-L., Zhang, X.-E., Bi, L.-J., and Wang, D.-C. (2013) Crystal structure of L, D-transpeptidase $Ldt_{Mt2}$ in complex with meropenem reveals the mechanism of carbapenem against Mycobacterium tuberculosis, *Cell research 23*, 728.
[38] The PyMOL Molecular Graphics System, V. S., LLC.
[39] Case, D., Darden, T., Cheatham III, T., Simmerling, C., Wang, J., Duke, R., Luo, R., Crowley, M., Walker, R., and Zhang, W. (2008) AMBER, version 10, *University of California: San Francisco, CA*.
[40] Hornak, V., Abel, R., Okur, A., Strockbine, B., Roitberg, A., Simmerling, C. (2006) Comparison of multiple Amber force fields and development of improved protein backbone parameters, *Proteins. Discipline. Protein biochemistry 65*, 712-725.
[41] Wang, J. M., Wolf, R. M., Caldwell, J. W., Kollman, P. A., Case, D. A. . (2004) Development and testing of a general amber force field, *J. Comput. Chem 25*, 1157–1174.
[42] Jorgensen, W. L., Chandrasekhar, J., Madura, J. D., Impey, R. W., and Klein, M. L. (1983) Comparison of simple potential functions for simulating liquid water, *J. Chem. Phys 79*, 926-935.
[43] Harvey M. J., F. G. D. (2009) An Implementation of the Smooth Particle Mesh Ewald Method on GPU Hardware, *J. Chem. Theory Comput 5*, 2371–2377.
[44] Ryckaert, J. P., Ciccotti, G., Berendsen, H. J. C. . (1977) Numerical integration of the cartesian equations of motion of a system with constraints: Molecular dynamics of N-alkanes, *J. Comput. Phys 23*, 327–341.
[45] Li, H., Robertson, A. D., and Jensen, J. H. (2005) Very fast empirical prediction and rationalization of protein pKa values, *Proteins. Discipline. Protein biochemistry 61*, 704-721.
[46] Frisch, M., Trucks, G., Schlegel, H., Scuseria, G., Robb, M., Cheeseman, J., Scalmani, G., Barone, V., Mennucci, B., and Petersson, G. (2009) Gaussian 2009, *See Supporting Information f or full citation*.
[47] Kapp, J., Remko, M., and Schleyer, P. v. R. (1996) H2XO and (CH3) 2XO Compounds (X= C, Si, Ge, Sn, Pb): Double Bonds vs Carbene-Like Structures Can the Metal Compounds Exist at All?, *J. Am. Chem. Soc. 118*, 5745-5751.
[48] Remko, M., Walsh, O. A., and Richards, W. G. (2001) Theoretical study of molecular structure, tautomerism, and geometrical isomerism of moxonidine: Two-layered ONIOM calculations, *J. Phys. Chem. A 105*, 6926-6931.
[49] Johnson, B. G., Gill, P. M., and Pople, J. A. (1993) The performance of a family of density functional methods, *J. Chem. Phys 98*, 5612-5626.
[50] Humbel, S., Sieber, S., and Morokuma, K. (1996) The IMOMO method: Integration of different levels of molecular orbital approximations for geometry optimization of large systems: Test for n-butane conformation and SN2 reaction: RCl+ Cl−, *J. Chem. Phys 105*, 1959-1967.
[51] Kohn, W., Becke, A. D., and Parr, R. G. (1996) Density functional theory of electronic structure, *J. Phys. Chem. A 100*, 12974-12980.
[52] Neumann, R., Nobes, R. H., and Handy, N. C. (1996) Exchange functionals and potentials, *Molecular Physics 87*, 1-36.
[53] Becke, A. D. (1993) Density-functional thermochemistry. III. The role of exact exchange, *J. Chem. Phys 98*, 5648-5652.
[54] Lee, C., Yang, W., and Parr, R. G. (1988) Development of the Colle-Salvetti correlation-energy formula into a functional of the electron density, *Physical review B 37*, 785.

[55] Hariharan, P. C., and Pople, J. A. (1973) The influence of polarization functions on molecular orbital hydrogenation energies, *Theoretica chimica acta 28*, 213-222.
[56] Rassolov, V. A., Pople, J. A., Ratner, M. A., and Windus, T. L. (1998) 6-31G* basis set for atoms K through Zn, *J. Chem. Phys 109*, 1223-1229.
[57] Vreven, T., Byun, K. S., Komáromi, I., Dapprich, S., Montgomery, J. A., Morokuma, K., and Frisch, M. J. (2006) Combining quantum mechanics methods with molecular mechanics methods in ONIOM, *J. Chem. Theory Comput 2*, 815-826.
[58] Laskowski, R. A., and Swindells, M. B. . (2011) Journal of Chemical Information and Modeling, *LigPlot+: multiple ligand–protein interaction diagrams for drug discovery 51*, 2778-2786.
[59] Panigrahi, S. K. (2008) Strong and weak hydrogen bonds in protein-ligand complexes of kinases: a comparative study, *Amino acids 34*, 617-633.
[60] Desiraju, G. R. (1996) The C− H··· O hydrogen bond: structural implications and supramolecular design, *Acc. Chem. Res 29*, 441-449.
[61] Panigrahi, S. K., and Desiraju, G. R. (2007) Strong and weak hydrogen bonds in the protein–ligand interface, *Proteins. Discipline. Protein biochemistry. 67*, 128-141.
[62] Dassault Systèmes BIOVIA, D. S. M. E., Release 2017, San Diego: Dassault Systèmes, 2016.
[63] Bader, R., and Molecules, A. I. (1990) A quantum theory, *Clarendon: Oxford, UK*.
[64] Popelier, P., and Bader, R. (1992) The existence of an intramolecular C・ H・ O hydrogen bond in creatine and carbamoyl sarcosine, *Chemical physics letters 189*, 542-548.
[65] Bianchet, M. A., Pan, Y. H., Basta, L. A. B., Saavedra, H., Lloyd, E. P., Kumar, P., Mattoo, R., Townsend, C. A., and Lamichhane, G. (2017) Structural insight into the inactivation of Mycobacterium tuberculosis non-classical transpeptidase Ldt $_{Mt2}$ by biapenem and tebipenem, *BMC Biochem. 18*, 8.
[66] Lu, Y., Wang, Y., Xu, Z., Yan, X., Luo, X., Jiang, H., and Zhu, W. (2009) C− X··· H Contacts in Biomolecular Systems: How They Contribute to Protein− Ligand Binding Affinity, *J. Phys. Chem. B 113*, 12615-12621.
[67] Patil, R., Das, S., Stanley, A., Yadav, L., Sudhakar, A., and Varma, A. K. (2010) Optimized hydrophobic interactions and hydrogen bonding at the target-ligand interface leads the pathways of drug-designing, *PloS one 5*, e12029.
[68] Bissantz, C., Kuhn, B., and Stahl, M. (2010) A medicinal chemist's guide to molecular interactions, *J. Med. Chem. 53*, 5061-5084.
[69] Parthasarathi, R., Amutha, R., Subramanian, V., Nair, B. U., and Ramasami, T. (2004) Bader's and reactivity descriptors' analysis of DNA base pairs, *J. Phys. Chem. A 108*, 3817-3828.
[70] Biegler-Konig, F., Schonbohm, J., and Bayles, D. (2001) Software news and updates-AIM2000-A program to analyze and visualize atoms in molecules, pp 545-559, John Wiley & Sons Inc 605 THIRD AVE, NEW YORK, NY 10158-0012 USA.
[71] Popelier, P. (1998) Characterization of a dihydrogen bond on the basis of the electron density, *J. Phys. Chem. A. 102*, 1873-1878.
[72] Bader, R. F. (1990) Atoms in Molecules: a quantum theory, International series of monographs on chemistry, 22, *Oxford University Press, Oxford Henkelman G, Arnaldsson A, Jónsson H (2006) A fast and robust algorithm for Bader decomposition of charge density. Comput Mater Sci 36*, 354-360.
[73] Nazari, F., and Doroodi, Z. (2010) The substitution effect on heavy versions of cyclobutadiene, *Int. J. Quantum Chem. 110*, 1514-1528.
[74] Mosapour Kotena, Z., Behjatmanesh–Ardakani, R., and Hashim, R. (2014) AIM and NBO analyses on hydrogen bonds formation in sugar-based surfactants (α/β-d-mannose and n-octyl-α/β-d-mannopyranoside): a density functional theory study, *Liquid Crystals 41*, 784-792.

# CHAPTER THREE

## ONIOM study of carbapenems binding interaction energies against L, D transpeptidase2 from *Mycobacterium tuberculosis* with explicit water molecule confined in the active site

**Thandokuhle Ntombela, [a] Zeynab Fakhar, [a] Gideon F. Tolufashe, [a] Collins U. Ibeji, [a] Thavendran Govender, [a] Glenn E. M. Maguire, [a, b] Gyanu Lamichhane, [c.] Bahareh Honarparvar, [a*] and Hendrik G. Kruger[a*]**

[a]Catalysis and Peptide Research Unit, School of Health Sciences, University of KwaZulu-Natal, Durban 4001, South Africa.

[b]School of Chemistry and Physics, University of KwaZulu-Natal, 4001 Durban, South Africa.

[c]Center for Tuberculosis Research, Division of Infectious Diseases, School of Medicine, Johns Hopkins University, Baltimore, MD 21205, USA.

***Corresponding authors:** Honarparvar@ukzn.ac.za (Dr Bahareh Honarparvar), (Prof. Hendrik G. Kruger) kruger@ukzn.ac.za, Telephone: + 27 31 2601845, Fax: +27 31 2603091, Catalysis and Peptide Research Unit, School of Health Sciences, University of KwaZulu-Natal, Durban 4041, South Africa.

### Abstract

L, D transpeptidase plays a significant role in *Mycobacterium tuberculosis* (*Mtb*) during the biosynthesis of an impermeable cell wall structure. $Ldt_{Mt2}$ protein has attracted substantial attention of researchers as a known therapeutic target from *Mtb*. β-lactam sub-class of antibiotics, carbapenems, have been deemed to have activity against this non-classical transpeptidases. In this study, a hybrid two-layered ONIOM method was employed to examine molecular and electronic properties when a bridging water molecule is added to carbapenem—$Ldt_{Mt2}$ complex binding interface. The active site residues (His187, Ser188, His203, Cys205 and Asn207) together with carbapenems and water molecule were modelled at QM (B3LYP/6-31+G(d)) level of theory and the remaining part of the enzyme was evaluated at MM level of theory (AMBER force field). The obtained theoretical binding free energies (ΔG) from ONIOM geometry optimization demonstrate that the presence of a water molecule in the carbapenem—$Ldt_{Mt2}$ complexes has a substantial role during complexation process. Both enthalpy (ΔH) and entropy (ΔS) had significant contributions in the binding free energies of carbapenem—$Ldt_{Mt2}$ complexes. Furthermore, AIM and NBO analysis corroborated the

significance of water in mediating hydrogen bond interactions which contributed to the stability and improved binding affinities of carbapenems. Our results revealed the importance of a bridging water molecule in the carbapenem—$Ldt_{Mt2}$ binding interfaces and this data could be useful in rational drug design.

***Keywords***: *Mycobacterium tuberculosis(Mtb)*, Carbapenems, $Ldt_{Mt2}$, ONIOM, AIM, NBO

## 1.0 Introduction

In recent years, public health care has been confronted by the increase in cases of multi-drug resistant (MDR) and extensively drug-resistant (XDR) strains of *M. tuberculosis*[1, 2]. Therefore, it is of great urgency to search for potent drug leads and explore new targets to counteract the burden of these increasingly dangerous species.

A major contribution towards elusive elimination of *Mtb* is its complex peptidoglycan layer comprising of 4→3 and 3→3 cross-linkages generated by D, D- Transpeptidase and L, D-Transpeptidase, respectively, during the last step of the biosynthesis process. Inactivation of these enzymes is by means of disrupting the peptidoglycan cell wall biosynthesis, which will consequently destroy the bacteria. A variety of bacterial species displays approximately 5–10% of 3→3 cross linkages generated by L, D-Transpeptidase known to perform a significant role during the biosynthesis of peptidoglycan[3]. *Mtb* is the only known mycobacterium to generate approximately 80% of 3→3 cross-linkages. Therefore, L, D-Transpeptidase 2 has been seen as an attractive target towards eradication of *Mtb* as it is essential for virulence, growth and morphology[4, 5].

One of the most potent classes of antibacterial that have been studied is the *β*-lactam[6] family of antibiotics. This class of compounds are characterized by their efficacious inhibitory activity against D, D-transpeptidases[6]. The inhibition of both enzymes, simultaneously, is essential for halting their significant cross-linking function. The *β*-lactam class of antibiotics targets peptidoglycan biosynthesis and is broadly used as the treatment for bacterial infections but they have been deemed to be impotent as TB treatment[7]. The inefficacious of *β*-lactams against *M. tuberculosis* has been impaired by the presence of the chromosomally encoded *β*-lactamases (*BlaC*), that hydrolyse the *β*-lactam ring thus resulting in drug deactivation.[8] However, the inhibition of *BlaC* has been achieved with clavulanate thus making it possible to repurpose and optimize the use of carbapenems as potential therapeutic drug candidates for TB.

Several studies have reported carbapenems to have anti-TB activity[9, 10]. *In-vitro* studies of biapenem, meropenem and tebipenem have indicated their potency/activity against *Mtb* even when administered alone or in combination[11, 12]. The structural data for $Ldt_{Mt2}$ bound to either peptidoglycan fragment or meropenem have been reported[5]. Several theoretical studies exploring the inhibition mechanism using different molecular methods have evolved[13-15]. The QM/MM molecular dynamic (MD) simulation and umbrella sampling approaches yielded insightful measures of the inactivation process rendered by meropenem and imipenem respectively. However, the theoretical values found for the calculated inhibition mechanism correspond with the kinetic experimental energy values[13]. Moreover, a 25 ns MD simulation study revealed the insightful binding free energy profiles of carbapenems against ex-$Ldt_{Mt2}$ using MM/GBSA and SIE methods[14]. Recently our group reported an extensive 140 ns molecular dynamics simulation study with explicit water solvent exploring the role of the $\beta$-hairpin flaps of $Ldt_{Mt2}$ during the complexation process which were assumed to have considerable influence in accommodating the substrate and inhibitor in the active site[15]. The results obtained in that study revealed that ertapenem and meropenem have lower binding free energies (-40.42 kcal $mol^{-1}$, -37.91 kcal $mol^{-1}$) than imipenem (-34.47 kcal $mol^{-1}$) and that was observed in a closed conformation of the $\beta$-hairpin flap[15]. Also, the study conducted by Bianchet *et al.*[16] conferred the crucial molecular interactions between carbapenems (biapenem and tebipenem) and the $Ldt_{Mt2}$ with a possible S-conjugation mechanism of inactivation prior to binding. According to their observations, biapenem and tebipenem bind to and inactivate the $Ldt_{Mt2}$ from an outer cavity of the binding site[16]. The study conducted by Lu *et al.*[17] revealed the significance of bridging water molecules in the GSK3 $\beta$-inhibitors interfaces by facilitating the hydrogen bonding interactions so as to induce the affinity of inhibitors and also improve the stability in the GSK3 $\beta$-inhibitor complexes. The role of water molecules in drug design is gaining attention and numerous studies have emphasized their influence in binding affinities of ligands[18].

The focus of this study was to exploit a two-layered ONIOM computational model to investigate the role played by the explicit water molecule to successfully bridge (hydrogen bonding) the carbapenems (biapenem, imipenem, meropenem and tebipenem) with $Ldt_{Mt2}$ during the complex formation. Also, we opted to ascertain the nature of binding nature and determine the binding interactions energies for carbapenem-water-$Ldt_{Mt2}$ upon complexation. Since water molecules are classified as a vital structural feature in protein-ligand complexes

that mediate intermolecular interactions (hydrogen bond formation), we believe that the stability of the carbapenem-$Ldt_{Mt2}$ complexes will be improved.

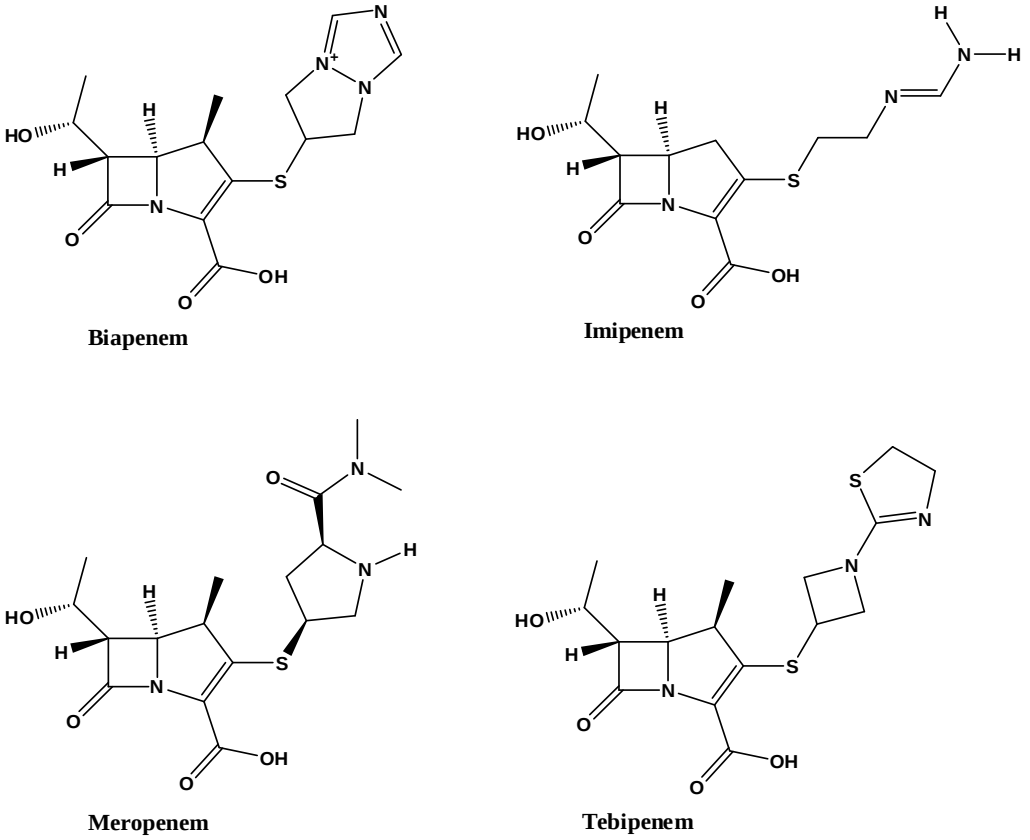


**Figure 1**. Structural representation of the studied carbapenems

## 2.0 Material and methods

### 2.1 System preparation

The PBD complex structures of *Mtb* $Ldt_{Mt2}$ were prepared by superimposing chain A of 3TUR[5] complexed with the natural substrate and 3VYP[19] meropenem-bound complex. The covalently bound meropenem from 3VYP[19] was restored by deletion of the covalent bond between the sulfur atom of cysteine residue and the carbonyl carbon of $\beta$-lactam ring. The $\beta$-lactam ring was restored; the hydrogen atoms were added, and the inhibitor was moved about 3.5 Å away from the R-SH (cysteine) group. A water molecule from the crystal structure (PDB ID: 3TUR[5]) was added between the inhibitor and the cysteine R-SH group. The meropenem-bound complex was then optimized. This optimized structure was then used as a reference to model other complexes by overlaying other inhibitors using PyMOL[20].

A molecular dynamics (MD) calculation was performed on the starting complex to affix the missing protons using X-leap[21] software. The MD simulations were carried out using Amber 14 with the ff99SB[22] force field (for proteins) and GAFF[23] for the inhibitors. The complexes were solvated with TIP3P[24] explicit water in a cubic box with 10 Å distance and counterions were added to neutralize the complexes. Partial Mesh Ewald (PME)[25] method was applied for long range electrostatic forces with cut-off of 12 Å. All bonds to hydrogen atoms was constrained using SHAKE algorithm[26]. Two-stage geometric minimization was performed by 2500 steps of steepest decent minimization followed by 2500 of conjugated gradient to remove clashes and bad contacts. To accurately assign the protonation states of the residues in the enzyme at pH=7.8, the empirical PropKa web server[27] was used.

The prepared complexes were then evaluated with a two-layered ONIOM[28-32] method. The ONIOM input files together with the optimized output files of all carbapenem-$Ldt_{Mt2}$ complexes are provided in PDB format with the supplementary materials.

**2.2 ONIOM hybrid (QM:MM) method**

An efficient hybrid method used for investigating large biosystems was applied and all calculations were executed using the Gaussian09 program[33]. The Becke3LYP[51, 52] functional has been applied in several studies[34-36] for it reliable accuracy of producing relatively good energies as to that of high-level *ab initio* methods. The ONIOM input files were prepared and visualized using Gauss View 5 program[33]. Using the DFT method, the best minimum energy conformations were achieved by full geometrical optimization of each conformer.

In this study, a two-layered ONIOM[28, 29, 37] hybrid approach (B3LYP/6-31G+(d): AMBER) as described by Morokuma *et al.*[38] was used to evaluate the role of water contribution in the binding affinities of the selected carbapenems against $Ldt_{Mt2}$. The computational ONIOM[28-32] model being investigated was evaluated with quantum mechanics (QM) and molecular mechanics (MM) methods in separate ONIOM layers. The selected FDA-approved inhibitors together with an explicit water molecule and the catalytic active site residues of $Ldt_{Mt2}$ enzyme (Cys205, His187, Ser188, His203, Asn207) were considered at QM level of theory and modeled using density functional theory (DFT)[39, 40], B3LYP[41, 42] functional and the 6-31+G(d)[43, 44] basis set. The residual portion of the complex was considered at MM[30, 45] and treated at low level of theory with the AMBER force field.

To verify the local stable minimum point of the potential energy surface for carbapenem-$Ldt_{Mt2}$ complexes, frequency calculations were performed using the optimized ONIOM output

structures and consequently the vibrational frequencies for all carbapenem-$Ldt_{Mt2}$ complexes were obtained with non-negative frequency. The total interaction energies are defined as:

$$\Delta E_{ONIOM} = \Delta E_{real,low} + \Delta E_{model,high} - \Delta E_{model,low} \quad (\mathbf{1})$$

Where, $\Delta E_{\text{model}}$ represent the energies of the model system defined at high and low level of theory and $\Delta E_{\text{real}}$ represent the whole (real) system. Thus, the equivalent binding interaction ONIOM energies of the complex systems are determined as follows:

$$\Delta G_{ONIOM} \approx \Delta G = G_{carbapenem-\text{LdtMt2}} - (G_{\text{LdtMt2}} + G_{\text{carbapenem}}) \quad (\mathbf{2})$$

The thermodynamic properties (enthalpies and entropies contributions) were also achieved from frequency calculations. The different entropic contributions (rotation, translation, and vibration) for carbapenem—$Ldt_{Mt2}$ complexes were calculated as follows:

$$\Delta S_{total} = \Delta S_{carbapenem-\text{LdtMt2}} - (\Delta S_{carbapenems} + \Delta S_{\text{LdtMt2}}) \quad (\mathbf{3})$$

After the procurement of the thermodynamic properties, the natural bond orbital (NBO)[46, 47] and quantum theory of atoms in molecules (QTAIM)[48] analysis were performed using the optimized structures to show the nature and stability of hydrogen bonds. Moreover, the topological properties i.e. electron density (ρ(r)) and its Laplacian (∇2ρ(r)) at bond critical points (BCPs), were computed based on Bader's QTAIM using the AIM2000 package[49].

## 3.0 Result and Discussion

It may be noted that the computational model exploited in this study consist of water molecule confined in the protein-ligand interfaces (active site) evaluated using a two-layered ONIOM method. To successfully understand the role of water during the binding process of FDA approved carbapenems, the binding free energy calculations of the carbapenem-water-$Ldt_{Mt2}$ complexes were executed using a two-layered ONIOM computational model (**Figure 2**). The structural water involvement in this setting was aimed to enhance the energetics of protein-ligand complexes by inducing carbapenems affinities towards $Ldt_{Mt2}$. The thermodynamic properties for the calculated theoretical results are reported in **Table 1** and are comparable to the experimental data, except for two outliers. As it was observed from the calculated theoretical binding free energies (ΔG) (**Table 1**), Tebi-$Ldt_{Mt2}$, Imi-$Ldt_{Mt2}$ and Mero-$Ldt_{Mt2}$ have approximately high theoretical values (-25.76 kcal $mol^{-1}$, -19.35 kcal $mol^{-1}$and -16.97 kcal $mol^{-1}$, respectively) compared to their experimental data, with Tebi-$Ldt_{Mt2}$ being one of the outliers

that reversed the trend. Also, Bia-$Ldt_{Mt2}$ have demonstrated comparable binding free energies (theoretical and experimental) even though it is an outlier.

**Table 1.** The ONIOM binding interaction energies of carbapenem—water**—**LdtMt2 complexes evaluated using (B3LYP/6-31+G (d): AMBER).

| *Complexes* | $\Delta G_{bind}(Exp)$ *kcal mol$^{-1}$* | $\Delta G_{bind}(Calc)$ *kcal mol$^{-1}$* | $\Delta H$ *kcal mol$^{-1}$* | $\Delta S_{Total}$ *cal mol$^{-1}$ K$^{-1}$* | $\Delta S_{trans}$ *cal mol$^{-1}$ K$^{-1}$* | $\Delta S_{rot}$ *cal mol$^{-1}$ K$^{-1}$* | $\Delta S_{vib}$ *cal mol$^{-1}$ K$^{-1}$* |
|---|---|---|---|---|---|---|---|
| **Tebi—$Ldt_{Mt2}$** | -9.35 | -25.76 | -41.31 | -52.18 | -43.68 | -36.27 | 27.77 |
| **Imi—$Ldt_{Mt2}$** | -9.82 | -19.35 | -35.15 | -53.07 | -42.95 | -34.79 | 24.67 |
| **Mero—$Ldt_{Mt2}$** | -8.16 | -16.97 | -33.69 | -56.07 | -43.68 | -35.98 | 23.59 |
| **Bia—$Ldt_{Mt2}$** | -8.96 | -7.94 | -25.66 | -59.44 | -43.43 | -35.48 | 19.48 |

Gibb's free energy (**$\Delta G$**), Enthalpy change (**$\Delta H$**), Entropy change **($\Delta S$)**, S translational (**$\Delta S_{trans}$**), S rotational (**$\Delta S_{rot}$**), S vibrational **($\Delta S_{vib}$)**.

The computed binding free energies of the four complexes did not follow the experimental data, except for two complexes (outliers), the order was reversed in Tebi-$Ldt_{Mt2}$ and Bia-$Ldt_{Mt2}$.

The ΔH value (-41.31 kcal mol$^{-1}$) of Tebi-$Ldt_{Mt2}$ complex (outlier) is the highest in all the investigated complexes. For Imi-$Ldt_{Mt2}$ and Mero-$Ldt_{Mt2}$ complexes, their ΔH values (-35.15 kcal mol$^{-1}$ and -33.69 kcal mol$^{-1}$) implies that are reasonable binders too. However, the Bia-$Ldt_{Mt2}$ complex shows the least enthalpy penalty than other complexes (**Table 1)**.

In the case of entropy contribution (ΔS), the Tebi-$Ldt_{Mt2}$ and Imi-$Ldt_{Mt2}$ complexes have less entropy penalty (-52.18 cal mol$^{-1}$ K$^{-1}$ and cal mol$^{-1}$ K$^{-1}$) than other complexes. However, the complexes (Bia-$Ldt_{Mt2}$ and Mero-$Ldt_{Mt2}$) that are weak binders in this study appear to have larger entropy penalty. The translational and rotational entropy contributions are in close range for all complexes. Interestingly, the major entropy contribution is from the vibrational component.

**Distance analysis of the carbapenem—$Ldt_{Mt2}$ complexes**

Distance is one of the significant measure in non-covalent interacting molecules. As a result, to understand and justify the obtained Gibb's binding free energies, the selected distances of each complex were measured before and after optimization to show the significant discrepancy between the carbonyl carbon of *β*-lactam ring (**C**), water (**O**) and sulfur atom of cysteine residue (**S**). The distances are reported in **Table 2**. It was observed that in all carbapenem-$Ldt_{Mt2}$-water calculations, the distances increased significantly after optimisation. When the C-O distances are compared, the figure for Tebi-$Ldt_{Mt2}$ (4.45 A) deviates considerably, from the values of the other complexes. For this complex, the C-S distance is the shortest of all complexes. It is possible these complexes are trapped in different local minima, leading to binding energies that differ from the experimental binding energies. Alternatively, it is possible that the subsequent activation energies are rate determining and that the energies of the precomplexes are not so crucial. This would mean that this model is not suitable for observing a correlation between the binding energies of the precomplexes, and the experimental binding energies.

**Table 2.** Distance analysis in angstroms (Å) between carbonyl carbon of *β*-lactam ring (**C**)-water(**O**)-sulfur(**S**)

| Complexes | Interactions | Before optimization | After optimization |
|---|---|---|---|
| **Bia—$Ldt_{Mt2}$—water** | C—O | 3.19 | 3.32 |
| | O—S | 2.35 | 3.31 |
| | C—S | 3.51 | 3.91 |
| **Imi—$Ldt_{Mt2}$—water** | C—O | 3.12 | 3.44 |
| | O—S | 2.35 | 3.42 |
| | C—S | 3.51 | 3.88 |
| **Mero—$Ldt_{Mt2}$—water** | C—O | 3.25 | 3.31 |
| | O—S | 2.35 | 3.30 |
| | C—S | 3.51 | 3.81 |
| **Tebi—$Ldt_{Mt2}$—water** | C—O | 3.24 | 4.45 |
| | O—S | 2.35 | 3.30 |
| | C—S | 3.51 | 3.76 |

**The hydrogen bond interactions of carbapenem—$Ldt_{Mt2}$—water complexes**

Bridging water molecules are of great significance in protein active site and they can also regulate the number of hydrogen bond interactions between the protein and ligands[18]. It is evident that water molecule interacted with both the carbapenems and $Ldt_{Mt2}$ by forming crucial

H-bond links that significantly stabilized the complex and improved the correlation between theoretical and the experimental binding free energy results (**Table 1**). The water molecule interacts (H-bond) with the hydroxyethyl group of the carbapenems while the oxygen of water also forms a H-bond with the carbonyl oxygen of carbapenems. The Ser192 and Asn207 serve as hydrogen donors to the carbapenem while Thr171 forms hydrophobic interaction with the carboxyl group of carbapenem and Cys205 serve as a H-bond acceptor (**Figure 2**). Also see other data in **Figure 1S**. In **Figure 2**, the hydrogen bond interactions of carbapenem-$Ldt_{Mt2}$ complexes obtained after geometry optimization (frequency calculations). The water molecule served as H-bond donor-acceptor in this scenario. To further examine the nature of binding interactions, the LigPlot[50] program was used to plot the electrostatic and hydrogen bond interactions for $Ldt_{Mt2}$ complexed with carbapenems. The plots are depicted in **Figure 3** and in the supplementary material (**Figure 2S**).

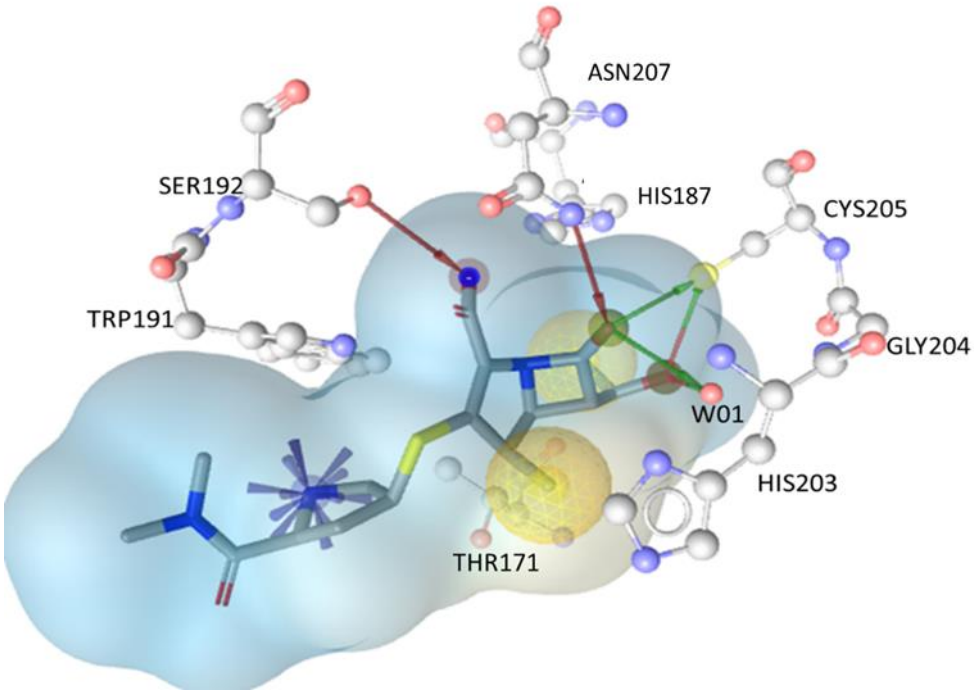


**Figure 2.** 3-D structural features of **t**he hydrogen bond and hydrophobic interactions of carbapenems, $Ldt_{Mt2}$ and the water molecule (W01).

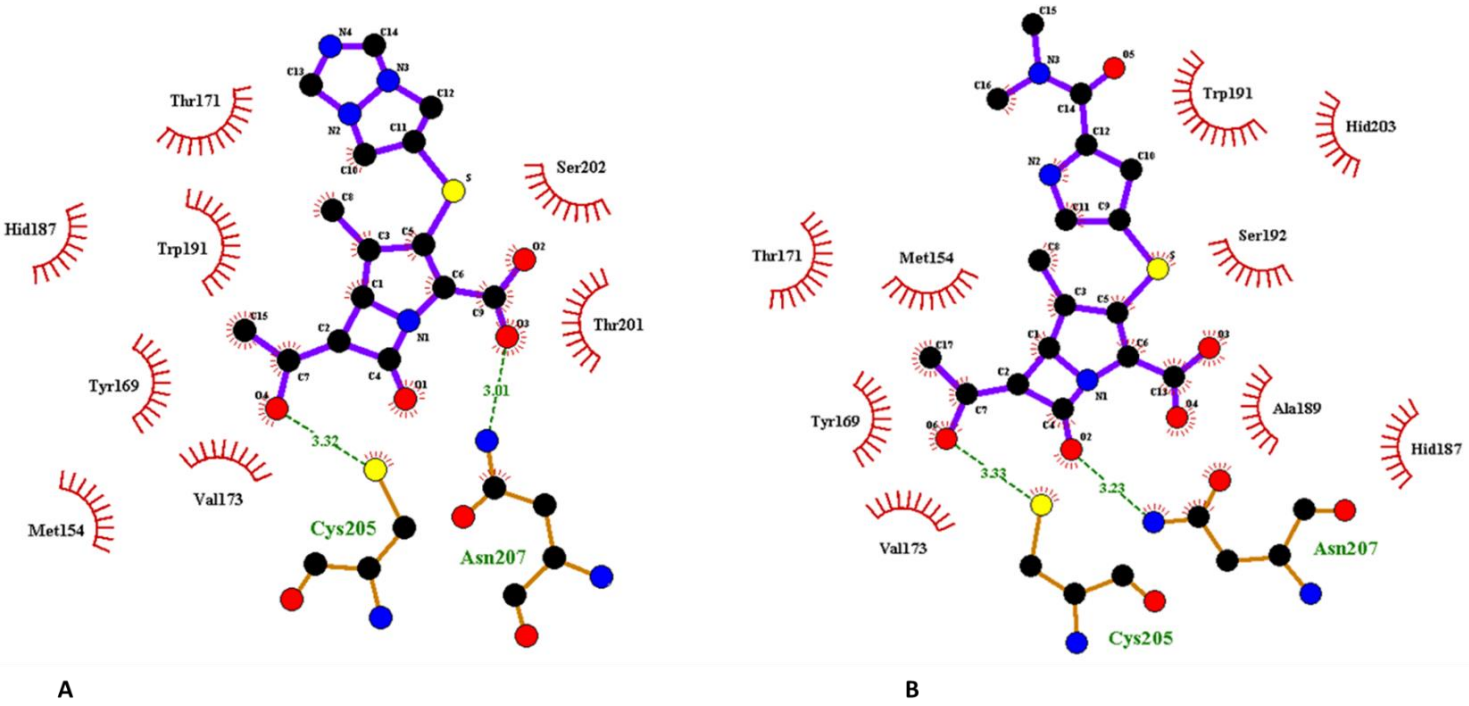


**Figure 3.** 2-D schematic representation of hydrogen bond and hydrophobic interactions between catalytic amino acid residues and the carbapenems (**A.** Biapenem and **B.** Meropenem). Red dotted lines represent hydrogen bond interactions.

### QTAIM analysis

The quantum theory of atoms in molecules (QTAIM) have been applied to describe and calculate the H-bond interactions for carbapenem-$Ldt_{Mt2}$ complexes[51, 52]. From the last optimized geometry of the carbapenem-$Ldt_{Mt2}$ complexes, the QM region comprising of the active site residues (His187, Ser188, His203, Cys205 and Asn207) and the selected carbapenems, were used to calculate the wave function using B3LYP/6-31G+(d). The resulting wave function output files were then employed to perform *ab initio* calculations to generate the electron topography of carbapenem-$Ldt_{Mt2}$ complexes using AIM2000 software package[53]. The topological parameters of these complexes were collected and analysed at each bond critical point (BCP) as shown by **HB** in **Figure 3** (**a.** Imi-$Ldt_{Mt2}$ and **b.** Bia-$Ldt_{Mt2}$ complexes). The topological parameters for the carbapenem-$Ldt_{Mt2}$ complexes are tabulated in **Table 2**. In general, the existence of hydrogen bonds are assumed by electron density $\rho(r)$ and Laplacian of electron density $\nabla^2 \rho(r)$ values that range between 0.002-0.035 a.u and 0.024-0.139 a.u., respectively[54].

The reported data for the $\rho(r)$ and $\nabla^2 \rho(r)$ in **Table 2** differs according to each bond critical point it was collected from as denoted by **HB**'s. However, the standard measure for both the $\rho(r)$ and $\nabla^2 \rho(r)$ in the carbapenem-$Ldt_{Mt2}$ complexes range from 0.0001-0.0434 and 0.0003-

0.1194 a.u, respectively. The $\rho(r)$ and $\nabla^2 \rho(r)$ shows the strength of the hydrogen bond interactions and validate the presence of hydrogen bonds at each BCP as shown in **Figure 4.**

It was observed in all complexes that both strong and weaker binders, the hydrogen bonds in the QM region, have more strength as measured by $\rho(r)$ and $\nabla^2 \rho(r)$ values in **Table 2**. It is worth noting that the sign of $\nabla^2 \rho(r)$ determines the charge density whether it is locally depleted $\nabla^2 \rho(r)>0$, or locally concentrated $\nabla^2 \rho(r)<0$. Furthermore, the strength of the hydrogen bonds is also determined by the $H(r)<0$ and $\nabla^2 \rho(r)<0$ for strong hydrogen bonds, while $H(r)<0$ and $\nabla^2 \rho(r)>0$, determine medium hydrogen bonds and $H(r)>0$, and $\nabla^2 \rho(r)>0$ denotes weak hydrogen bond interactions[48]. The sign of the $\nabla^2 \rho(r)$ and $H(r)$ values (**Table 2**) indicate the nature of the bonds i.e. positive value of $\nabla^2 \rho(r)$ and the negative value of $H(r)$ indicates that the bond type is partially covalent-partially electrostatic (Pc-Pe)[55]. See details for other complexes in **Table 1S**.

**Table 3**. AIM topological parameters of carbapenem—$Ldt_{Mt2}$ complexes calculated at the B3LYP/6-31+G(d). Electron density (**ρ**) and their Laplacian of electron density (**$\nabla^2\rho$**) in a.u. and energetic parameters **G(r)**, **H(r)**, and **V(r)** in (kcal/mol)

| Hydrogen bonds | Complexes interactions | ρ (r) | $\nabla^2\rho$ (r) | G(r) | H(r) | V(r) | Ellipticity (ε) |
|---|---|---|---|---|---|---|---|
| | **Imi—$Ldt_{Mt2}$** | | | | | | |
| **HB1** | $C_{80}H\cdots C_{39}$ | 0.0001 | 0.0003 | 0.00005 | -0.00003 | 0.00002 | 2.7859 |
| **HB2** | $O_{71}\cdots H_{34}C$ | 0.0169 | 0.0559 | 0.0137 | -0.0003 | 0.0134 | 0.0430 |
| **HB3** | $O_{90}\cdots H_{72}O$ | 0.0217 | 0.0723 | 0.0184 | 0.0003 | 0.0187 | 0.0270 |
| **HB4** | $O_{82}\cdots H_{73}O$ | 0.0329 | 0.1064 | 0.0274 | 0.0008 | 0.0282 | 0.1092 |
| **HB5** | $O_{71}\cdots H_{30}N$ | 0.0143 | 0.0526 | 0.0124 | -0.0007 | 0.0117 | 0.0865 |
| **HB6** | $O_{90}H\cdots S_{53}$ | 0.0198 | 0.0495 | 0.0127 | 0.0004 | 0.0131 | 0.0271 |
| **HB7** | $O_{108}\cdots H_{67}N$ | 0.0163 | 0.0644 | 0.0149 | -0.0012 | 0.0137 | 0.0370 |
| **HB8** | $C_{89}H\cdots C_{11}$ | 0.0050 | 0.0162 | 0.0030 | -0.0010 | 0.0020 | 0.2725 |
| | **Bia—$Ldt_{Mt2}$** | | | | | | |
| **HB1** | $C_{83}H\cdots C_{39}$ | 0.0027 | 0.0095 | 0.0018 | -0.0006 | 0.0012 | 1.0611 |
| **HB2** | $S_{71}\cdots H_{40}C$ | 0.0009 | 0.0026 | 0.0005 | -0.0002 | 0.0003 | 1.4043 |
| **HB3** | $C_{77}H\cdots O_{115}$ | 0.0060 | 0.0213 | 0.0043 | -0.0010 | 0.0033 | 0.4363 |
| **HB4** | $O_{107}\cdots H_{115}O$ | 0.0247 | 0.0794 | 0.0206 | 0.0007 | 0.0213 | 0.0875 |
| **HB5** | $O_{115}\cdots H_{34}C$ | 0.0192 | 0.0630 | 0.0157 | -0.00004 | 0.0157 | 0.0739 |
| **HB6** | $O_{72}\cdots H_{117}O$ | 0.0233 | 0.0760 | 0.0194 | 0.0004 | 0.0199 | 0.0422 |
| **HB7** | $O_{115}H\cdots S_{53}$ | 0.0093 | 0.0368 | 0.0075 | -0.0016 | 0.0059 | 0.5410 |
| **HB8** | $O_{72}\cdots H_{30}N$ | 0.0086 | 0.0333 | 0.0074 | -0.0010 | 0.0064 | 0.0579 |
| **HB9** | $O_{107}H\cdots S_{53}$ | 0.0205 | 0.0516 | 0.0134 | 0.0005 | 0.0138 | 0.0484 |
| **HB10** | $C_{105}H\cdots C_{11}$ | 0.0065 | 0.0218 | 0.0042 | -0.0013 | 0.0029 | 0.0332 |
| **HB11** | $C_{84}O\cdots H_{67}N$ | 0.0136 | 0.0549 | 0.0124 | -0.0013 | 0.0111 | 0.0962 |

KEG, Lagrangian kinetic energy density ***G(r)***, KEK, Hamiltonian kinetic energy density ***H(r)***, VIR, Virial filed function ***V(r)***.

## NBO analysis

The last optimized ground state geometries of the QM region of the carbapenem-$Ldt_{Mt2}$ complexes were used to calculate the distribution of electron density in atoms using the B3LYP/6-311+G(d). In the NBO analysis[46], occupied Lewis and a set of unoccupied non-Lewis localized orbitals are explained based on the electronic wave function. The NBO donor-acceptor (bond-antibonding) interactions were assessed. The strengths of the delocalization interactions $E^{(2)}$ are approximated by second order perturbation theory[46]. The stabilization energies associated with delocalization of electrons in the strongest in **HB**'s with S···· H─O

and O···H—O type of interactions being mediated by water across all the carbapenem-$Ldt_{Mt2}$ complexes. In the Imi-$Ldt_{Mt2}$ complex, the dominant interatomic interactions are observed in **HB2**, **HB3**, **HB6** and **HB7**. For Tebi-$Ldt_{Mt2}$, it was demonstrated that **HB4**, **HB5** and **HB9** have the strongest stabilization energy as shown in **Table 3**.

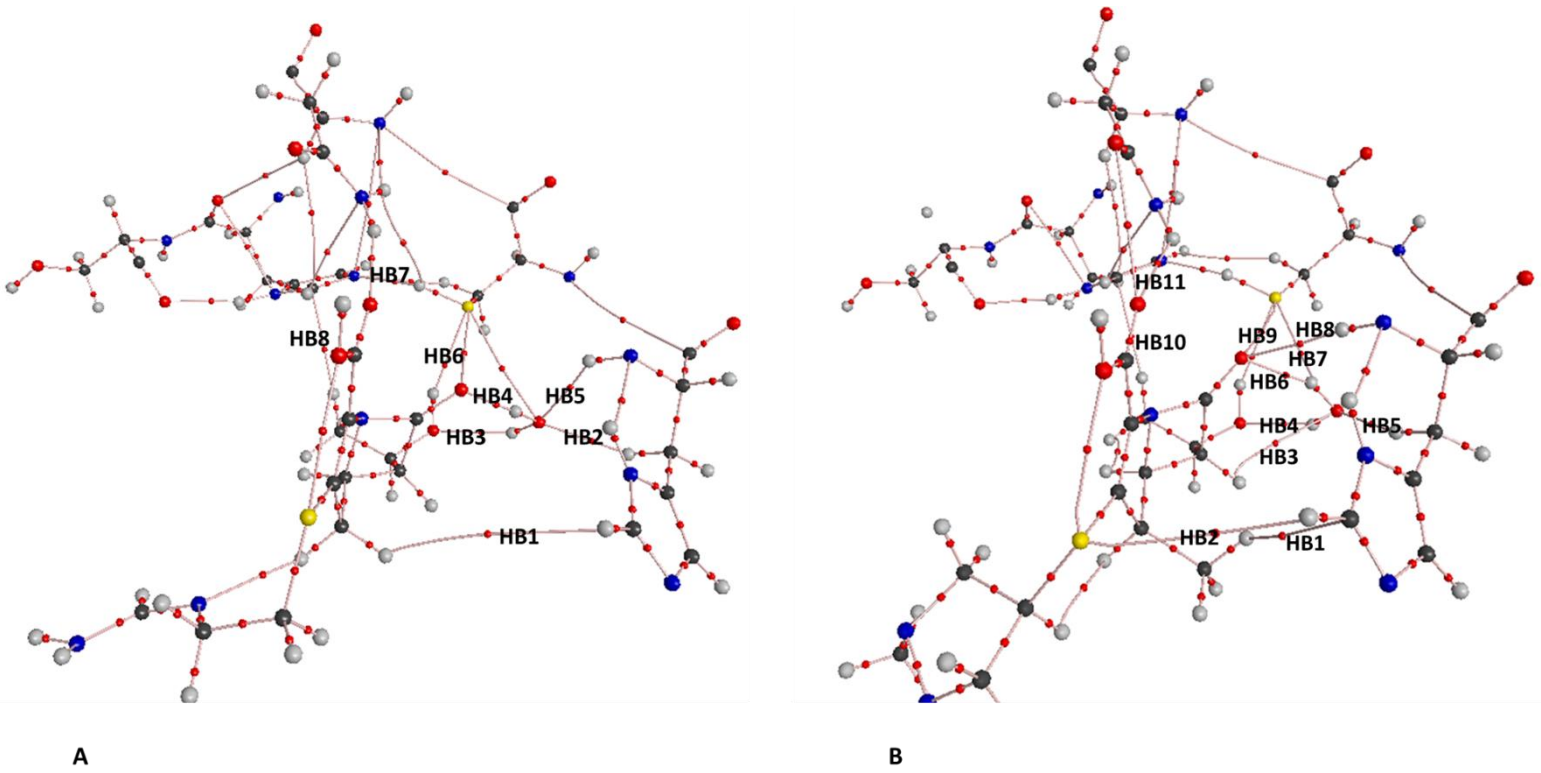


**Figure 4**. Molecular graph of **A**. Imi—$Ldt_{Mt2}$ and **B**. Bia—$Ldt_{Mt2}$ complexes generated using AIM2000 software. Small red spheres and lines correspond to the bond critical points (BCP) and the bond paths, respectively. See details of the molecular graph for other complexes in **Figure 3S**

It is worth pointing out that other **HB**'s from carbapenem-$Ldt_{Mt2}$ complexes contributed significantly in electron charge transfer. This observation reveals that there was a great deal of electron charge transfer from donor to acceptor units in the presence of water molecule (**Table 3**). The charge transfer between the lone pair (LP) and the anti-bonding (BD*) orbitals are shown in **Figure 5** and **Figure 4S**. The hydrogen bonds between interacting atoms provide satisfactory evidence for significant electron charge transfer from the lone pair orbital to anti-bonding orbital. Therefore, the NBO analysis corresponds with the QTAIM results in qualifying the stability of the carbapenem-$Ldt_{Mt2}$ complexes as represented by the ONIOM Gibbs binding free energies.

**Table 4**. Second-order perturbation energies E $^{(2)}$ (kcal mol$^{-1}$) corresponding to the most important charge transfer interaction (donor→ acceptor) in the carbapenem-$Ldt_{Mt2}$ complexes at the B3LYP/6-31+G (d) level. **Table 1S**

| **Complex/ Interactions** | **Donor NBO(*i*) *n*(O)** | **Acceptor NBO(*j*) σ*(O─H)** | ***E*** $^{(2)}$ **(kcalmol$^{-1}$) (O)→σ*(O─H)** |
|---|---|---|---|
| **Imi—$Ldt_{Mt2}$** | | | |
| **HB1** | BD (1) C80─H88 | BD*(1) C39─H40 | - |
| **HB2** | BD (1) O71 | BD*(1) C33─H34 | 0.13 |
| | LP (1) O71 | BD*(1) C33─H34 | 5.06 |
| **HB3** | BD (1) O90─H107 | BD*(1) O71─H72 | 0.20 |
| | LP (1) O90 | BD*(1) O71─H72 | 2.06 |
| | LP (2) O90 | BD*(1) O71─H72 | 4.35 |
| **HB4** | BD (1) C76─O82 | BD*(1) O71─H73 | 0.22 |
| **HB5** | BD (1) N29─H30 | BD*(1) O71─H72 | 0.27 |
| | BD (1) O71─H72 | BD*(1) N29─H30 | 0.23 |
| | LP (1) O71 | BD*(1) N29─H30 | 1.67 |
| | LP (2) O71 | BD*(1) N29─H30 | 0.77 |
| **HB6** | BD (1) S53─H54 | BD*(1) O90─H107 | 0.20 |
| | LP (1) S53 | BD*(1) O90─H107 | 1.10 |
| | LP (1) S53 | BD*(1) O90─H107 | 12.11 |
| **HB7** | BD (1) C81─H108 | BD*(1) N66─H67 | 0.12 |
| | LP (1) O108 | BD*(1) N66─H67 | 6.34 |
| | LP (2) O108 | BD*(1) N66─H67 | 0.10 |
| **HB8** | BD (1) C11─N13 | BD*(1) C89─H94 | 0.20 |
| | BD (2) C11─N13 | BD*(1) C89─H94 | 0.26 |
| | BD (2) C11─N13 | BD*(1) C89─H94 | 0.27 |

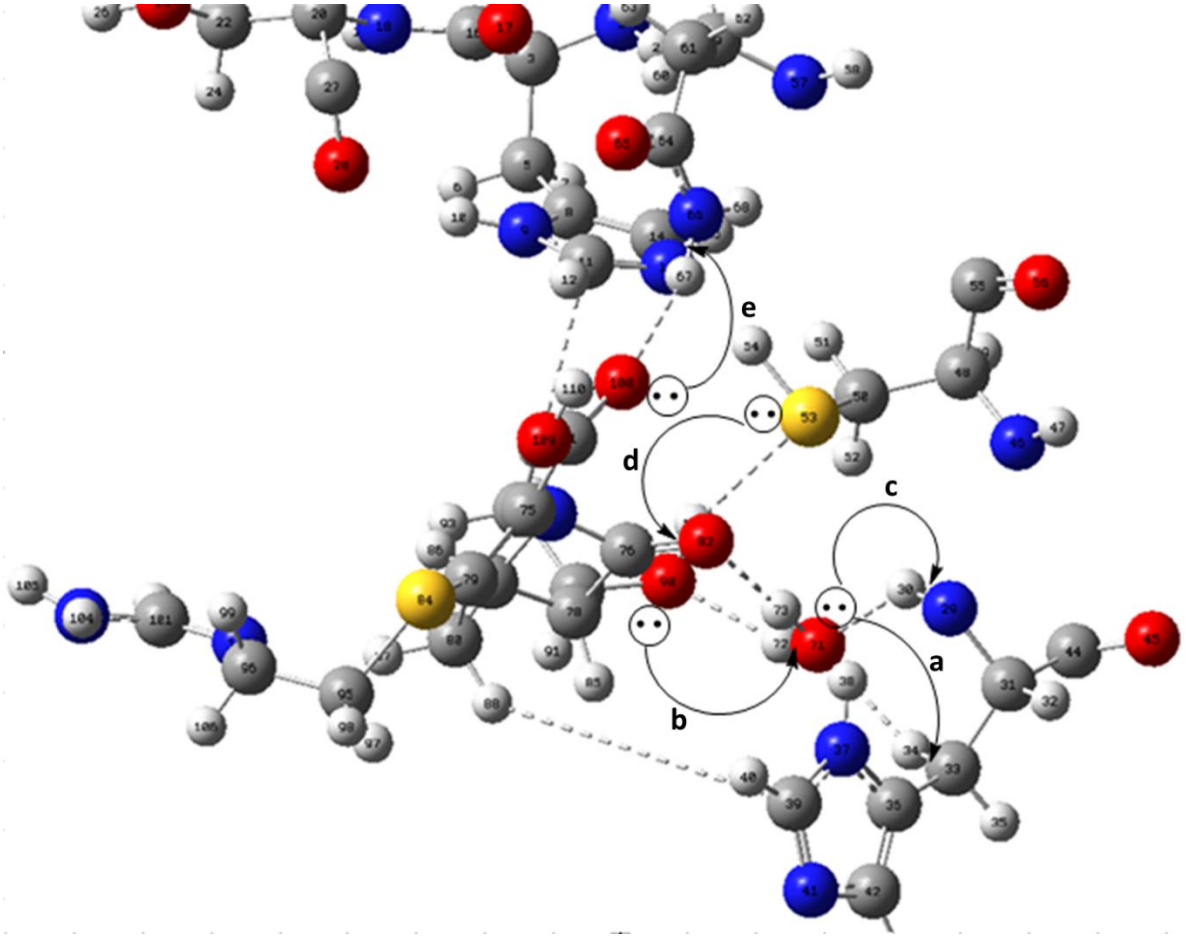


**Figure 5**. Depiction of electron transfers for Imi—$Ldt_{Mt2}$ complex derived by second-order perturbation theory of NBO analysis. The curved arrows (**a, b, c, d** and **e**) depict the direction of charge transfer: (**a**) LP (O) → σ* (C─H) (**b**) LP (O) → σ* (O─H) (**c**) LP (O) → σ* (N─H) (**d**) LP (S) → σ* (O─H) and (**e**) LP (O) → σ* (N─H) listed in **Table 3**. See other depictions in **Figure 4S.**

## 4.0 Conclusion

In this study, the role of the catalytic water molecule at the protein active site of $Ldt_{Mt2}$ complexed with four FDA approved carbapenems. A two-layered ONIOM method was applied to evaluate the effect of bridging water molecule in the protein-inhibitor interface. In the context of the binding event, the solvent plays a significant role in the interactions. The results for Tebi-$Ldt_{Mt2}$, Imi-$Ldt_{Mt2}$, Mero-$Ldt_{Mt2}$ and Bia-$Ldt_{Mt2}$ complexes reflect reasonable Gibb's binding free energies which corresponded with the experimental data with exceptions of two outliers. The Gibb's order for the binding free energies of Tebi-$Ldt_{Mt2}$ and Bia-$Ldt_{Mt2}$ complexes was reversed. The contribution of the water molecule in mediating hydrogen bond formation/breaking varied significantly in each carbapenem-$Ldt_{Mt2}$ complex as seen in the binding free energy results. It is worth mentioning that the distance between carbapenem; water and the protein have a significant impact in binding free energy. The QTAIM and NBO

analysis were carried out to assess the hydrogen bond interactions and delocalization of electron charge, respectively, to ascertain the nature and stability of hydrogen bond interactions and electron charge transfer in the protein-ligand-water interfaces.

The precision of the water modelling is vital for accurate prediction of binding free energy and insightful binding kinetics of ligands. The data provided in this study can be used to improve the reliability of the computational model by using suitable methods for calculating the energy contribution of water molecules in the protein-ligand complexes. Future studies should determine whether any of these precomplexes are trapped in a local minimum and if that can be overcome by optimising all complexes with the same constrained interatomic distances (see **Table 2**). Alternatively, the activation energies of the bond formation step should be calculated.

## Competing interests

The authors declare that they have no competing interests.

## Acknowledgements

We thank the College of Health Sciences (CHS) and National Research Foundation (NRF) for financial support. We are also grateful to the CHPC (www.chpc.ac.za) for computational resources.

# References


[1] Fauci, A. S., and Group, N. T. W. (2008) Multidrug-resistant and extensively drug-resistant tuberculosis: the National Institute of Allergy and Infectious Diseases Research agenda and recommendations for priority research, *J Infect Dis. 197*, 1493-1498.

[2] Gandhi, N. R., Nunn, P., Dheda, K., Schaaf, H. S., Zignol, M., Van Soolingen, D., Jensen, P., and Bayona, J. (2010) Multidrug-resistant and extensively drug-resistant tuberculosis: a threat to global control of tuberculosis, *The Lancet 375*, 1830-1843.

[3] Mainardi, J.-L., Villet, R., Bugg, T. D., Mayer, C., and Arthur, M. (2008) Evolution of peptidoglycan biosynthesis under the selective pressure of antibiotics in Gram-positive bacteria, *FEMS microbiology reviews 32*, 386-408.

[4] Lavollay, M., Arthur, M., Fourgeaud, M., Dubost, L., Marie, A., Veziris, N., Blanot, D., Gutmann, L., and Mainardi, J.-L. (2008) The peptidoglycan of stationary-phase Mycobacterium tuberculosis predominantly contains cross-links generated by L, D-transpeptidation, *J. Bacteriol. 190*, 4360-4366.

[5] Erdemli, S. B., Gupta, R., Bishai, W. R., Lamichhane, G., Amzel, L. M., and Bianchet, M. A. (2012) Targeting the cell wall of Mycobacterium tuberculosis: structure and mechanism of L,D-transpeptidase 2, *Struct. 20*, 2103-2115.

[6] Fisher, J. F., Meroueh, S. O., and Mobashery, S. (2005) Bacterial resistance to β-lactam antibiotics: compelling opportunism, compelling opportunity, *Chem. Rev. 105*, 395-424.

[7] Walsh, C. (2003) *Antibiotics: actions, origins, resistance*, American Society for Microbiology (ASM), Washington.

[8] Hugonnet, J.-E., Tremblay, L. W., Boshoff, H. I., Barry, C. E., and Blanchard, J. S. (2009) Meropenem-Clavulanate Is Effective Against Extensively Drug-Resistant Mycobacterium tuberculosis, *Science 323*, 1215-1218.

[9] Cordillot, M., Dubée, V., Triboulet, S., Dubost, L., Marie, A., Hugonnet, J.-E., Arthur, M., and Mainardi, J.-L. (2013) In vitro cross-linking of Mycobacterium tuberculosis peptidoglycan by l, d-transpeptidases and inactivation of these enzymes by carbapenems, *Antimicrob. Agents Chemother. 57*, 5940-5945.

[10] Rullas, J., Dhar, N., McKinney, J. D., García-Pérez, A., Lelievre, J., Diacon, A. H., Hugonnet, J.-E., Arthur, M., Angulo-Barturen, I., and Barros-Aguirre, D. (2015) Combinations of β-Lactam Antibiotics Currently in Clinical Trials Are Efficacious in a DHP-I-Deficient Mouse Model of Tuberculosis Infection, *Antimicrob. Agents Chemother. 59*, 4997-4999.

[11] Horita, Y., Maeda, S., Kazumi, Y., and Doi, N. (2014) In vitro susceptibility of Mycobacterium tuberculosis isolates to an oral carbapenem alone or in combination with β-lactamase inhibitors, *Antimicrob. Agents Chemother. 58*, 7010-7014.

[12] Kaushik, A., Makkar, N., Pandey, P., Parrish, N., Singh, U., and Lamichhane, G. (2015) Carbapenems and rifampin exhibit synergy against Mycobacterium tuberculosis and Mycobacterium abscessus, *Antimicrob. Agents Chemother. 59*, 6561-6567.

[13] Silva, J. R. A., Govender, T., Maguire, G. E., Kruger, H. G., Lameira, J., Roitberg, A. E., and Alves, C. N. (2015) Simulating the inhibition reaction of Mycobacterium tuberculosis L, D-transpeptidase 2 by carbapenems, *Chem. Commun. 51*, 12560-12562.

[14] Silva, J. R. A., Bishai, W. R., Govender, T., Lamichhane, G., Maguire, G. E., Kruger, H. G., Lameira, J., and Alves, C. N. (2016) Targeting the cell wall of Mycobacterium tuberculosis: a molecular modeling investigation of the interaction of imipenem and meropenem with L, D-transpeptidase 2, *J. Biomol. Struct. Dyn. 34*, 304-317.

[15] Fakhar, Z., Govender, T., Maguire, G. E. M., Lamichhane, G., Walker, R. C., Kruger, H. G., and Honarparvar, B. (2017) Differential flap dynamics in l,d-transpeptidase2 from mycobacterium tuberculosis revealed by molecular dynamics, *Molecular BioSystems 13*, 1223-1234.

[16] Townsend, C. A., Lloyd, E. P., Lamichhane, G., Saavedra, H., Basta, L. A. B., Bianchet, M. A., Kumar, P., Mattoo, R., and Pan, Y. H. (2017) Structural insight into the inactivation of Mycobacterium

tuberculosis non-classical transpeptidase Ldt Mt2 by biapenem and tebipenem, *BMC biochemistry 18*, 8.

[17] Lu, S. Y., Jiang, Y. J., Lv, J., Zou, J. W., and Wu, T. X. (2011) Role of bridging water molecules in GSK3β-inhibitor complexes: Insights from QM/MM, MD, and molecular docking studies, *J. Comput. Chem. 32*, 1907-1918.

[18] Duan, L., Feng, G., Wang, X., Wang, L., and Zhang, Q. (2017) Effect of electrostatic polarization and bridging water on CDK2–ligand binding affinities calculated using a highly efficient interaction entropy method, *Phys. Chem. Chem. Phys. 19*, 10140-10152.

[19] Li, W.-J., Li, D.-F., Hu, Y.-L., Zhang, X.-E., Bi, L.-J., and Wang, D.-C. (2013) Crystal structure of L, D-transpeptidase LdtMt2 in complex with meropenem reveals the mechanism of carbapenem against Mycobacterium tuberculosis, *Cell research 23*, 728.

[20] The PyMOL Molecular Graphics System, V. S., LLC.

[21] Case, D., Darden, T., Cheatham III, T., Simmerling, C., Wang, J., Duke, R., Luo, R., Crowley, M., Walker, R., and Zhang, W. (2008) AMBER, version 10, *University of California: San Francisco, CA*.

[22] Hornak, V., Abel, R., Okur, A., Strockbine, B., Roitberg, A., Simmerling, C. (2006) Comparison of multiple Amber force fields and development of improved protein backbone parameters, *Proteins. Discipline. Protein biochemistry. 65*, 712-725.

[23] Wang, J. M., Wolf, R. M., Caldwell, J. W., Kollman, P. A., Case, D. A. . (2004) Development and testing of a general amber force field, *J. Comput. Chem. 25*, 1157–1174.

[24] Jorgensen, W. L., Chandrasekhar, J., Madura, J. D., Impey, R. W., and Klein, M. L. (1983) Comparison of simple potential functions for simulating liquid water, *J. Chem. Phys. 79*, 926-935.

[25] Harvey M. J., F. G. D. (2009) An Implementation of the Smooth Particle Mesh Ewald Method on GPU Hardware, *J. Chem. Theory Comput 5*, 2371–2377.

[26] Ryckaert, J. P., Ciccotti, G., Berendsen, H. J. C. . (1977) Numerical integration of the cartesian equations of motion of a system with constraints: Molecular dynamics of N-alkanes, *J. Comput. Phys. 23*, 327–341.

[27] Li, H., Robertson, A. D., and Jensen, J. H. (2005) Very fast empirical prediction and rationalization of protein pKa values, *Proteins. Discipline. Protein biochemistry. 61*, 704-721.

[28] Dapprich, S., Komáromi, I., Byun, K. S., Morokuma, K., and Frisch, M. J. (1999) A new ONIOM implementation in Gaussian98. Part I. The calculation of energies, gradients, vibrational frequencies and electric field derivatives, *Comput. Theor. Chem. 461*, 1-21.

[29] Svensson, M., Humbel, S., Froese, R. D., Matsubara, T., Sieber, S., and Morokuma, K. (1996) ONIOM: A multilayered integrated MO+ MM method for geometry optimizations and single point energy predictions. A test for Diels-Alder reactions and Pt (P (t-Bu) 3) 2+ H2 oxidative addition, *J. Phys. Chem. 100*, 19357-19363.

[30] Vreven, T., and Morokuma, K. (2000) On the application of the IMOMO (integrated molecular orbital+ molecular orbital) method, *J. Comput. Chem. 21*, 1419-1432.

[31] Karadakov, P. B., and Morokuma, K. (2000) ONIOM as an efficient tool for calculating NMR chemical shielding constants in large molecules, *Chem. Phys. Lett. 317*, 589-596.

[32] Banáš, P., Jurečka, P., Walter, N. G., Šponer, J., and Otyepka, M. (2009) Theoretical studies of RNA catalysis: hybrid QM/MM methods and their comparison with MD and QM, *Methods 49*, 202-216.

[33] Kapp, J., Remko, M., and Schleyer, P. v. R. (1996) H2XO and (CH3) 2XO Compounds (X= C, Si, Ge, Sn, Pb): Double Bonds vs Carbene-Like Structures Can the Metal Compounds Exist at All?, *J. Am. Chem. Soc. 118*, 5745-5751.

[34] Remko, M., Walsh, O. A., and Richards, W. G. (2001) Theoretical study of molecular structure, tautomerism, and geometrical isomerism of moxonidine: Two-layered ONIOM calculations, *J. Phys. Chem. A 105*, 6926-6931.

[35] Johnson, B. G., Gill, P. M., and Pople, J. A. (1993) The performance of a family of density functional methods, *J. Chem. Phys. 98*, 5612-5626.
[36] Humbel, S., Sieber, S., and Morokuma, K. (1996) The IMOMO method: Integration of different levels of molecular orbital approximations for geometry optimization of large systems: Test for n-butane conformation and SN2 reaction: RCl+ Cl−, *J. Chem. Phys. 105*, 1959-1967.
[37] Morokuma, K. (2009) Theoretical studies of structure, function and reactivity of molecules— A personal account, *Proc Jpn Acad Ser B Phys Biol Sci 85*, 167-182.
[38] Kohn, W., Becke, A. D., and Parr, R. G. (1996) Density functional theory of electronic structure, *J. Phys. Chem. 100*, 12974-12980.
[39] Neumann, R., Nobes, R. H., and Handy, N. C. (1996) Exchange functionals and potentials, *Mol. Phys. 87*, 1-36.
[40] Becke, A. D. (1993) Density-functional thermochemistry. III. The role of exact exchange, *J. Chem. Phys. 98*, 5648-5652.
[41] Lee, C., Yang, W., and Parr, R. G. (1988) Development of the Colle-Salvetti correlation-energy formula into a functional of the electron density, *Physical review B 37*, 785.
[42] Hariharan, P. C., and Pople, J. A. (1973) The influence of polarization functions on molecular orbital hydrogenation energies, *Theoretica chimica acta 28*, 213-222.
[43] Rassolov, V. A., Pople, J. A., Ratner, M. A., and Windus, T. L. (1998) 6-31G* basis set for atoms K through Zn, *J. Chem. Phys. 109*, 1223-1229.
[44] Vreven, T., Byun, K. S., Komáromi, I., Dapprich, S., Montgomery, J. A., Morokuma, K., and Frisch, M. J. (2006) Combining quantum mechanics methods with molecular mechanics methods in ONIOM, *J. Chem. Theo. Comp. 2*, 815-826.
[45] Reed, A. E., Curtiss, L. A., and Weinhold, F. (1988) Intermolecular interactions from a natural bond orbital, donor-acceptor viewpoint, *Chem. Rev. 88*, 899-926.
[46] Weinhold, F., and Glendening, E. D. (2001) NBO 5.0 Program Manual: Natural Bond Orbital Analysis Programs, *Theoretical Chemistry Institute and Department of Chemistry, University of Wisconsin, Madison, WI 53706*.
[47] Bader, R. F. (1990) Atoms in Molecules: a quantum theory, International series of monographs on chemistry, 22, *Oxford University Press, Oxford Henkelman G, Arnaldsson A, Jónsson H (2006) A fast and robust algorithm for Bader decomposition of charge density. Comput Mater Sci 36*, 354-360.
[48] Bader, R. AIM2000 Program Package, Version 2.0; McMaster University: Hamilton, Ontario, Canada, 2002, *There is no corresponding record for this reference*.
[49] Laskowski, R. A., and Swindells, M. B. . (2011) Journal of Chemical Information and Modeling, *LigPlot+: multiple ligand–protein interaction diagrams for drug discovery 51*, 2778-2786.
[50] Bader, R., and Molecules, A. I. (1990) A quantum theory, *Clarendon: Oxford, UK*.
[51] Parthasarathi, R., Amutha, R., Subramanian, V., Nair, B. U., and Ramasami, T. (2004) Bader's and reactivity descriptors' analysis of DNA base pairs, *J. Phys. Chem. A 108*, 3817-3828.
[52] Biegler-Konig, F., Schonbohm, J., and Bayles, D. (2001) Software news and updates-AIM2000-A program to analyze and visualize atoms in molecules, pp 545-559, John Wiley & Sons Inc 605 THIRD AVE, NEW YORK, NY 10158-0012 USA.
[53] Popelier, P. (1998) Characterization of a dihydrogen bond on the basis of the electron density, *J. Phys. Chem. A 102*, 1873-1878.
[54] Nazari, F., and Doroodi, Z. (2010) The substitution effect on heavy versions of cyclobutadiene, *Int. J. Quantum Chem. 110*, 1514-1528.

# CHAPTER FOUR

# CONCLUSION

Understanding the inactivation mechanisms of carbapenems against L, D transpeptidase 2 ($Ldt_{Mt2}$) is of great importance. In this regard, carbapenems have been shown to have a remarkable activity against L, D-transpeptidases, particularly $Ldt_{Mt2}$. In this thesis, a highly efficient hybrid ONIOM approach was applied to investigate the no-covalent interactions in carbapenems— $Ldt_{Mt2}$ complexes which regulates the efficiency of carbapenems against $Ldt_{Mt2}$.

A comprehensive study established in chapter two of this thesis examined the binding free energies of the carbapenems against the significant non-classical L, D-Transpeptidase 2 from *Mycobacterium tuberculosis* using a hybrid two-layered ONIOM approach. The QM/MM geometry optimization of the four FDA approved carbapenems complexed with $Ldt_{Mt2}$ were performed using hybrid two-layered ONIOM (B3LYP/6-31G+(d):AMBER) model, where the density functional theory [B3LYP/6-31G(d)] was used for QM region and MM region evaluated with Amber force field. It was observed that the theoretically calculated relative binding free energies ($\Delta G$) for FDA approved carbapenems complexed with $Ldt_{Mt2}$ correspond with the experimentally observed data.

In addition, the important amino acid residues which were in proximity with the ligand were involved in hydrogen bond formation which thus had a significant contribution in the Gibbs binding free energies and stability of the complexes. The quantum theory of atoms in molecules (QTAIM) authenticated the existence of hydrogen bond interactions. Furthermore, the stabilization energy, $E^{(2)}$, obtained by NBO second-perturbation energy analysis revealed the electron charge transfer between carbapenems and active residues of $Ldt_{Mt2}$. These analyses agreed in principle with the calculated Gibb's binding free energies. For further model refinement to justify our observation, we investigated the water involvement in the binding site by adding explicit water molecule in the active site to ascertain more insight in the binding process.

The role of water molecules in drug design is increasingly being considered to strengthen the binding kinetics of the ligands. Previously, our group explored the six-membered ring mechanistic study involving catalytic water and the observed thermochemical outcomes revealed the significance of water which motivated us to consider water molecule in this study.

A study established in chapter three of this thesis demonstrated the effect of water confined in the active site of $Ldt_{Mt2}$ complexed with carbapenems. The water molecule, active site residues and carbapenem were considered at the QM [B3LYP/6-31G(d)] level of theory. It was revealed that the calculated relative binding free energies for the carbapenem—$Ldt_{Mt2}$—water complexes followed the experimental trend, exceptions for two outliers. The trend in Bia—$Ldt_{Mt2}$ and Tebi—$Ldt_{Mt2}$ was reversed. Also, the distance discrepancies between the carbonyl carbon of *β*-lactam ring (**C**), water (**O**) and sulfur atom of cysteine residue (**S**) demonstrated a significant contribution to the binding free energies ($\Delta G$). In addition, the QTAIM and NBO analysis revealed the great deal of hydrogen bond interactions and electron charge delocalization in the interface that contributed to the binding free energies ($\Delta G$). This analysis corroborated with the reported theoretical and experimental results.

In conclusion, the overall calculated binding free energies reported in this study for carbapenem─$Ldt_{Mt2}$ complexes correlated with the experimental data except for two outliers evaluated and discussed in chapter three of this thesis. Also, this could infer from our study that ONIOM approach can be used as a reliable molecular orbital technique to compute the binding free energies for carbapenem─$Ldt_{Mt2}$ complexes. The data obtained in this study can be tailored for rational drug design of potent therapeutic drugs for TB.

**Recommendation**

Future studies should involve the optimization of inhibitor plus one water molecule precomplexes with the same constrained interatomic distances since it seems that some of them are trapped in a local minimum. Afterwards, the optimization of these complexes without any constraints must be performed to observe if the energies then follow experiment. Alternative, the activation energies of the bond formation in the acylation step should be calculated. Also, to validate the potential role of water in the reaction mechanism, the activation energies for these inhibitors can be calculated the using a 6-membered ring TS model with water and the enzyme residues.

# APPENDIX A

## Supplementary Material for Chapter Two

## ONIOM study of the binding interaction energies for the carbapenems complexed with L, D-Transpeptidase 2 from *Mycobacterium tuberculosis*

**Thandokuhle Ntombela, [a] Zeynab Fakhar, [b] Collins U. Ibeji, [a] Thavendran Govender, [a] Glenn E. M. Maguire, [a, c] Gyanu Lamichhane, [d] Hendrik G. Kruger[a*] and Bahareh Honarparvar[a*]**

The supplementary material for the investigated carbapenem—$Ldt_{Mt2}$ complexes.

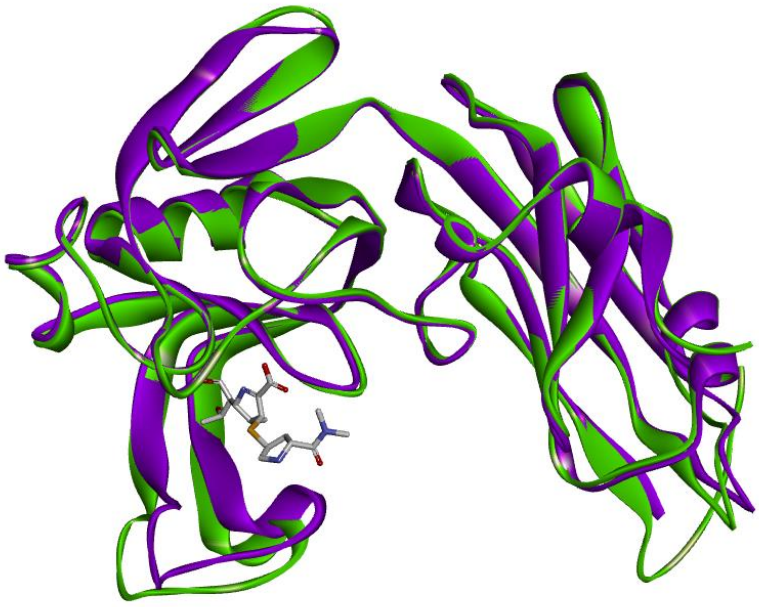

**Figure 1S.** The superimposed 3D structures of 3TUR ($Ldt_{Mt2}$ in complex with peptidoglycan fragment as natural substrate) in purple and 3VYP (meropenem—$Ldt_{Mt2}$ adduct) in green for the selected carbapenem—$Ldt_{Mt2}$ complexes.

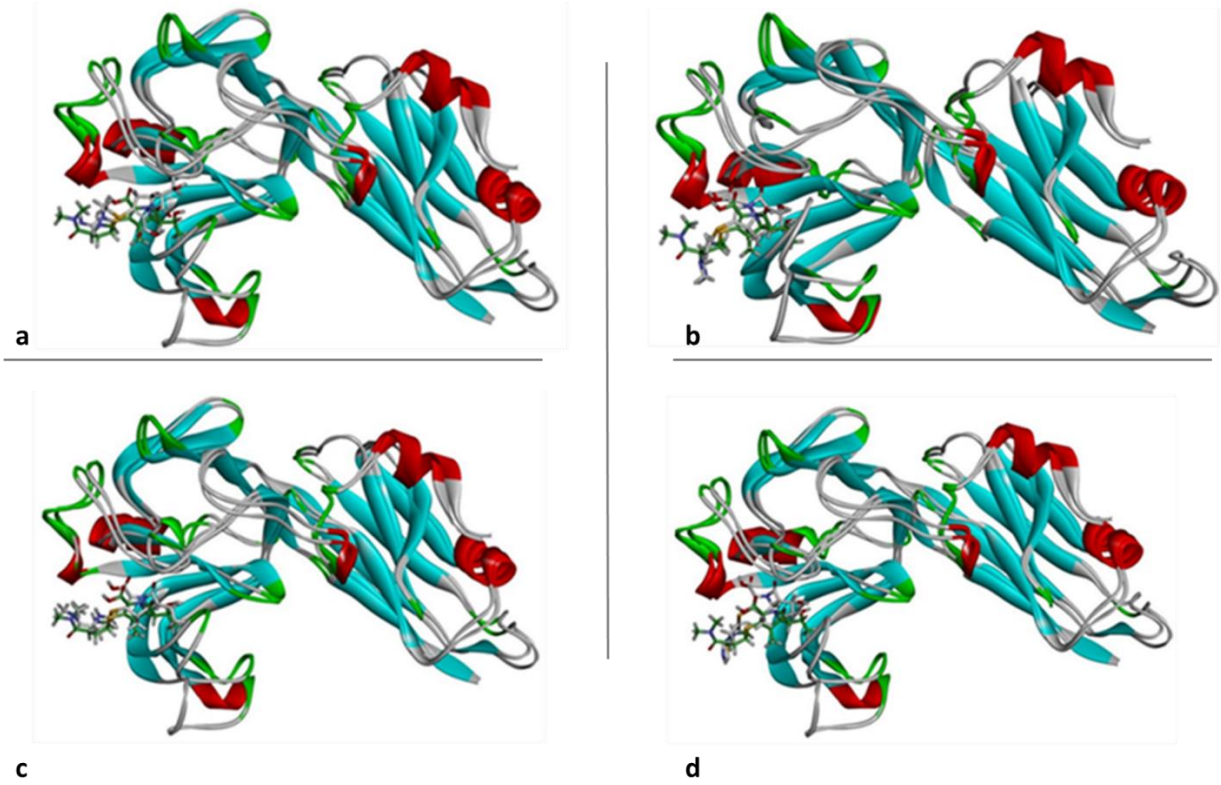


**Figure 2S.** The 3D structures of 3TUR superimposed with carbapenem—$Ldt_{Mt2}$ complexes. (a) Biapenem—$Ldt_{Mt2}$ (b) Imipenem—$Ldt_{Mt2}$ (c) Meropenem—$Ldt_{Mt2}$ (d) Tebipenem—$Ldt_{Mt2}$

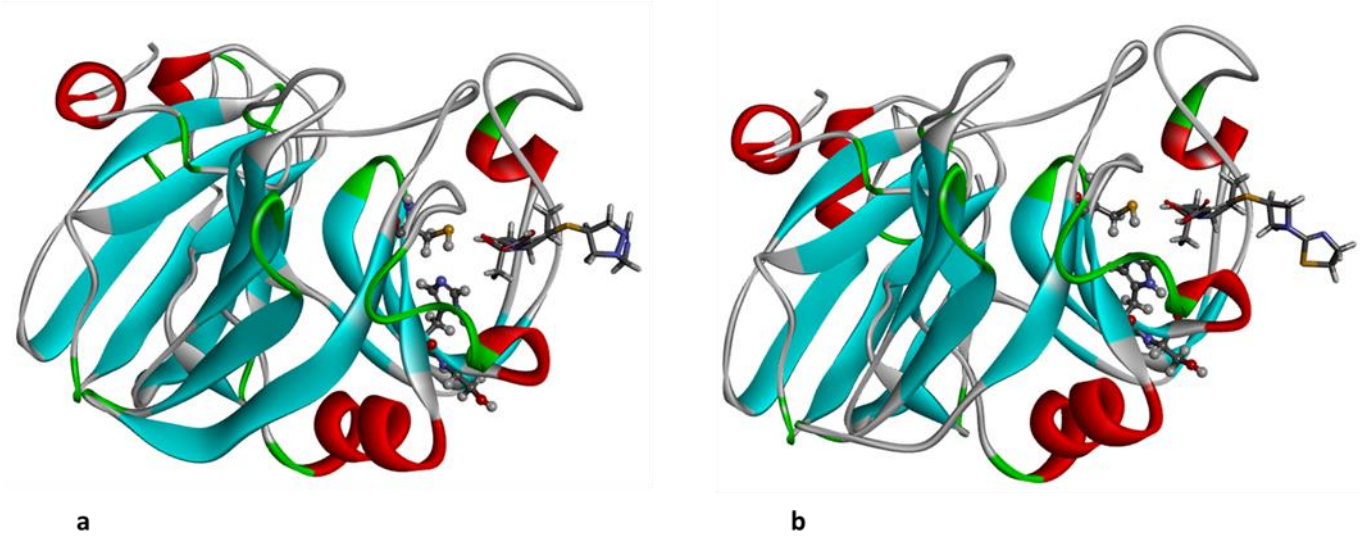


**Figure 3S.** 3D-structures of carbapenem—$Ldt_{Mt2}$ complexes showing poses obtained after frequency calculations. (**A**) Biapenem—$Ldt_{Mt2}$ (**B**) Tebipenem—$Ldt_{Mt2}$

**Table 1S:** The ONIOM binding interaction energies of carbapenem—$Ldt_{Mt2}$ complexes evaluated using (B3LYP/6-31+G (d): AMBER).

| Complexes | ΔG | ΔH | ΔS | $\Delta S_{trans}$ | $\Delta S_{rot}$ | $\Delta S_{vib}$ |
|---|---|---|---|---|---|---|
| | kcal $mol^{-1}$ | kcal $mol^{-1}$ | cal $mol^{-1}$ $K^{-1}$ | cal $mol^{-1}$ $K^{-1}$ | cal $mol^{-1}$ $K^{-1}$ | cal $mol^{-1}$ $K^{-1}$ |
| **Tebi-$Ldt_{Mt2}$** | -35.92 | -52.74 | -56.42 | -43.68 | -36.26 | 23.52 |
| **Imi-$Ldt_{Mt2}$** | -30.38 | -46.49 | -54.05 | -42.95 | -34.80 | 23.70 |
| **Bia-$Ldt_{Mt2}$** | -25.03 | -42.84 | -59.75 | -43.43 | -35.49 | 19.17 |
| **Mero-$Ldt_{Mt2}$** | -24.27 | -48.73 | -54.42 | -43.68 | -36.00 | 25.26 |

Gibb's free energy (**Δ*G***), Enthalpy change (**Δ*H***), Entropy change **(Δ*S***), S translational (**Δ$S_{trans}$**), S rotational (**Δ$S_{rot}$**), S vibrational **(Δ$S_{vib}$**).

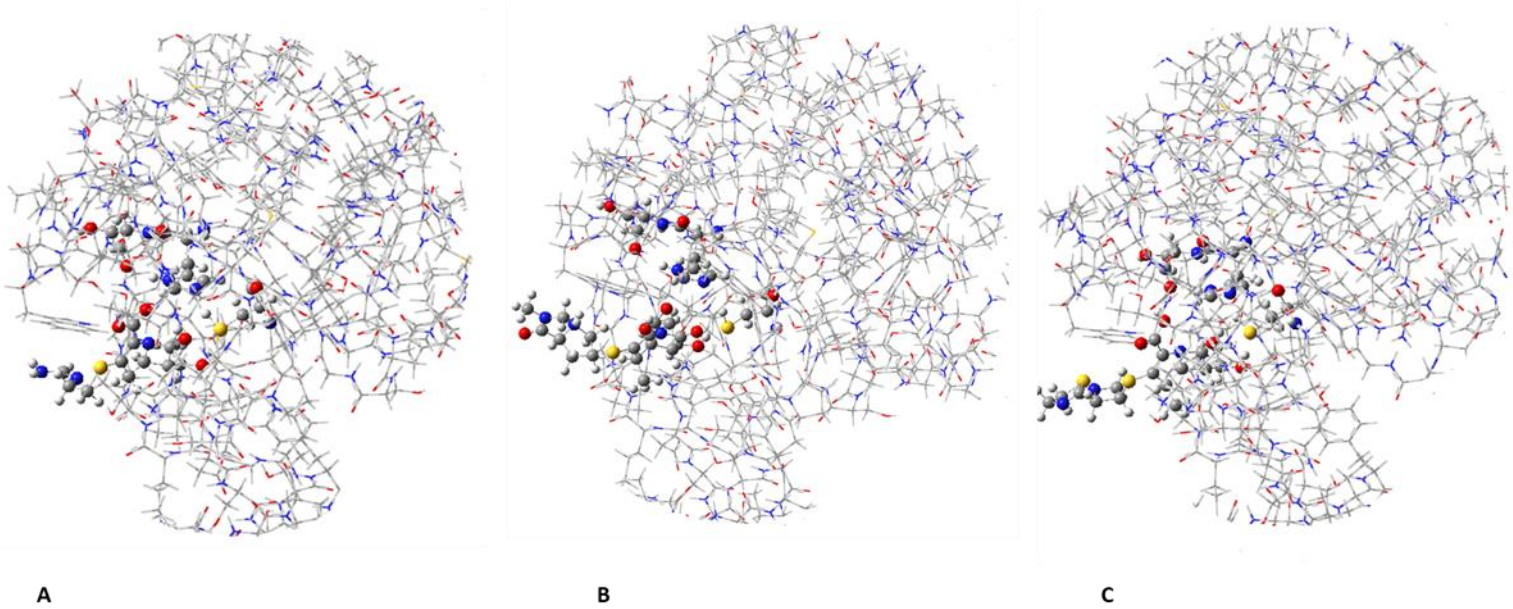


**Figure 4S** A two-layered QM:MM ONIOM (B3LYP/6-31G+(d): AMBER) model of (**A**)Imi—$Ldt_{Mt2}$, (**B**) Mero—$Ldt_{Mt2}$ and (**C**)Tebi—$Ldt_{Mt2}$ complexes. Active site residues His187, Ser188 and Cys205 were also treated at the same QM level.

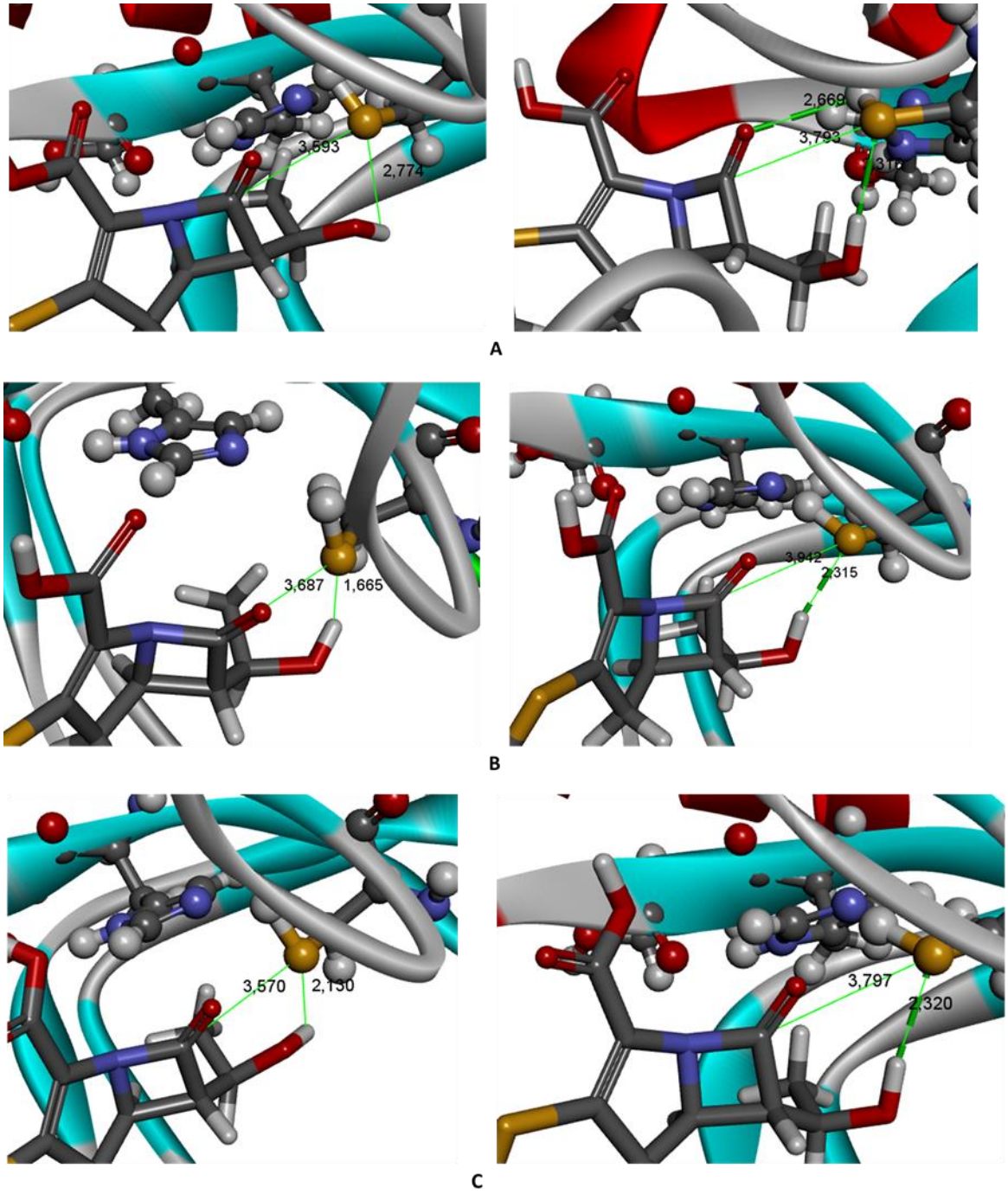


**Figure 5S**: Schematic representation of hydrogen bond and intermolecular interactions and their respective distances before and after optimization. **A.** Bia—$Ldt_{Mt2}$ **B**. Imi—$Ldt_{Mt2}$ and **C**. Tebi—$Ldt_{Mt2}$

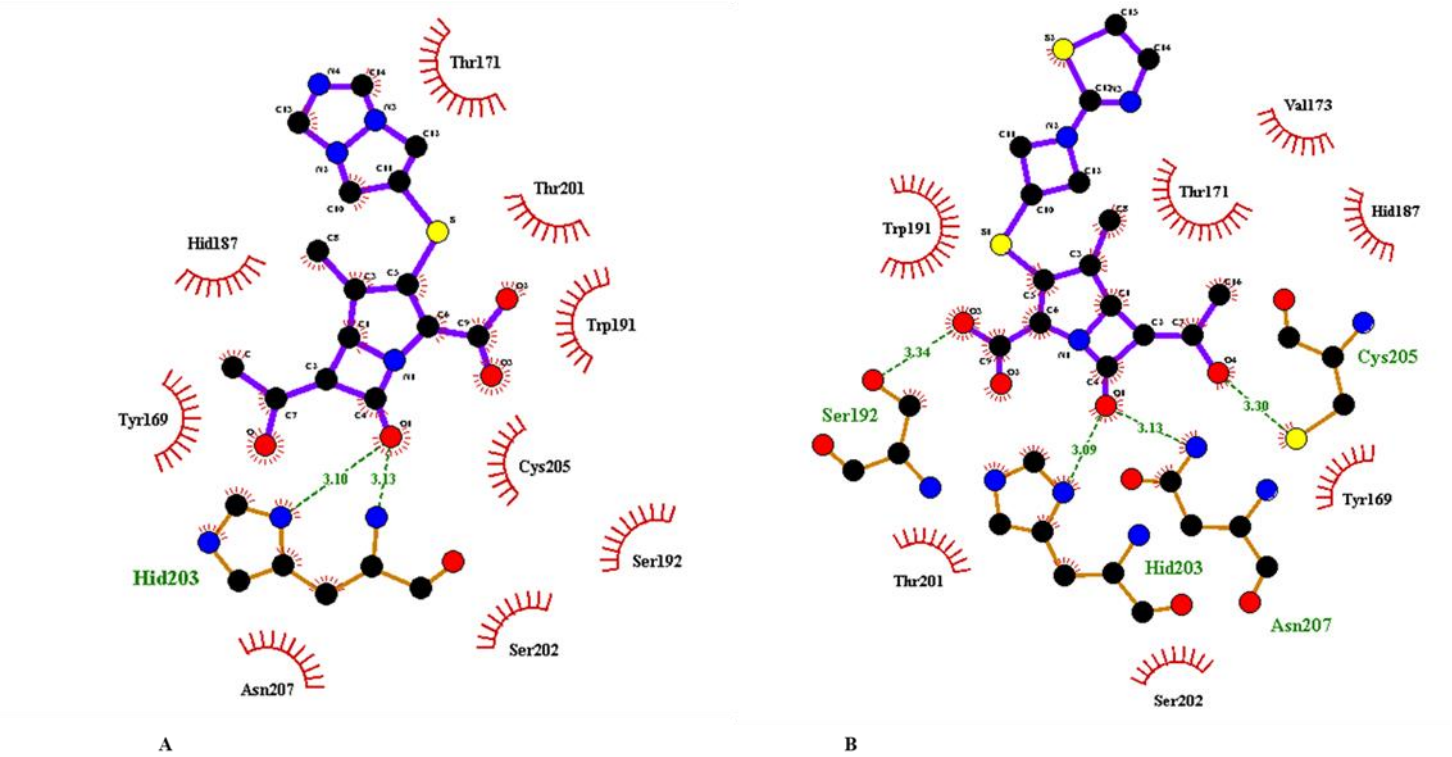


**Figure 6S.** A 2-D schematic representation of hydrogen bond and hydrophobic interactions between catalytic amino acid residues and the carbapenems **A.** Bia—$Ldt_{Mt2}$ and **B.** Tebi—$Ldt_{Mt2}$. Hydrogen bonds are denoted with dashed line and hydrophobic interactions are shown as arcs. Both the figures were made using LigPLOT program.

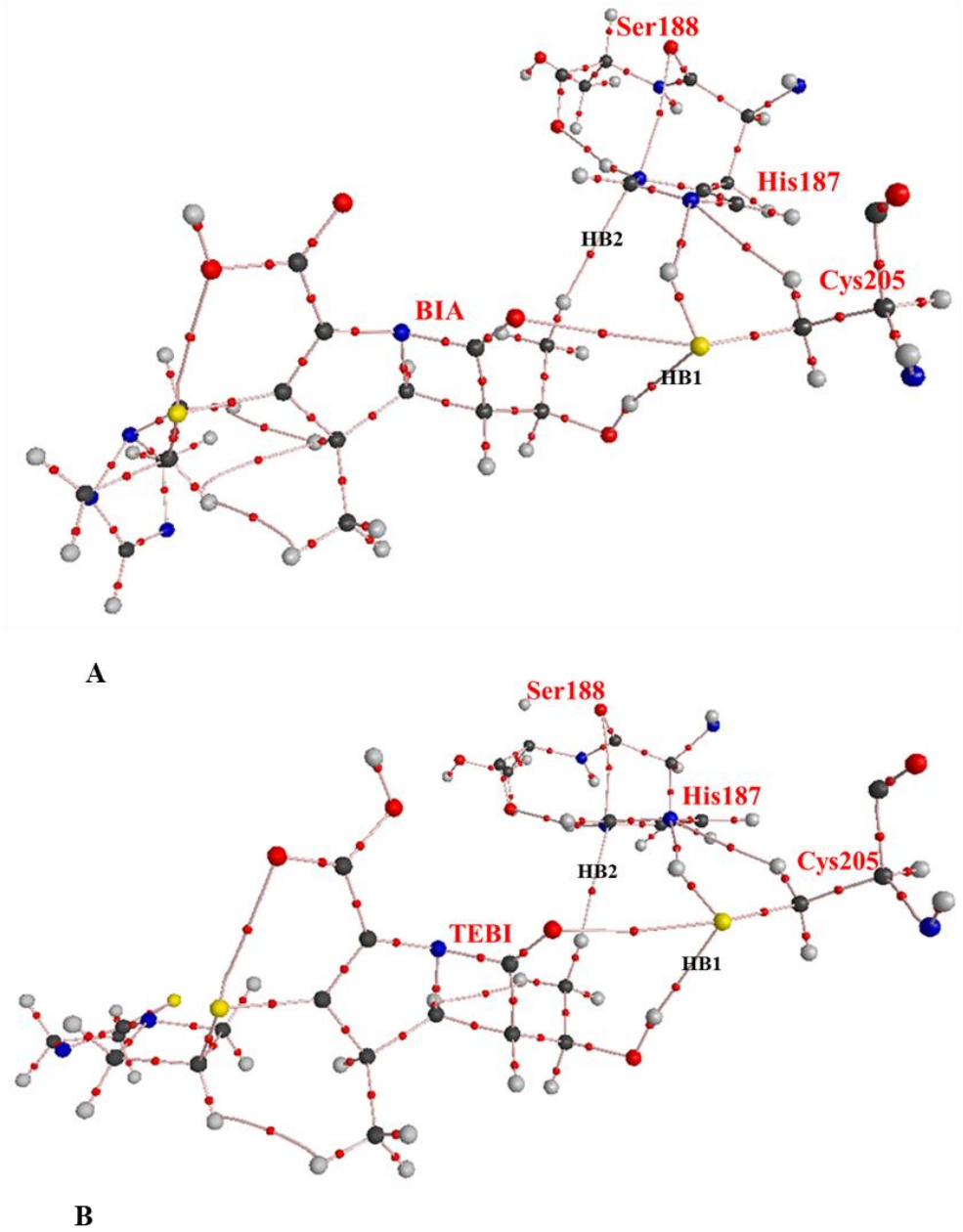


**Figure 7S.** Molecular graph of **A**. Bia—$Ldt_{Mt2}$ and **B**. Tebi—$Ldt_{Mt2}$ complexes generated using AIM2000 software. Small red spheres and lines correspond to the bond critical points (BCP) and the bond paths, respectively.

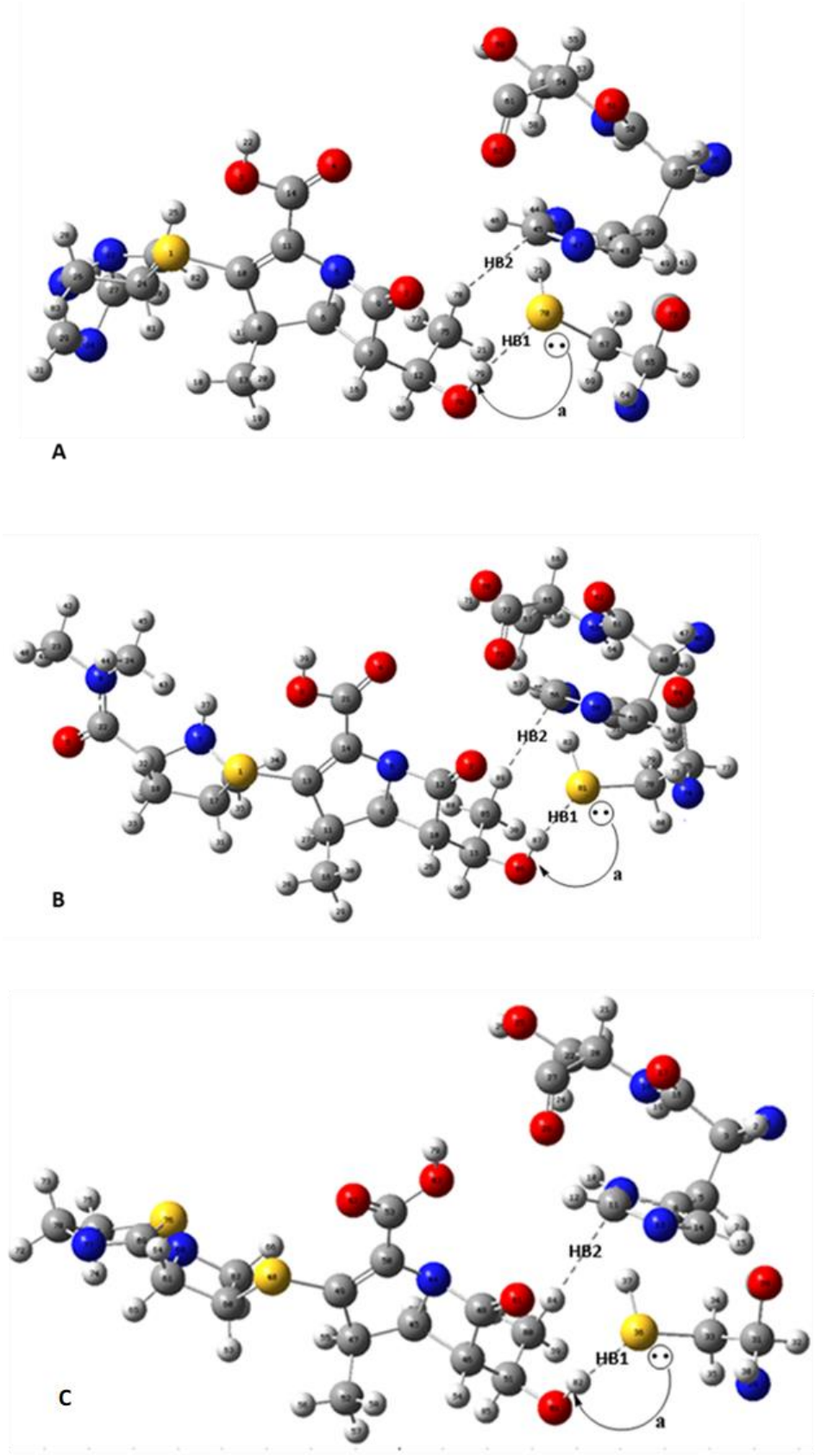


**Figure 8S**. Depiction of electrons transfer for carbapenem—$Ldt_{Mt2}$ complexes derived by second-order perturbation theory of NBO analysis. The curved arrow (**a**) depict the direction of charge transfer from lone pair to antibonding (LP→ σ*): (**A**) Bia—$Ldt_{Mt2}$ (**B**) Mero—$Ldt_{Mt2}$ and (**C**) Tebi—$Ldt_{Mt2}$ as listed in **Table 3.**

# APPENDIX B

## Supplementary Material for Chapter Three

## ONIOM study of carbapenems binding interaction energies against L, D transpeptidase2 from *Mycobacterium tuberculosis* with explicit water molecule confined in the active site

**Thandokuhle Ntombela, [a] Zeynab Fakhar, [a] Gideon F. Tolufashe, [a] Thavendran Govender, [a] Glenn E. M. Maguire, [a, b] Gyanu Lamichhane, [c.] Bahareh Honarparvar, [a*] and Hendrik G. Kruger[a*]**

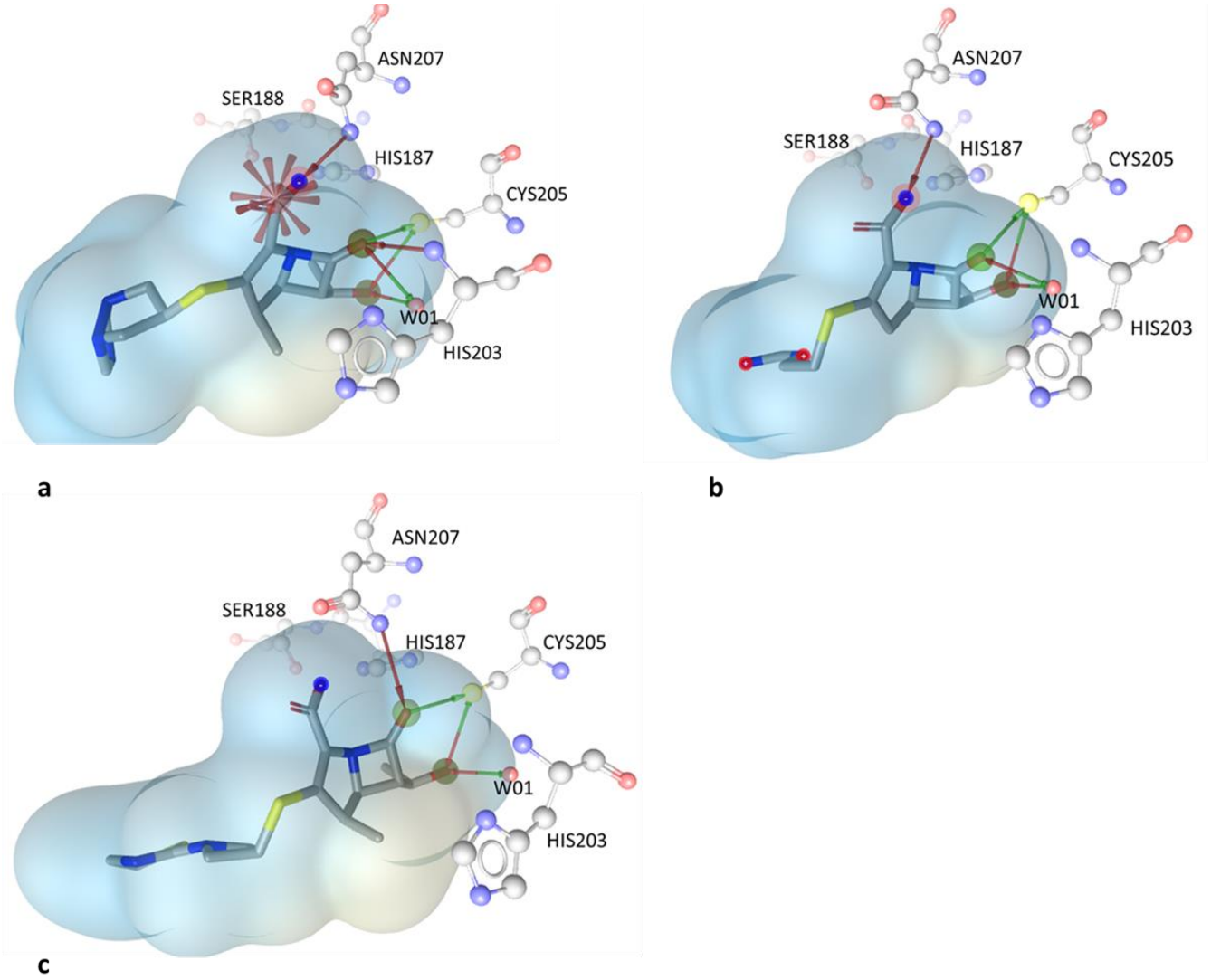


**Figure 1S.** 3-D structural features (hydrogen bond and hydrophobic interactions) of carbapenems— $Ldt_{Mt2}$—water complexes. Water molecule is denoted as **W01**

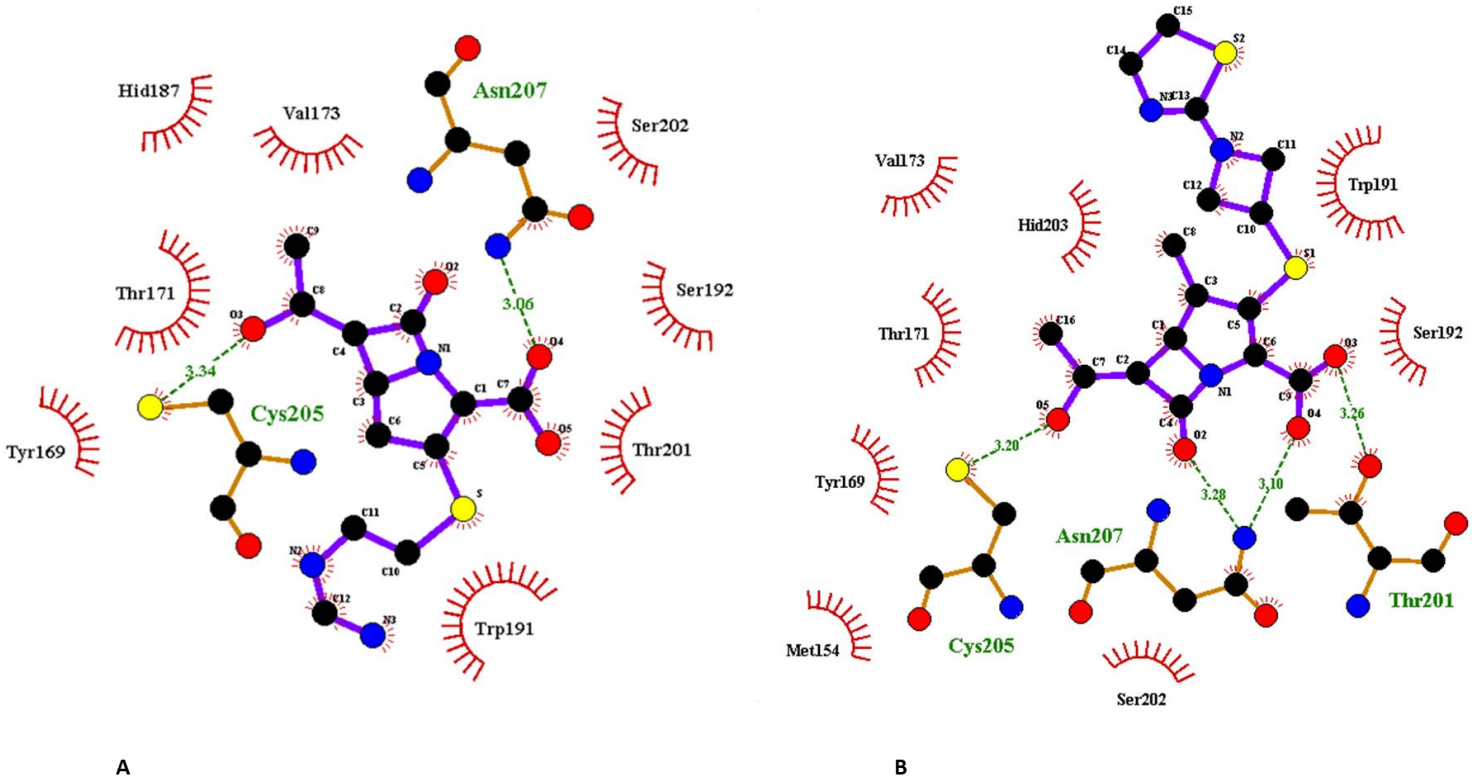


**Figure 2S.** 2-D schematic representation of hydrogen bond and hydrophobic interactions between catalytic amino acid residues and the carbapenems (**A.** Biapenem and **B.** Meropenem). Red dotted lines represent hydrogen bond interactions

**Table 1S**. AIM topological parameters including electron density (**ρ**) and their Laplacian of electron density (**$\nabla^2\rho$**) in a.u. and energetic parameters **G(r)**, **H(r)**, and **V(r)** in (kcal/mol) in carbapenem—$Ldt_{Mt2}$ complexes calculated at the B3LYP/6-31+G(d).

| Hydrogen bonds | Complexes interactions | ρ (r) | $\nabla^2\rho$ (r) | G(r) | H(r) | V(r) | Ellipticity (ε) |
|---|---|---|---|---|---|---|---|
| | **Mero—$Ldt_{Mt2}$** | | | | | | |
| **HB1** | $C_{89}H\cdots N_{37}$ | 0.0033 | 0.0109 | 0.0021 | -0.0006 | 0.0016 | 0.8872 |
| **HB2** | $O_{71}\cdots H_{34}C$ | 0.0201 | 0.0671 | 0.0167 | -0.00009 | 0.017 | 0.0852 |
| **HB3** | $C_{83}H\cdots O71$ | 0.0096 | 0.0336 | 0.0073 | -0.0011 | 0.0062 | 0.2154 |
| **HB4** | $O_{120}\cdots H_{72}O$ | 0.0242 | 0.0761 | 0.0198 | 0.0008 | 0.0201 | 0.0857 |
| **HB5** | $O_{75}\cdots H_{73}O$ | 0.0176 | 0.0578 | 0.0145 | 0.00009 | 0.0146 | 0.0562 |
| **HB6** | $O_{71}H\cdots S_{53}$ | 0.0103 | 0.0406 | 0.0084 | -0.0017 | 0.0068 | 0.3375 |
| **HB7** | $O_{120}H\cdots S_{53}$ | 0.0188 | 0.0495 | 0.0124 | 0.00007 | 0.0125 | 0.0601 |
| **HB8** | $O_{75}\cdots H_{67}N$ | 0.0101 | 0.0374 | 0.0085 | -0.0008 | 0.0077 | 0.0627 |
| **HB9** | $C_{119}H\cdots C_{11}$ | 0.0049 | 0.0164 | 0.0031 | -0.0010 | 0.0021 | 0.1342 |
| **HB10** | $O_{76}H\cdots O_{65}C$ | 0.0426 | 0.1401 | 0.0356 | 0.0005 | 0.0361 | 0.0305 |
| **HB11** | $C_{94}O\cdots H_{12}C$ | 0.0061 | 0.0238 | 0.0050 | -0.0010 | 0.0040 | 0.0427 |
| | **Tebi—$Ldt_{Mt2}$** | | | | | | |
| **HB1** | $C_{86}H\cdots N_{37}$ | 0.0040 | 0.0127 | 0.0026 | -0.0006 | 0.0019 | 1.4200 |
| **HB2** | $O_{71}\cdots H_{34}C$ | 0.0170 | 0.0520 | 0.0131 | 0.00009 | 0.0132 | 0.0524 |
| **HB3** | $O_{71}\cdots H_{30}N$ | 0.0072 | 0.0267 | 0.0058 | -0.0009 | 0.0049 | 0.1881 |
| **HB4** | $O_{115}\cdots H_{73}O$ | 0.0370 | 0.1194 | 0.0310 | 0.0012 | 0.0322 | 0.0334 |
| **HB5** | $O_{115}H\cdots S_{53}$ | 0.0260 | 0.0593 | 0.0166 | 0.0018 | 0.0184 | 0.0446 |
| **HB6** | $O_{75}\cdots H_{67}N$ | 0.0097 | 0.0634 | 0.0083 | -0.0008 | 0.0074 | 0.04616 |
| **HB7** | $O_{75}\cdots H_{12}C$ | 0.0014 | 0.0058 | 0.0010 | -0.0004 | 0.0006 | 0.4056 |
| **HB8** | $C_{114}H\cdots C_{11}$ | 0.0048 | 0.0154 | 0.0029 | -0.0010 | 0.0019 | 0.0991 |
| **HB9** | $O_{77}H\cdots O_{65}$ | 0.0434 | 0.1380 | 0.0357 | 0.0012 | 0.0369 | 0.0126 |

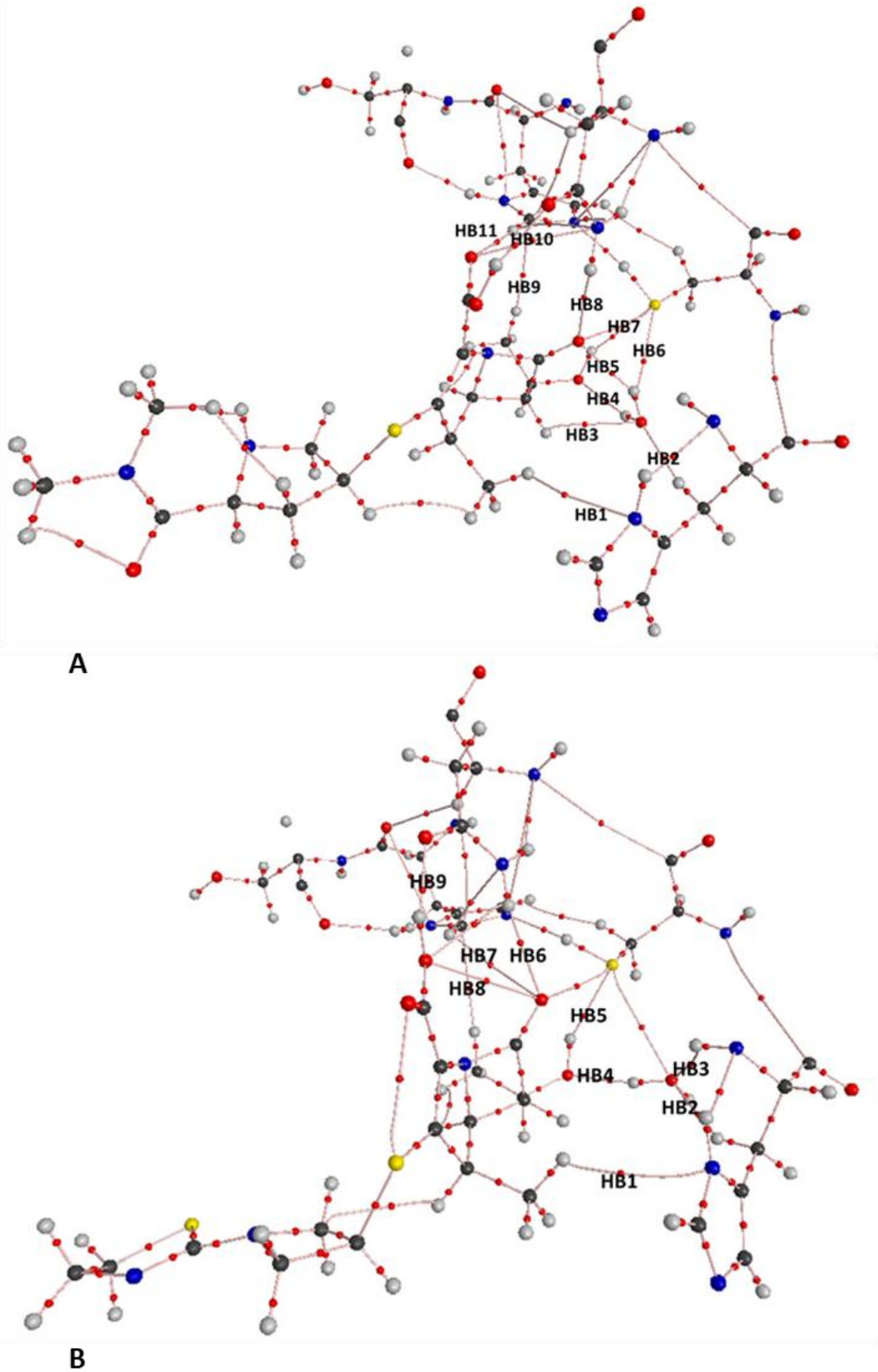


**Figure 3S.** Molecular graph of **A**. Mero—$Ldt_{Mt2}$ and **B**. Tebi—$Ldt_{Mt2}$ complexes generated using AIM2000 software. Small red spheres and lines correspond to the bond critical points (BCP) and the bond paths, respectively. See details of the molecular graph for other complexes in

**Table 2S**. Second-order perturbation energies E $^{(2)}$ (kcal mol$^{-1}$) corresponding to the most important charge transfer interaction (donor→ acceptor) in the carbapenem-$Ldt_{Mt2}$ complexes at the B3LYP/6-31+G(d) level.

| **Complex/ Interactions** | **Donor NBO(i) n(O)** | **Acceptor NBO(j) σ*(O─H)** | ***E*** $^{(2)}$ **(kcalmol$^{-1}$) (O)→σ*(O─H)** |
|---|---|---|---|
| **Tebi—$Ldt_{Mt2}$** | | | |
| **HB1** | LP (1) N37 | BD*(1) C86─H92 | 0.17 |
| **HB2** | BD (1) C33—H34 | BD*(1) O71─H73 | 0.12 |
| | BD*(1) O71─H73 | BD*(1) C33─H34 | 0.54 |
| | LP (1) O71 | BD*(1) C33—34 | 5.28 |
| **HB3** | LP (1) O71 | BD*(1) N29─H30 | 0.44 |
| | LP (2) O71 | BD*(1) N29─H30 | 0.60 |
| **HB4** | BD (1) O115─H116 | BD*(1) O71─H73 | 0.95 |
| | LP (1) O115 | BD*(1) O71─H73 | 2.04 |
| | LP (2) O115 | BD*(1) O71─H73 | 15.50 |
| **HB5** | BD (1) S53─H54 | BD*(1) O115─H116 | 0.48 |
| | LP (1) S53 | BD*(1) O115─H116 | 1.49 |
| | LP (2) S53 | BD*(1) O115─H116 | 17.75 |
| **HB6** | LP (1) O75 | BD*(1) N66─H67 | 1.42 |
| | LP (2) O75 | BD*(1) N66─H67 | 1.59 |
| **HB7** | — | — | — |
| **HB8** | BD (1) C11─H12 | BD*(1) C114─H118 | 0.14 |
| | BD (2) C11─N13 | BD*(1) C114─H118 | 0.39 |
| **HB9** | BD (1) C64—O65 | BD*(1) O77—H113 | 0.79 |
| | BD (2) C64—O65 | BD*(1) O77—H113 | 0.49 |
| | LP (1) O65 | BD*(1) O77—H113 | 7.84 |
| | LP (2) O65 | BD*(1) O77—H113 | 19.04 |
| **Mero—$Ldt_{Mt2}$** | | | |
| **HB1** | LP (1) N37 | BD*(1) C89—H103 | |
| **HB2** | BD (1) C33—H34 | BD*(1) O71—H72 | 0.27 |
| | LP (1) O71 | BD (1) C33—H34 | 0.47 |
| | LP (2) O71 | BD (1) C33—H34 | 7.74 |
| **HB3** | — | — | — |
| **HB4** | BD (1) O120—H121 | BD*(1) O71—H72 | 0.30 |

| | | | |
|---|---|---|---|
| | LP (1) O120 | BD*(1) O71—H72 | 1.59 |
| | LP (2) O120 | BD*(1) O71—H72 | 6.42 |
| **HB5** | BD (1) O75—C85 | BD*(1) O71—H72 | 0.21 |
| | LP (1) O75 | BD*(1) O71—H72 | 1.04 |
| | LP (2) O75 | BD*(1) O71—H72 | 3.29 |
| **HB6** | LP (1) S53 | BD*(1) O71—H73 | 1.34 |
| | LP (2) S53 | BD*(1) O71—H73 | 0.14 |
| **HB7** | LP (1) S53 | BD*(1) O120—H121 | 1.12 |
| | LP (2) S53 | BD*(1) O120—H121 | 10.89 |
| **HB8** | LP (1) O75 | BD*(1) N66—H67 | 1.29 |
| | LP (2) O75 | BD*(1) N66—H67 | 1.59 |
| **HB9** | BD (2) C11—N13 | BD*(1) C119—H123 | 0.54 |
| **HB10** | BD (1) C64—O65 | BD*(1) O76—H112 | 0.93 |
| | BD (2) C64—O65 | BD*(1) O76—H112 | 2.36 |
| | LP (1) O65 | BD*(1) O76—H112 | 11.58 |
| | LP (2) O65 | BD*(1) O76—H112 | 13.35 |
| **HB11** | BD (1) O77—C34 | BD*(1) C11—H12 | 0.15 |
| | LP (1) O77 | BD*(1) C11—H12 | 1.15 |
| | LP (1) O77 | BD*(1) C11—H12 | 0.51 |
| **Bia—Ldt$_{Mt2}$** | | | |
| **HB1** | BD (1) C39—N41 | BD*(1) C83—H90 | 0.10 |
| **HB2** | - | - | - |
| **HB3** | LP (1) O115 | BD*(1) C77—H86 | 0.13 |
| | LP (1) O115 | BD*(1) C77—H86 | 0.15 |
| **HB4** | BD (1) O107—H110 | BD*(1) O115—H116 | 0.32 |
| | LP (1) O107 | BD*(1) O115—H116 | 1.85 |
| | LP (2) O107 | BD*(1) O115—H116 | 6.14 |
| **HB5** | BD (1) C33—H34 | BD*(1) O115—H116 | 0.31 |
| | BD (1) O115—H116 | BD*(1) C33—H34 | 0.46 |
| | LP (1) O115 | BD (1) C33—H34 | 0.76 |
| | LP (2) O115 | BD (1) C33—H34 | 7.06 |
| **HB6** | BD (2) O72—C79 | BD*(1) O115—H117 | 0.25 |
| **HB7** | LP (1) S53 | BD*(1) O115—H117 | 1.00 |

| | | | |
|---|---|---|---|
| | LP (2) S53 | BD*(1) O115—H117 | 0.16 |
| **HB8** | BD (1) O72—C79 | BD*(1) N29—H30 | 0.46 |
| | LP (1) O72 | BD*(1) N29—H30 | 1.24 |
| **HB9** | BD (1) S53—H54 | BD*(1) O107—H110 | 0.20 |
| | LP (1) S53 | BD*(1) O107—H110 | 1.30 |
| | LP (2) S53 | BD*(1) O107—H110 | 12.94 |
| **HB10** | - | - | - |
| **HB11** | LP (1) O74 | BD*(1) N66—H67 | 3.40 |
| | LP (2) O74 | BD*(1) N66—H67 | 0.72 |

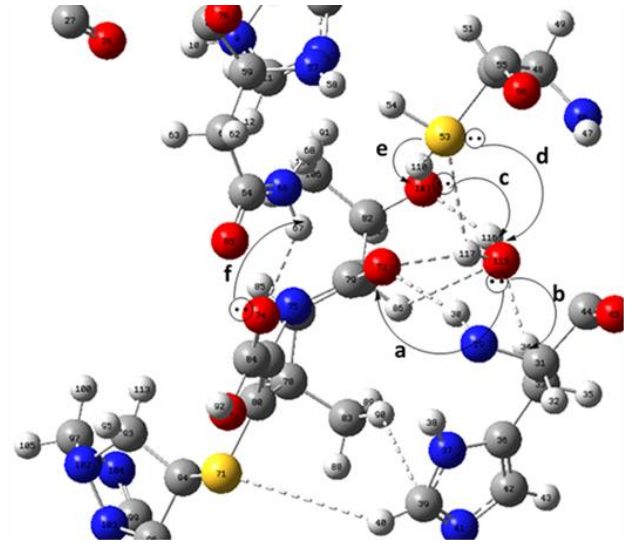


A

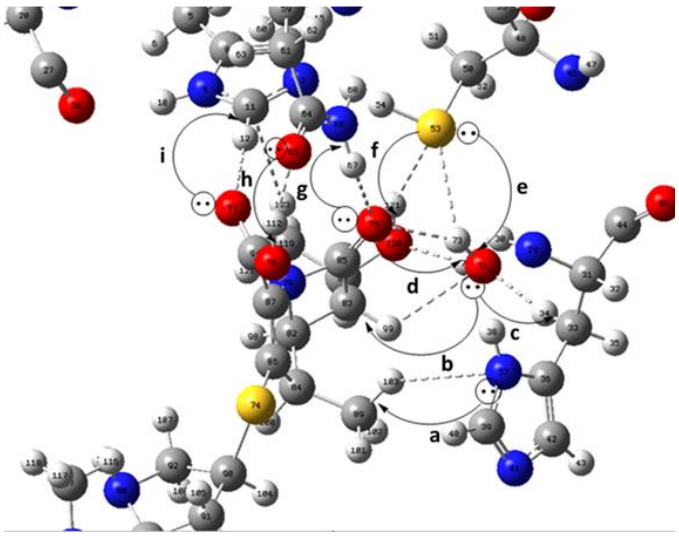


B

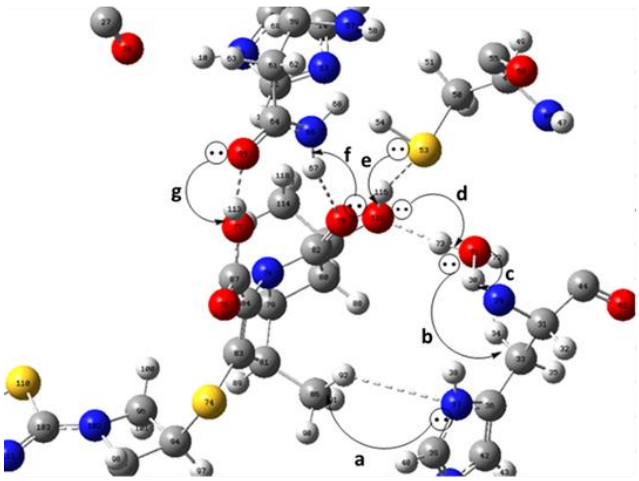


C

**Figure 4S**. Depiction of electron transfers for Imi—$Ldt_{Mt2}$ complex derived by second-order perturbation theory of NBO analysis. The curved arrows (**a, b, c, d, e, f, g, h** and i) depict the direction of charge transfer: **Table 2S**